

UNIVERSITY OF NATURAL RESOURCES AND LIFE SCIENCES,
VIENNA

Department of Food Sciences and Technologies
Institute of Food Biotechnology



&

NORWEGIAN UNIVERSITY OF LIFE SCIENCE
Department of Chemistry, Biotechnology and Food Sciences
Protein Engineering and Proteomics group



Master Thesis

Structural features important for electron transfer in cellobiose dehydrogenase

Daniela Gamperl

This project was done at the Institute of Food Biotechnology under supervision of:

Priv.-Doz. Dr. Roland Ludwig
and Dipl.-Ing. Alfons Felice

Vienna/Ås 2014-2015

Eidesstattliche Erklärung des Verfassers/-in

Ich erkläre ehrenwörtlich, dass ich die Arbeit selbständig angefertigt, keine anderen als die angegebenen Hilfsmittel benutzt und alle aus ungedruckten Quellen, gedruckter Literatur oder aus dem Internet im Wortlaut oder im wesentlichen Inhalt übernommenen Formulierungen und Konzepte gemäß den Richtlinien wissenschaftlicher Arbeiten zitiert, durch Fußnoten gekennzeichnet bzw. mit genauer Quellenangabe kenntlich gemacht habe. Diese Arbeit wurde in gleicher oder ähnlicher Form noch bei keinem/r anderen Prüfer/in als Prüfungsleistung eingereicht. Mir ist bekannt, dass die Verwendung unerlaubter Hilfsmittel rechtliche Schritte nach sich ziehen kann.

Acknowledgements

I would like to express my sincere gratitude to my supervisor Priv.-Doz. Dr. Roland Ludwig for enabling me to realize this thesis in his group and his encouragement and valuable remarks along this research.

My special thanks goes to my co-supervisor Dipl.-Ing. Alfons Felice for his immense support, motivation and constant patience throughout the whole Master thesis. His great guidance helped me in all the time of research and writing of this thesis.

My sincere thanks also goes to Prof. Dr. Vincent Eijsink and Dr. Bjørge Westereng at the Norwegian University of Life Science for providing me the great opportunity to join their team and their helpful support during my stay there.

I also want to thank my fellow lab mates and all workers at the Institute of Food Biotechnology for their help and pleasant atmosphere during my work.

Diese Arbeit widme ich meinen Eltern, Elisabeth und Wolfgang, die mich nicht nur in guten, sondern auch in schwierigen Situation immer unterstützen und an mich glauben. Ihre stete, nicht nur finanzielle, sondern auch emotionale und moralische Unterstützung haben diese Arbeit erst möglich gemacht. Vielen, vielen Dank!

Table of Contents

1. Abstract	5
2. Introduction.....	7
2.1 Aims of the study.....	12
3. Materials & Methods	14
3.1 Chemicals.....	14
3.1.1 Buffers	14
3.2 Media.....	16
3.3 Molecular Biology	18
3.2.1 Biological material.....	18
3.2.2 Primers	18
3.2.3 Enzymes.....	19
3.2.4 Vectors.....	19
3.2.5 Kits	20
3.4 Site directed mutagenesis of <i>NcCDH IIA</i> and preparation for expression in <i>P. pastoris</i>	20
3.4.1 Site-directed mutagenesis.....	20
3.4.2 PCR.....	21
3.4.3 Agarose Gel Electrophoresis	23
3.4.4 DNA Digestion	24
3.4.5 Transformation of chemically competent <i>E. coli</i> strain NEB 5-alpha.....	24
3.4.6 Sequencing	24
3.4.7 Electroporation of competent <i>P. pastoris</i> cells	25
3.4.8 Preparation of a cryo stock culture	25
3.5 96 – Deep well plate cultivation	25
3.6 Hightroughput activity screening	26
3.6.1 2,6-Dichloroindophenol (DCIP) assay.....	28
3.6.2 Cytochrome <i>c</i> assay.....	29
3.6.3 Amplex red assay.....	30
3.6.4 Bradford assay	31
3.7 Fermentation.....	32
3.8 Purification	32

3.8.1	Hydrophobic interaction chromatography (HIC).....	33
3.8.2	Ion exchange chromatography (IEC)	33
3.9	Enzyme characterisation	34
3.9.1	Steady-state kinetic studies.....	34
3.9.2	Presteady – state kinetic studies.....	34
3.10	Kinetic studies of CDH-LPMO interaction on soluble and insoluble substrates.....	36
3.11	UV/visible spectra.....	40
3.12	SDS-PAGE.....	41
4.	Results & Discussion.....	42
4.1	Mutagenic studies of <i>NcCDH IIA</i>	42
4.2	High-throughput activity screening.....	44
4.3	Production of CDH variants	49
4.4	Protein purification.....	51
4.5	Characterization	53
4.5.1	Steady-state kinetic constants	53
4.5.2	Presteady-state kinetic studies	55
4.6	Comparison of HTS versus kinetic parameters.....	60
4.7	Kinetic studies of CDH-LPMO interaction on solid substrates	61
4.7.1	Kinetic studies of CDH-LPMO interaction on the soluble substrate cellopentaose.....	62
4.7.2	Kinetic studies of CDH-LPMO interaction on the insoluble substrate Avicel	65
4.7.3	Comparison ESI-MS vs MALDI-TOF MS.....	68
5.	Conclusions & Outlook	70
6.	References.....	73
7.	Appendix.....	77
7.1	List of figures	77
7.2	List of tables.....	80
7.3	List of abbreviations	82
7.4	Supplemental information	83

1. Abstract

Cellulose is earth's most abundant biopolymer and a renewable and economically important resource that can substitute fossil resources for the production of second generation biofuel, chemicals and materials. Recently, a novel, bi-enzymatic system was identified with potential to increase the efficiency of saccharification processes and thereby to reduce the high costs of biofuel production. The two enzymes involved are the extracellular flavocytochrome cellobiose dehydrogenase (CDH) and the copper-dependent lytic polysaccharide monoxygenase (LPMO). However, despite intensive research, there are still major questions concerning the electron transfer inbetween the two enzymes and the mechanism that controls their interaction. The aim of this study was to elucidate the influence of varying electron transfer rates inbetween CDH (IET) on the catalytic efficiency of LPMO in solution as well as adsorbed on its natural substrate cellulose. During this study a robust and simple high-throughput-screening method was established combining four photometric enzyme activity assays. It allows for fast determination of active CDH-LPMO combinations in culture supernatant. The screening exhibits six interesting CDH variants, which were successfully produced in *P. pastoris* and characterized in detail. Kinetic features of the variants were determined by stopped-flow and MS-techniques for CDH-LPMO interaction studies in solution and on cellulose, respectively. Rapid kinetic analysis of the CDH variants provided evidence that the length and composition of the linker peptide as well as mutations adjacent the heme-*b* cofactor strongly contribute to the intra- and inter-electron transfer mechanism. Hydrophobic and electrostatic repulsion or attraction forces are shown to substantially affect the domain interaction. For conversion experiments on cellopentaose and cellulose two CDH/LPMO combinations with CDHs showing either fast or slow IET rates were used. Remarkably, both combinations showed very similar substrate conversion velocities, revealing the LPMO substrate conversion reaction rate and its property to be the overall rate limiting step.

This work provides insight into the electron transfer mechanism of this elaborate biodegradation enzymatic system. It elucidates the reaction mechanism in solution as well as under in vivo conditions on cellulose. A comprehensive picture of this bi-enzymatic system is crucial for an improved enzymatic conversion of plant biomass towards a cost-saving and efficient production of biofuels.

1. Zusammenfassung

Zellulose ist weltweit das am häufigsten vorkommende Biopolymer. Dieser nachwachsende Rohstoff stellt eine wirtschaftlich und ökologisch wertvolle Alternative zu fossilen Brennstoffen für die Herstellung von Biokraftstoffen der 2. Generation, diversen Basischemikalien und Materialien dar. Erst kürzlich entdeckte man ein viel versprechendes Exoenzymsystem in holzabbauenden Pilzen, das einen effizienten hydrolytischen Abbau von Lignocellulose und somit eine Senkung der Herstellungskosten für Biotreibstoffe ermöglicht. Hierzu zählen das extrazelluläre Flavocytochrom, Cellobiosedehydrogenase (CDH), und die Kupfer-abhängige lytische Polysaccharidmonooxygensase (LPMO). Trotz immenser Forschungsarbeit in den letzten Jahren, bleiben immer noch etliche Unklarheiten bezüglich des Elektronentransfers innerhalb CDH und LPMO und des Interaktionskontrollierenden Mechanismus. Das Ziel der Arbeit war es, den Einfluss verschieden schneller intramolekularer Elektronentransferraten (IET) innerhalb der CDH auf die katalytische Effizienz von LPMO zu untersuchen. Während dieser Arbeit wurde eine robuste und einfache High-Throuput-Screening Methode entwickelt. Sie erlaubt die schnelle Ermittlung von aktiven CDH-LPMO Kombination in Kulturüberständen. Das Screening ergab sechs interessante CDH Varianten, die in *P. pastoris* erfolgreich produziert wurden, gefolgt von einer detaillierten Charakterisierung. Kinetische Eigenschaften aller Varianten in Lösung, sowie auf Zellulose wurden jeweils mittels Stopped-flow Spektrophotometrie und Massenspektrometrie ermittelt. Presteady-state kinetische Untersuchungen der CDH Varianten zeigten, dass die Länge und Zusammensetzung des Linkerpeptides, sowie Mutationen an den Aminosäureresten nahe des Häm-*b* Kofaktors maßgeblich an dem intra- und inter- Elektronentransfermechanismus beteiligt sind. Ausschlaggebend für die Domäneninteraktion waren hierbei hydrophobische und elektrostatische Kräfte. Für die enzymatische Umsetzung von Zellulose und Cellopentaose wurden zwei verschiedene CDH/LPMO-Kombinationen eingesetzt, mit jeweils einer CDH mit schnellem bzw. langsamem IET. Beide Kombinationen zeigten keinen oder nur geringen Einfluss auf die Substratumsatzrate. Daraus lässt sich auf die Geschwindigkeit der LPMO Reaktion schließen und schlussfolgern, dass diese der geschwindigkeitslimitierende Schritt ist.

Die Arbeit bietet nähere Einblicke in den Elektronentransfermechanismus dieses ausgefeilten Biomasse abbauenden enzymatischen Systems. Dabei wurde sowohl die CDH-LPMO-Reaktion in Lösung als auch unter in vivo Bedingungen auf Zellulose untersucht. Eine vollständige Aufklärung der Interaktion dieser zwei Enzyme ist entscheidend für einen verbesserten enzymatischen Abbau von pflanzlicher Biomasse und somit für eine kostensparende und effiziente Biotreibstoff-Produktion.

2. Introduction

Cellulosic biomass is the largest source of biopolymers on earth and the biological exploitation of this carbohydrate as an energy source plays a critical role in the carbon cycle and the planet's ecology. Industrial production of fuels and chemicals from this economically important and renewable resource holds potential to substitute fossil resources and promotes energy self-sufficiency. (Langston et al., 2011). In 2011, the US Department of Energy stated that more than 1.3 billion tons of plant biomass could be sustainably produced annually for biofuel production, which is equivalent to one-third of the current demand for transportation fuels in the USA (Perlack et al., 2011, 2005). Currently, the most common biofuel, bioethanol, is mainly produced from starch or sugar, both potential food sources. Therefore great efforts are being made to develop so called second generation biofuels based on non-food biomass such as lignocellulosic biomass (Horn et al., 2012). However, the main bottleneck in the development of lignocellulosic fuels or chemicals lies in the cost-intensive conversion of plant cell wall polysaccharides to fermentable sugars by thermochemical pre-treatment and enzymatic hydrolysis. The expense is related to the recalcitrance of lignocellulose when comparing with other feedstocks like sucrose or starch (Beeson et al., 2015). Plant biomass has evolved complex structures to resist assaults on its structural sugars from microorganisms and animals. In the context of saccharification processes, the inaccessibility of the plant cell wall and the recalcitrant of its individual components prevents not only the penetration by hydrolytic enzymes, but even by small molecules like water and thus increases conversion costs tremendously (Himmel et al., 2007).

Lignocellulosic biomass is mainly composed of three major components: cellulose (35-50%), hemicellulose (20-35%) and lignin (5-30%) (Lynd et al., 2002). The main component of lignocellulose, cellulose, is a linear polysaccharide consisting of several hundred to more than ten thousand β -1,4 linked glucose units. In crystalline cellulose, cellobiose forms repeating units due to a rotation by 180 degrees of consecutive sugar molecules. The cellulose chains aggregate into microfibriles via hydrogen bonding contributing to the resistance of crystalline cellulose to degradation. While its recalcitrance to enzymatic saccharification is challenging, a big advantage of cellulose is its homogeneity. Complete depolymerisation yields just one product, namely glucose. In contrast, hemicellulose, the second most abundant component of hemicellulose, is typically composed of various hexoses and pentoses such as arabinose, galactose, glucose, mannose and xylose, depending on the plant type. It links cellulose fibres into microfibriles and cross-links with lignin, creating a complex network of bonds that provide structural strength. Lignin is a three-dimensional macromolecule that consists of three major phenolic components – *p*-coumaryl alcohol (H), coniferyl alcohol (G) and sinapyl alcohol (S) – and acts like glue to hold the lignocellulosic matrix together. It

fills the spaces in the cell wall between cellulose, hemicellulose and pectin. Lignin is covalently linked to hemicellulose providing compressive strength to the individual cellulose fibres and stiffness to the plant cell wall (Figure 1, Horn et al., 2012; Ritter, 2008; Rubin, 2008).

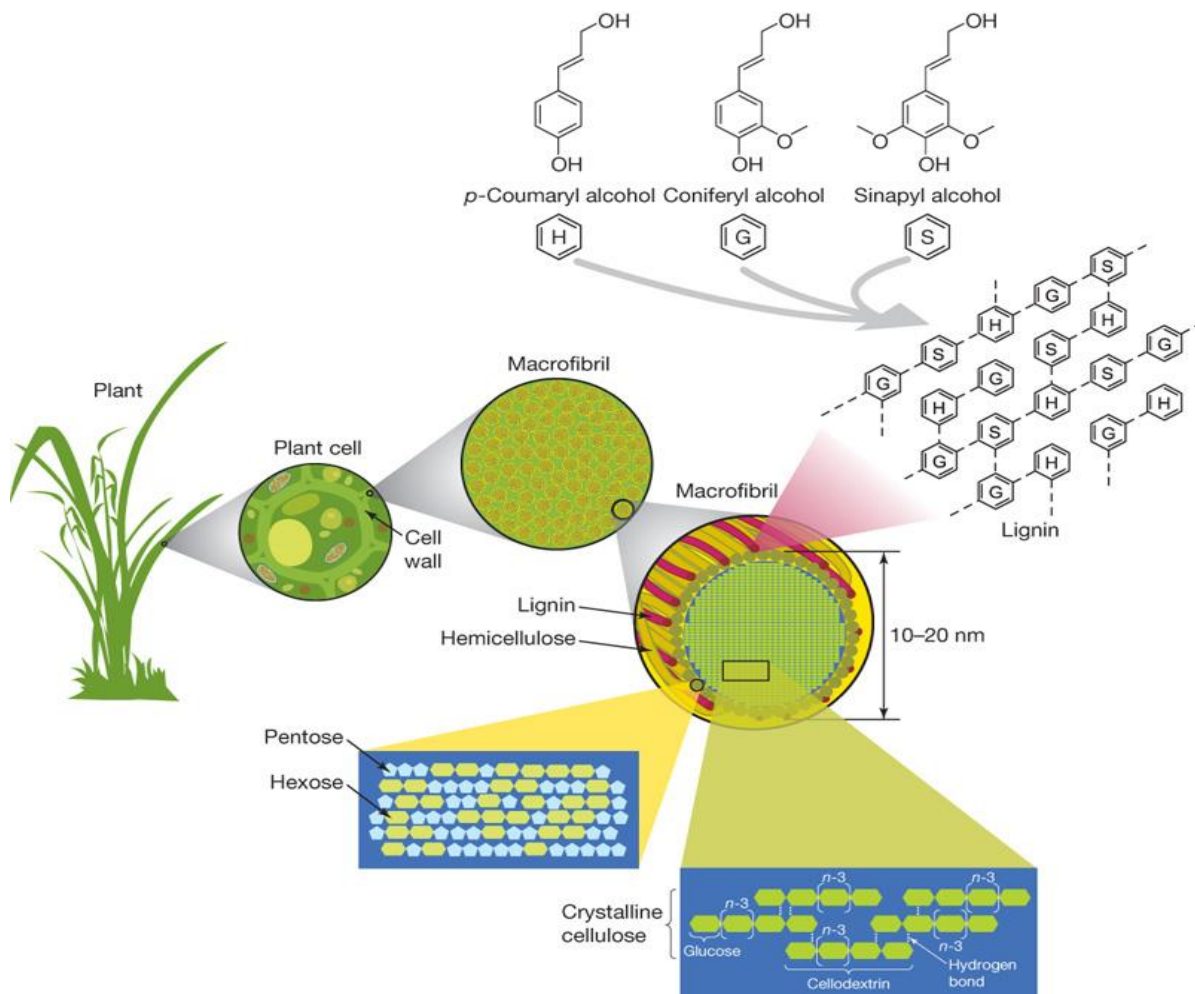


Figure 1: Structure of lignocellulosic biomass (Rubin, 2008)

The cellulose-hemicellulose-lignin matrix has a complex, physically and chemically robust structure and thus isn't able to be efficiently degraded to sugars by enzymes alone. Thermochemical pre-treatment is necessary, followed by enzymatic hydrolysis and sugar fermentation to ethanol and other fuels (Himmel et al., 2007). In nature, rot fungi and bacteria have developed highly sophisticated enzymes for biomass degradation and are the most important factors contributing in the recycling of lignocellulosic-based biomass. Efficient saccharification of cellulose has historically been assigned to the synergetic action of three classes of enzymes (Tan et al., 2015). Exo-1,4- β -glucanases or cellobiohydrolases (CBH) attack the reducing (CBH I) and non-reducing (CBH II) ends of the cellulose polymer. Endo-1,4- β -glucanases cleave internal bonds in the amorphous cellulose chain,

increasing the accessibility of cellulose to exoglucanases by creating new chain ends. The third class is represented by β -glucosidases that convert cellobiose to glucose. (Horn et al., 2012)

Intense research in the recent years discovered a novel, oxidative bi-enzymatic system in wood degrading fungi, which assists cellulases in the degradation of cellulose (Phillips et al., 2011). The enzymes involved are the extracellular fungal flavocytochrome cellobiose dehydrogenase (CDH) and the copper dependent lytic polysaccharide monooxygenase (LPMO). CDH and LPMO act synergistically as LPMO receives reduction equivalents from CDH to be able to catalyse redox-mediated glycosidic bond cleavage in crystalline cellulose and hemicellulose. Thereby, stimulating cellulases activity and thus enhancing the degradation efficiency of crystalline regions in cellulose (Horn et al., 2012). The discovery of the CDH-LPMO system has fundamentally changed the long-accepted paradigm of fungal cellulose utilization. A model for fungal cellulose degradation including LPMO and CDH is depicted in Figure 2.

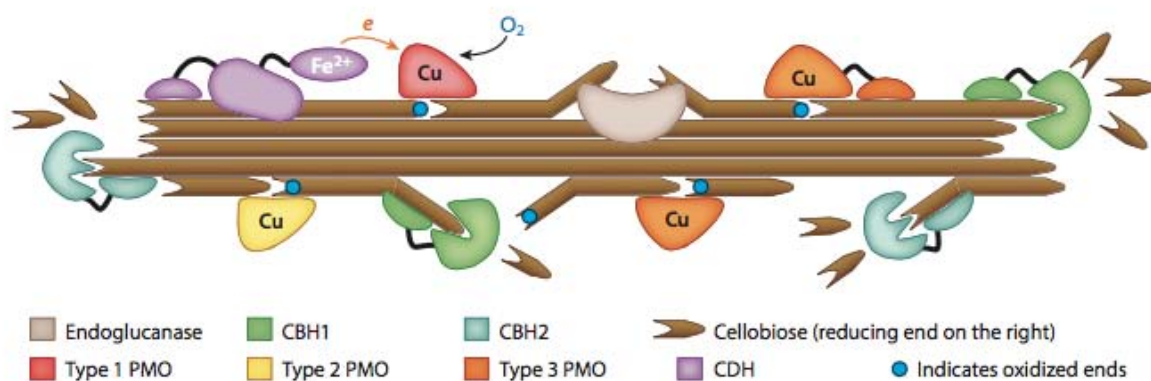


Figure 2 : Scheme of fungal cellulolytic enzyme system. Exoglucanases (CBH1 and CBH2) act on chain ends. Endoglucanases (grey) and LPMO (here PMO – red, yellow and orange) cleave internal bonds in amorphous and crystalline cellulose, respectively, creating new chain ends for exoglucanases. CDH (violet) provides electrons for LPMO-dependent oxygen activation. Picture taken from Beeson et al., (2015).

Cellobiose dehydrogenase (EC 1.1.99.18) was first discovered and isolated in 1974 from the wood degrading fungus *Phanerochaete chrysosporium* by Westermarck and Eriksson (1974). The only known extracellular fungal flavocytochrome is produced by a variety of wood-degrading fungi within the phyla of Basidiomycota and Ascomycota. CDH can be divided into two main classes; while class-I CDHs occur in basidiomycetes and lack an additional carbohydrate-binding module (CBM), class-II CDHs are produced by ascomycetes either with or without a CBM, corresponding to class IIA and IIB, respectively (Zamocky et al., 2006; 2004).

Generally, CDH consist of two distinct domains. A dehydrogenase domain (DH) with a flavin adenine dinucleotide (FAD) as a cofactor and a cytochrome domain (CYT) including a *b*-type heme. The

domains are connected by a long and flexible linker peptide of about 20 amino acids, that keeps the two domains in close proximity and allows intra electron transfer (IET) between them (Cameron and Aust, 2001). Recently, crystal structures of open and closed states of two CDHs from *Neurospora crassa* and *Myrococcum thermophilum* as well as one LPMO, NCU-02916 also from *N. crassa*, were reported, providing a structural platform for detailed investigations of the interaction mechanism between CDH and LPMO (Tan et al., 2015).

The overall reaction of cellobiose dehydrogenase can be divided into a reductive and an oxidative half-reaction. The catalytic site is located in the flavoprotein domain, where the reductive half-reaction proceeds by oxidation of the natural substrate of CDH, β -D-cellobiose, to cellobione-1,5-lactone and the concomitant two-electron reduction of FAD to FADH₂. During the oxidative half-reaction, the FADH₂ is reoxidized to FAD by transferring electrons either directly to a two-electron acceptor or to CYT heme *b*, presumably by a single-electron transfer (Hallberg et al., 2002, 2000). Several in vivo functions have been proposed for CDH (Baminger et al., 2001; Cameron and Aust, 2001; Harreither et al., 2011). The most accepted theory in the last decade was the participation of CDH in the degradation and modification of polymers such as cellulose by generating hydroxyl radicals via a Fenton's type reaction. Recent studies in the last years provided strong evidence that the main purpose of CDH in vivo is to transfer electrons acquired from substrate oxidation to LPMO, formerly classified as family 61 glycoside hydrolases (GH61) (Langston et al., 2011; Phillips et al., 2011; Quinlan et al., 2011).

LPMOs are relatively small enzymes that contain a catalytic surface-exposed copper centre in which the copper is coordinated by three nitrogen ligands including two histidine residues. These enzymes depolymerize cellulose through an oxidative mechanism involving hydroxylation of cellulose at the C₁ (class-I LPMOs) or C₄ (class-II LPMOs) carbon. This leads to subsequent destabilizing and breaking of the glycosidic bond and formation of either aldonic acid (C1) or 4-ketoaldose (C4). The reaction requires both molecular oxygen and an extracellular electron source that can be derived from CDH or small-molecule reductants present in lignocellulosic biomass (Beeson et al., 2015). The evidence for CDH electron transfer via its heme to LPMO, which are used to activate oxygen for C-H bond insertion, and its contribution to efficient cellulose degradation seems striking.

In 2011, Phillips et al. showed that the deletion of CDH-1 (CDH IIA) in *N. crassa* decreased cellulolytic activity by 37 – 49%, which could be recovered by addition of purified CDH. Furthermore, analysis of several hundred fungal genomes approved the crucial role of CDH for LPMO function. In fungi that contain multiple LPMOs and the accepted cellobiohydrolases, CDH was overwhelming conserved, whereas in fungi that contain no LPMOs, CDH is always absent (Beeson et al., 2015; Grigoriev et al.,

2014). In Figure 3 a summary of the overall electron transfer mechanism of the CDH-LPMO-cellulose –interaction is illustrated. It can be separated into four sub steps: First the FAD cofactor of CDH gets reduced during substrate conversion (k_1), followed by a subsequent inter domain electron transfer (IET) from FAD to the heme in CYT (k_2). Finally, the reduced CYT domain donates electrons to the type-2 copper center of LPMO (k_3) to activate molecular oxygen for the cleavage of cellulose (k_4) (Ludwig et al., 2013).

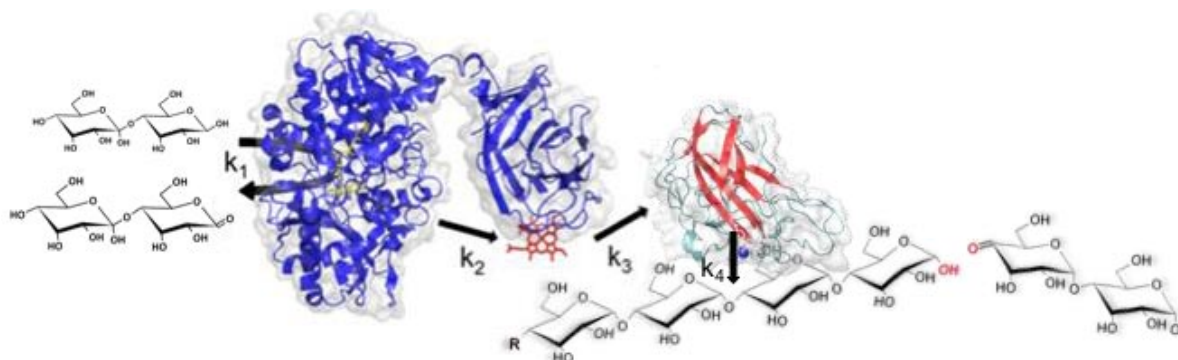


Figure 3: Electron transfer steps of CDH and LPMO (provided by Alfons Felice)

The discovery of the CDH-LPMO system as a major stimulatory factor for lignocellulose degradation might be a significant breakthrough in reducing enzyme loading required for hydrolysis of plant biomass and therefore the high costs of cellulosic biofuels. However, a comprehensive understanding of this elaborate biodegradable machinery has remained elusive, despite intensive research during the last years. In a very recent study (Tan et al., 2015) the structural basis for electron transfer between FAD and heme in CDH was presented. Furthermore, evidence was provided that direct ET occurs only between CYT and LPMO, whereas DH alone is unable to reduce Cu(II) in LPMO.

Nevertheless, very little is known about the electron transfer inbetween CDH and LPMO and the influence of varying IET rates in CDH on the catalytic efficiency of LPMO. In general, more experimental work is needed to fully unravel the mechanism that controls the CDH-LPMO interaction in solution as well as on cellulose.

The cellulolytic filamentous fungus *N. crassa* has been used as model organism for more than 90 years to study genetics, biochemistry and fungal biology. Its genome encodes two different CDHs – one with a C-terminal CBM (*NcCDH IIA*) and one without (*NcCDH IIB*) – and 14 LPMO genes, rendering it as an interesting candidate for investigations on the mechanism of oxidative cellulose degradation. When the fungus is grown on *Miscanthus* the *NcCDH IIA* and *NCU-02916* gene was upregulated 160- and 85-fold, respectively, whereas the expression level of the *NcCDH IIB* gene

increased only three times (Tian et al., 2009). A sequence alignment of *NcCDH IIA* and *NcCDH IIB* showed a very low sequence identity of only 53% (Harreither et al., 2011). Thus it is not surprising that a detailed characterization of both *NcCDHs* by Sygmund et al., (2012) revealed significant differences in terms of size, redoxpotential and physical and catalytical properties. Especially their differences in intra and inter electron transfer rates inbetween CDH itself as well as to its reaction partner LPMO offer a promising basis to gain insight into the electron transfer mechanisms of the CDH-LPMO system. To study the interaction of *NcCDH* with its proposed natural reaction partner, NCU-02916 from the same organism was chosen for this study. It is a class-II LPMO that oxidizes solely the C₄ position of the non-reducing moiety, leading to the formation of 4-keto sugars. NCU-02916 has the ability to use, beside microcrystalline cellulose, also soluble cellodextrins as a substrate (Isaksen et al., 2014), a finding that facilitates kinetic studies of CDH-LPMO substrate interaction in solution.

2.1 Aims of the study

In this study, the kinetic regularities of this two-enzyme system were investigated with major focus on the electron transfer within CDH (k_2) as well as from CDH to LPMO (k_3). The two CDHs from the ascomycete *N. crassa* and one of its LPMOs (NCU-02916 or LPMO9C) served as fundament for this study. Based on these three cellulolytic enzymes, the recently published crystal structure of *NcCDH IIA* and the sophisticated analytical tools available at the Institute of Food Biotechnology, two major goals were defined in respect to study the interaction mechanism between CDH and LPMO:

1. By comparing the three-dimensional structures and the structural differences of the already successfully characterized CDHs *NcCDH IIA* and *NcCDH IIB* (Sygmund et al., 2012) a rational enzyme design approach was chosen to obtain CDHs with different intra electron transfer rates (IET). These variants could then be used to elucidate the influence of varying IETs on the electron transfer rate to LPMO in solution as well as to LPMO in presence of its natural substrate cellulose.
2. A 96-well plate based high-throughput screening should be established by combining four easy-to-use assays (DCIP, cyt *c*, ARAA, Bradford) applicable in the crude supernatant of *P. pastoris* to identify active CDH variants with altered intra- and inter-electron transfer property .

The present work describes the implementation of this easy-to-use high-throughput-screening and the detailed characterization of genetically engineered *NcCDH* variants by steady-state and presteady-state kinetics with stopped-flow techniques. During a two-months stay at the Norwegian

University of Life Science, kinetic studies of CDH-LPMO interaction under *in vivo* conditions with cellulose or cellopentaose were performed. The released reaction products were analysed by MS-techniques and successfully quantified to determine the reaction rates of the enzymes in presence of a solid substrate.

3. Materials & Methods

3.1 Chemicals

All chemicals used during this work were of analytical grade or highest purity available and purchased from Fluka (Vienna, Austria), Sigma-Aldrich (Vienna, Austria), Merck (Darmstadt, Germany) or Roth (Karlsruhe, Germany) if not stated otherwise.

All aqueous solutions were prepared with deionized reserved osmosis water (>16 MΩcm).

3.1.1 Buffers

Activity assay buffer

As standard buffer for activity assays and kinetic measurements, a 50 mM potassium phosphate buffer, pH 6.0 was used.

Potassium phosphate buffer (KPB) 50mM, pH 6.0

KH_2PO_4	5.9 g L ⁻¹
K_2HPO_4	1.1 g L ⁻¹

Mass spectrometry analysis buffers

20 mM sodium acetat buffer (NaAc)⁻, pH 5.5

$\text{CH}_3\text{COONa} \cdot 3\text{H}_2\text{O}$	2.31 g L ⁻¹
$\text{CH}_3\text{CO}_2\text{H}$	174 μl L ⁻¹

5 mM sodium acetat buffer (NaAc)⁻, pH 5.5

$\text{CH}_3\text{COONa} \cdot 3\text{H}_2\text{O}$	0.58 g L ⁻¹
$\text{CH}_3\text{CO}_2\text{H}$	43.5 μl L ⁻¹

The pH was adjusted with either 4 M NaOH or 4 M acetic acid to a pH of 5.5.

Hydrophobic interaction chromatography (HIC) buffer system

Buffer A: 25 mM sodium acetate buffer adjusted to pH 5.5 with 4 M NaOH containing 30% ammonium sulfate

BufferB: 25 mM sodium acetate buffer adjusted to pH 5.5 with 4 M NaOH

Ion exchange chromatography (IEC) buffer system

Buffer A: 25 mM sodium acetate buffer adjusted to pH 5.5 with 4 M NaOH

BufferB: 25 mM sodium acetate buffer adjusted to pH 5.5 with 4 M NaOH containing 1 M NaCl

SDS-PAGE running buffer

Tris (Tris(hydroxymethyl)aminomethane)	3.63 g L ⁻¹
glycine	14.4 g L ⁻¹
SDS (sodium dodecyl sulfate)	1 g L ⁻¹

TAE buffer 50x

Tris	40 mM
Acetic acid	20 mM
EDTA	1 mM

The buffer was diluted 1:5 to obtain a 10x concentrated one.

3.2 Media

All media were prepared according to the Easy select *Pichia* Expression Kit manual as well as to the *Pichia* Fermentation Process Guidelines supplied by Invitrogen (California, USA).

Antibiotics, if needed, were added to the temperate media in the following concentrations:

Zeocin	25 mg L ⁻¹	for <i>E. coli</i>
	100 mg L ⁻¹	for <i>P. pastoris</i>

a) Medium for *E. coli* cultivation

Lysogeny Broth (LB) low salt

Peptone from casein	10 g L ⁻¹
Yeast extract	5 g L ⁻¹
Sodium chloride	5 g L ⁻¹

For agar plates:

Agar-agar	15 g L ⁻¹
-----------	----------------------

→ Autoclaved for 15 min at 121°C

b) Media for *P. pastoris* cultivation

Yeast Peptone Dextrose (YPD)

Peptone from casein	20 g L ⁻¹
Yeast extract	10 g L ⁻¹
D-Glucose	4 g L ⁻¹

For agar plates:

Agar-agar	15 g L ⁻¹
-----------	----------------------

→ Autoclaved for 15 min at 121°C

c) Deep well plate cultivation:

Buffered minimal dextrose (BMD) medium (100 ml)

H₂O 59.8 ml

→ Autoclaved for 15 min at 121°C

Following solutions were sterile filtered and added aseptically:

KPB (1M) 20 ml

10x YNB (13.4% yeast nitrogen base) 10 ml

500x Biotin (0.02%) 0.2 ml

10x Glucose (110 g L⁻¹) 10 ml

Buffered minimal methanol 2 (BMM2) medium (100 ml)

H₂O 59.8 ml

→ Autoclaved for 15 min at 121°C

Following solutions were sterile filtered and added aseptically:

KPB (1M) 20 ml

10x YNB (13.4% yeast nitrogen base) 10 ml

500x Biotin (0.02%) 0.2 ml

10x Methanol (10%) 10 ml

Buffered minimal methanol 10 (BMM10) medium (100 ml)

H₂O 59.8 ml

→ Autoclaved for 15 min at 121°C

Following solutions were sterile filtered and added aseptically:

KPB (1M) 20 ml

10x YNB (13.4% yeast nitrogen base) 10 ml

500x Biotin (0.02%) 0.2 ml

10x Methanol (50%) 10 ml

d) Large scale fermentation

Fermentation basal salts medium (1 L)

Phosphoric acid 85%	26.7 ml
Calcium sulfate	0.93 g L ⁻¹
Potassium sulfate	18.2 g L ⁻¹
Magnesium sulfate·7H ₂ O	4.13 g L ⁻¹
Glycerol	40.0 g L ⁻¹
H ₂ O	to 1 L

→ Autoclaved for 15 min at 121°C

Added sterile filtered and aseptically:

<i>Pichia</i> trace metals (PTM) solution	4.35 ml
---	---------

3.3 Molecular Biology

3.2.1 Biological material

All strains were provided by the culture collection of the Institute of Food Technology from the University of Natural Resources and Life Science, Vienna.

<i>E. coli</i> NEB5-alpha	New England Biolabs
<i>P. pastoris</i> X33	Invitrogen

3.2.2 Primers

For the site directed experiment six primer pairs (see Table 1), a forward and the corresponding reverse primer, were designed by the free DNA analysing tool GeneRunner. While only the forward primer contains the point mutation, both primers have an overlapping region of 15-20 bp and an extended region of 10-15 bp length. The melting temperature doesn't exceed a temperature of about 65°C.

The primers were ordered from Microsynth (Vienna, Austria) and diluted with sterile MQ-water to a concentration of 100 µM. For the application in PCRs and DNA sequencing primer stocks were frozen as 1:10 dilutions.

Table 1: List of primers used during the project

Name	Position	Sequence	Sequ. new	Sequence (5' to 3')
fw_Q198F_IIA	Q198F	LSQHD	LSFHD	ATCACTCTCAGTTTCCATGACAACGGTATGG
rv_Q198F_IIA				ACTGAGAGTGATCTGGGTAG
fw_A96Q_IIA	A96Q	RGAMT	RGQMT	TCTCTCAGAGGC CAA ATGACCAACAATCTACTCATTAC
rv_A96Q_IIA				GCCTCTGAGAGAAACACC
fw_E629Q_IIA	E629Q	SFETP	SFQTP	GAGGGCAGCTTCC CAA ACCCCCGACGGC
rv_E629Q_IIA				GAAGCTGCCCTCGAC
fw_Y716P_IIA	Y716P	VTYQS	VTPQS	CAACCCGTAACCC CCA CAATCCCGCCGC
rv_Y716P_IIA				GGTTACGGGTTGCTTG
fw_D200N_IIA	D200N	QHDNG	QHNGG	CTCAGTCAGCAT AACA ACGGTATGGGCCAG
rv_D200N_IIA				ATGCTGACTGAGAGTGATC
fw_link_IIA	linker			GTTCCA ACTGGTTCTGA ACCACCAGCTGA ACCAACCAGTATTGCCGCC
rv_link_IIA				ACCAGTTGGA ACTGGATCAGA AGCACCACTGCAAGTACCG

3.2.3 Enzymes

All restriction enzymes as well as DNA-polymerases (listed in Table 2) were acquired from Thermo Fisher Scientific (Vienna, Austria), New England Biolabs (Ipswich, USA) or Promega (Fitchburg, USA). If not stated otherwise, all digestion reactions were carried out according to the standard manuals provided by the supplier.

Table 2: List of enzymes used during the project

Restriction Enzymes	Buffer	Application
DpnI	Tango	Degradation of methylated (parental) DNA
MssI (PmeI)	B	Linearization of vector DNA for electroporation
DNA Polymerases		
GoTaq Polymerase		Colony PCR
Phusion high fidelity DNA Polymerase		Site directed mutagenesis

3.2.4 Vectors

The vector pPICZ α (Figure 4) provided by Invitrogen (Vienna, Austria) was used for the expression of CDH in *P. pastoris*. It contains the AOX1 promoter which allows high-level, methanol inducible expression of the gene of interest and the native α -factor secretion signal of *Saccharomyces cerevisiae* for efficient secretion. An additional feature of this vector is a *Sh ble gene* for the selection of successfully transformed *E. coli* as well as *P. pastoris*.

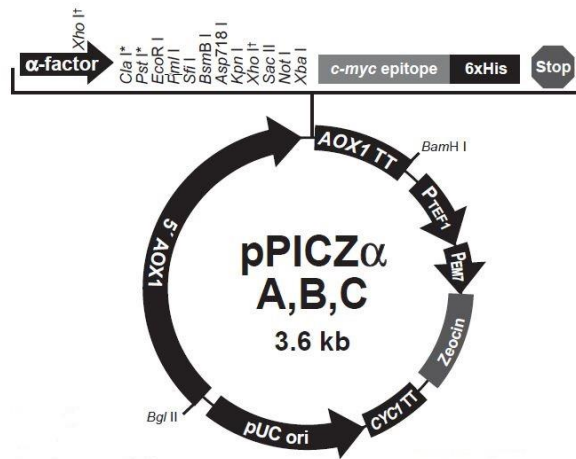


Figure 4: Map of pPICZ α vector. Adapted from (Invitrogen, 2010)

The recombinant plasmid pNCU00206 (*NcCDH IIA*), as recently described in Sigmund et al. (2012), was used for the genetic engineering of the CDH variants.

3.2.5 Kits

Table 3: List of kits used during the project

Kit	Company	Application
PureYield™ Plasmid Miniprep System	Promega (Fitchburg, USA)	Plasmid isolation from <i>E. coli</i>
GFX PCR DNA and Gel Band Purification Kit	GE Healthcare Life Science (Uppsala, Sweden)	Purification of DNA fragments from agarose gel slices

3.4 Site directed mutagenesis of *NcCDH IIA* and preparation for expression in *P. pastoris*

3.4.1 Site-directed mutagenesis

In vitro site-directed mutagenesis is a versatile and easy-to-use technique for studying protein structures and mechanisms of enzymatic reactions. It is based on detailed information on protein sequence, 3-dimensional structure and knowledge of the reaction mechanism, which helps to discover promising amino acids crucial for the target function of the protein (Adrio and Demain, 2014). Then chosen amino acids get replaced with another defined one. In contrast to random

approaches rational design leads to smaller, high quality libraries and reduces the time consuming screening work (Lutz, 2010).

For the mutagenesis a Phusion-PCR method with two overlapping oligosaccharide primers was used to create linearized PCR fragments with the point mutated CDH insert. After purification with an agarose gel a DpnI digestion was performed in order to disintegrate non-mutated methylated templates. PCR products were then transformed to *E. coli* chemically competent cells and selected on LB zeocin plates. The proliferated plasmids were recovered from *E. coli* again. The success of the mutagenesis is controlled by sequencing and further used for *P. pastoris* transformation (scheme see Figure 5).

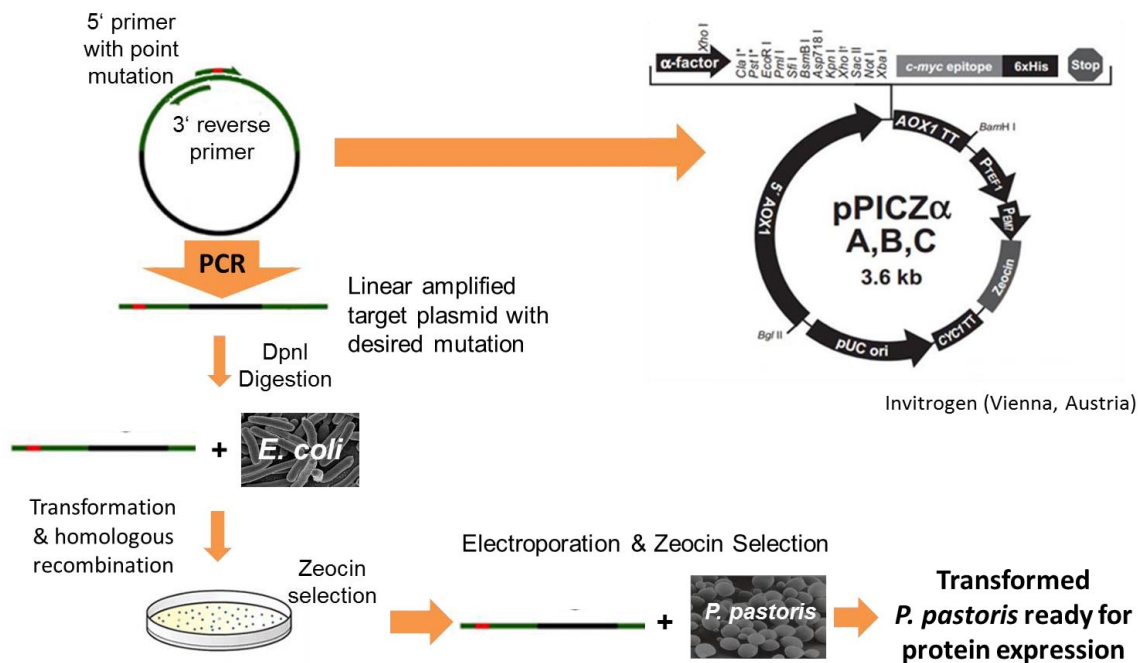


Figure 5: schematic overview of the site-directed mutagenesis

3.4.2 PCR

All PCR methods were conducted in a C1000 Thermal Cycler (BioRad, USA).

Phusion PCR

The point mutations were introduced with the Phusion High-Fidelity PCR system (Thermo Fisher Scientific) using the recombinant vector containing the wild type gene NCU05923 as template.

Table 4: Pipetting scheme for Phusion Master mix

Reagents	
ddH ₂ O	1012.5 µL
5x HF buffer green	750.0 µL
10mM dNTP (Promega)	75.0 µL
Phusion DNA polymerase	37.5 µL

Table 5: Pipetting scheme for Phusion PCR reaction

Reagents	1x
Phusion Mastermix	12,5 µL
Template 1:10	1 µL
ddH ₂ O	7,5 µL
fwd-Primer (1:10)	2 µL
rev-Primer (1:10)	2 µL
Sum	25 µL

The lid of the Thermal Cycler was always preheated to 105°C in order to avoid condensation of water. The annealing step was performed at different temperatures simultaneously to find optimal conditions.

Table 6: Protocol for Phusion PCR reaction

Step	Temperature	Time	Cycles
Initial	98°C	∞	1x
Denaturation	98°C	30 s	
Annealing	55 – 67°C	10 s	32x
Extension/elongation	72°C	3 min	
Final elongation	72°C	3 min	1x
Final hold	8°C	∞	

Colony PCR

The colony PCR was conducted to quickly screen for successful insertion of the CDH gene into the plasmid directly from *P. pastoris* colonies. As the plasmid was integrated into the *P. pastoris* genome at the AOX1 locus the 5'AOX and 3'AOX standard primers were used, yielding in PCR product if insert is present. A fresh colony was picked with a sterile pipette tip, suspended in 30 μ l sterile MQ-water and cooked at 99°C for 10 min followed by a 10 min – cooling step to break up the cells. After centrifugation at maximum speed for 10 min, 10 μ l of the supernatant was used as template for the following PCR reaction.

Table 7: Pipetting scheme for Colony-PCR reaction

Reagents	1x
5x GoTaq-buffer	5 μ L
10 mM dNTPs	0.5 μ L
fwd-Primer 5'AOX (10 pg μ l ⁻¹)	1 μ L
rev-Primer 3'AOX (10 pg μ l ⁻¹)	1 μ L
GoTaq DNA polymerase	0.5 μ L
ddH ₂ O	7 μ L
Template	10 μ L
Sum	25 μ L

Table 8: Protocol for Colony-PCR reaction

Step	Temperature	Time	Cycles
Initial	95 °C	2 min	1x
Denaturation	95 °C	30 s	
Annealing	60 °C	30 s	32x
Extension/elongation	72 °C	2 min	
Final elongation	72 °C	7 min	
Final hold	4 °C	∞	1x

3.4.3 Agarose Gel Electrophoresis

In order to isolate the PCR products Agarose gel electrophoresis was used. For that reason a 0.8% agarose gel was prepared with 1x TAE-buffer and mixed with 20000x peq-GREEN (Peqlab, Erlangen, Germany) as fluorescence DNA dye. Every sample as well as 10 μ l of a GeneRuler DNA-ladder

(Thermo Scientific) were applied to the gel, which then was run in 1x TAE buffer at 90 V for 30 min and further analysed under UV-light with a Gel Doc 2000 (BioRad Laboratories).

The DNA bands were cut out and transferred to a sterile tube for subsequent purification with a GFX PCR DNA and Gel Band Purification Kit (GE Healthcare).

3.4.4 DNA Digestion

The purified PCR products were incubated with the restriction enzyme DpnI at 37°C for at least two hours to disintegrate the methylated non-mutated (parental) DNA.

Table 9: Pipetting scheme for DpnI digestion

Reagents	
Tango-buffer	3 µL
DpnI	1 µL
PCR-Product	30 µL

3.4.5 Transformation of chemically competent *E. coli* strain NEB 5-alpha

According to the standard *High Efficiency Transformation Protocol* supplied by New England BioLabs (Ipswich, USA) the plasmid DNA including the point mutation was transformed into NEB 5-alpha competent *E. coli* cells (New England BioLabs).

After incubation of the transformed cells at 37°C for one hour and 125 rpm, the cell suspension was centrifuged at 12000 rpm for 1 min, 500 µl of the supernatant was discarded and the cell pellet resuspended. The cells were selected on LB-LS agar plates containing zeocin and incubated upside down over night at 37°C.

The positive clones formed after 24 h on the LB-LS zeocin plates were used to inoculate LB-LS zeocin liquid cultures to produce sufficient cell mass for the isolation of sufficient amounts of DNA for the transformation into competent X33 *P. pastoris* cells.

3.4.6 Sequencing

Sequencing of the mutated DNA fragments was done to check if the mutagenesis worked.

Therefore proliferated plasmids were extracted from *E. coli* according to the *PureYield™ Plasmid Miniprep System Protocol* (Promega). A mixture of 13 µl purified plasmid and 2 µL of a primer was then sent for sequencing to Microsynth (Vienna, Austria).

3.4.7 Electroporation of competent *P. pastoris* cells

The plasmid was cut with MSS1 (PmeI) and incubated for one hour at 37°C for more efficient transformation.

Table 10: Pipetting scheme for MSS1 digestion

Reagents	
Plasmid	17 µL
Buffer B	2 µL
MSS1	1 µL

Before the actual transformation 50 µl of electrocompetent X33 cells were thawed on ice for about 10 min and mixed with 4 µl of the linearized DNA in a chilled cuvette (BioRad Laboratories – 1mm). The electroporation was conducted at 1.5 kV for 2 ms. Immediately afterwards 500 µl of 1M sorbitol and 500 µl of YPD medium were added and transferred to a 2 ml Eppendorf tube. The suspension was incubated at 30°C for 3 – 4 h and then plated out on zeocin-containing YPD selection plates, which were incubated at 30°C for 2-3 days.

3.4.8 Preparation of a cryo stock culture

For the conservation of an *E. coli* or a *P. pastoris* culture a single colony was inoculated in either 3 ml LB-LS zeocin or YPD medium respectively and grown at 37°C or 25°C over night. Afterwards 3 ml of sterile 30% glycerol were added and 1 ml of the mixture distributed to three sterile cryo tubes. The tubes were frozen and stored at -80°C.

3.5 96 – Deep well plate cultivation

The cultivation and expression of all CDH variants for the CDH screening were done with 96-deep-well-plates adapted from Sygmund et al., 2012.

For each CDH mutant five transformants were picked from the transformation plate and regrown on YPD zeocin plates, which then were used for inoculation. A schematic illustration of a 96-deep well plate cultivation with five different colonies of each cell type - the *NcCDH* IIA wild-type (positive controle), six CDH mutants and the empty X33 cells (negative controle) - is shown in Figure 6.

	1	2	3	4	5	6	7	8	9	10	11	12
A												
B		AAA ₁	link2 ₁	link1 ₁	D200N ₁	Q198F ₁	A96Q ₁	E629Q ₁	Y716P ₁	X33 ₁		
C		AAA ₂	link2 ₂	link1 ₂	D200N ₂	Q198F ₂	A96Q ₂	E629Q ₂	Y716P ₂	X33 ₂		
D		AAA ₃	link2 ₃	link1 ₃	D200N ₃	Q198F ₃	A96Q ₃	E629Q ₃	Y716P ₃	X33 ₃		
E		AAA ₄	link2 ₄	link1 ₄	D200N ₄	Q198F ₄	A96Q ₄	E629Q ₄	Y716P ₄	X33 ₄		
F		AAA ₅	link2 ₅	link1 ₅	D200N ₅	Q198F ₅	A96Q ₅	E629Q ₅	Y716P ₅	X33 ₅		
G												
H												

Figure 6: Plate design for 96-deep well plate cultivation with *NcCDH* IIA wild-type, six CDH mutants and X33 cells.

The cells were grown in 250 µl BMD medium at 30°C and shaken in an Infors shaking incubator at 350 rpm. By sealing the plates with an oxygen permeable membrane an evaporation of water was successfully prevented. After approximately 65 h the stationary growth phase was reached and induction was started by the addition of 250 µl of BMM2 medium to reach a final concentration of 0.5% methanol. In order to maintain inducing conditions 50 µl BMM10 were added after 8, 24 and 48 h. All pipetting steps were done with an electronic multichannel pipette (Sartorius, Göttingen, Germany).

The cultivation was stopped after 136 h by the centrifugation of the deep-well plates at 3500 rpm and 4°C for 15 min.

3.6 Hightroughput activity screening

High-throughput-screening was used for determination of active CDH variants with altered electron transfer properties. As described above the 96-deep well plate cultivation was ended by centrifugation and the supernatant subjected to the screening assays. To facilitate the handling a pipetting robot (Janus, Perkin Elmer) was employed to transfer aliquots of the culture supernatant automatically from the cultivation plate to replica plates as shown in Figure 7.

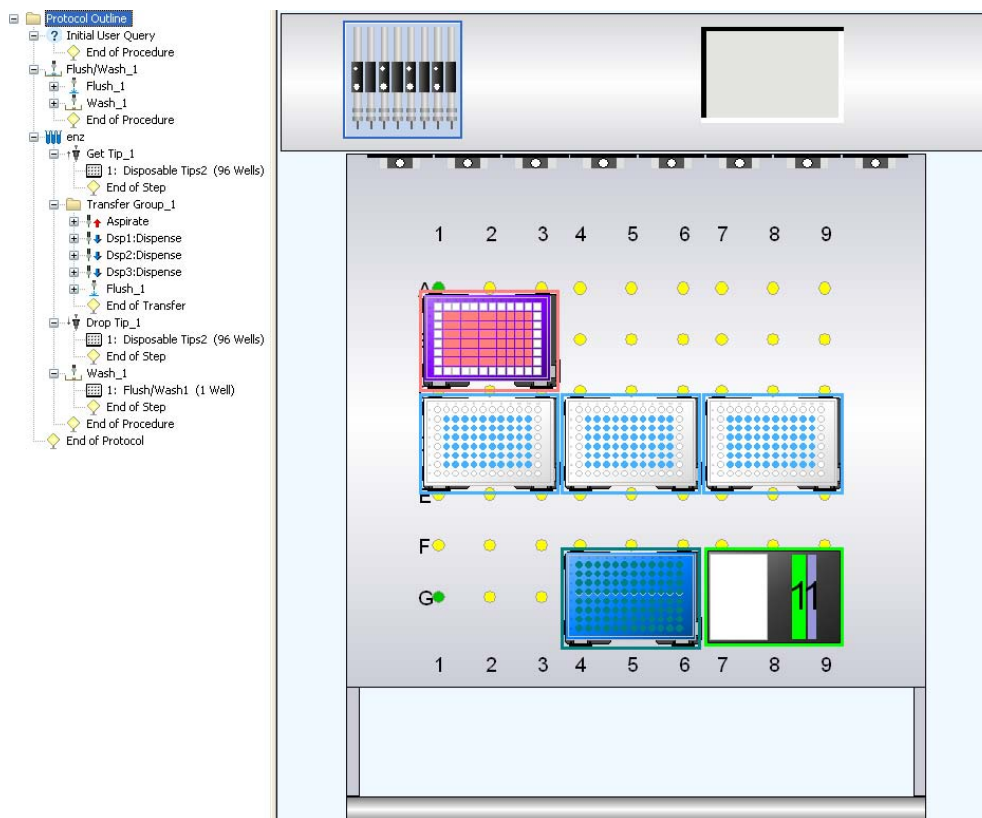


Figure 7: Layout of the pipetting robot for the transfer of supernatant: After a flushing and a washing step of the fixed tips (1), the robot picks up eight disposable tips (blue), takes up the supernatant from the deep well plate (violet) and transfers either 20 μ l or 10 μ l into the three microtiter plates (blue) until all wells are filled with culture supernatant. This procedure was repeated twice.

The screening was performed by combining four easy-to-use enzymatic assays (protocols are given below), which enables identification of changes in the intra-domain electron transfer on the one hand and additionally of improved CDH-LPMO interaction on the other hand. Figure 8 presents a schematic overview of the screening procedure.

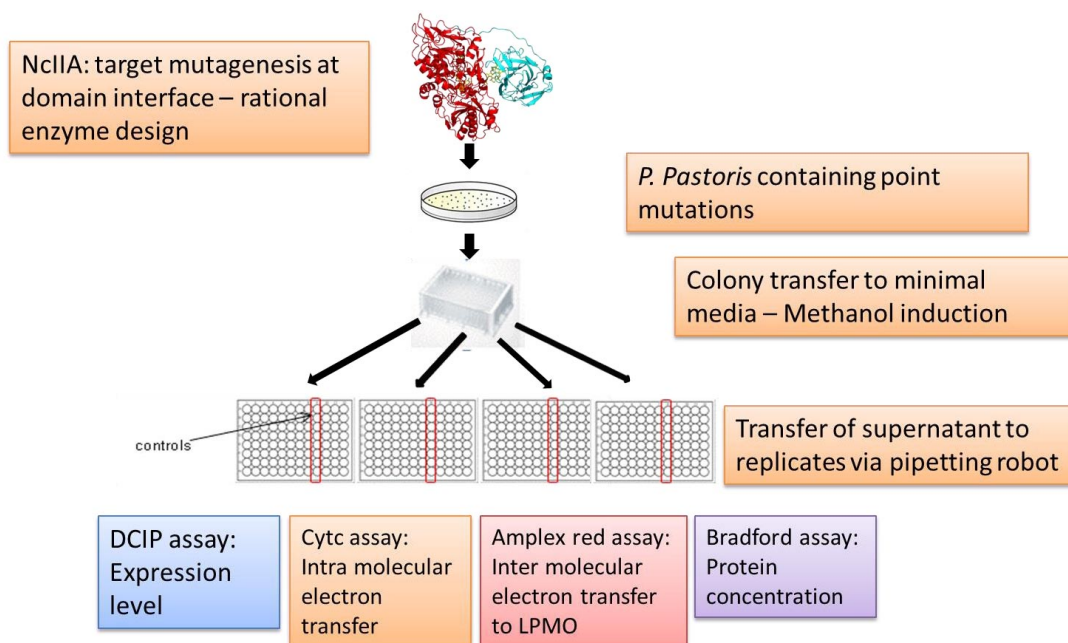


Figure 8: High-throughput-screening used for the detection of active CDH variants with intact electron transfer properties inbetween CDH as well as to LPMO

The enzymatic reactions of the DCIP-, cyt *c*- and Bradford assays were followed in a Tecan microplate reader, while the Amplex red assay was performed in a Perkin Elmer EnSpire Multimode plate reader.

3.6.1 2,6-Dichloroindophenol (DCIP) assay

DCIP is a redox indicator, which oxidized form is blue and changes to colourless during reduction. The reduction is independent from CYT and takes two electrons directly from the FAD. Therefore it is a useful assay to determine the expression level of CDH and to standardize the results obtained from the other assays.

The absorption was measured at room temperature with a kinetic method over 300 s. The result is a linear decrease of the absorbance at 520 nm. The pipetting scheme is presented below (Table 11).

Table 11: Pipetting scheme for DCIP assay.

Reagents	for 100 wells	in one well
3 mM DCIP	2 ml	20 μ l
600 mM Lactose	2 ml	20 μ l
50mM KPB pH 6.0	14 ml	140 μ l
Enzyme (Supernatant)		20 μ l

All reagents except for the enzyme solution were mixed and 180 μl of the stock solution added to the microtiter plate with a multichannel pipette, to start the reaction.

3.6.2 Cytochrome *c* assay

Cyt *c* (obtained from bovine heart) is an efficient acceptor of only one electron and it can solely be reduced at CYT. Thus it serves as an indicator for improved or reduced IET properties of CDH. The reaction was followed for 300 s at room temperature and recorded at 550 nm. During the reduction cyt *c* changes its colour from reddish to pink. Since the cyt *c* assay is more sensitive compared to the DCIP assay, the reactants used in the assay were consumed too fast and pseudo-first order linear dependencies were not given. In order to get a linear increase of the absorption over the entire 300 s the cyt *c* concentration was changed – compared to standard protocol – from 1 mM to 5 mM and the supernatant was diluted 2-fold compared to the supernatant used for DCIP measurements. The pipetting scheme is shown in Table 12.

Table 12: Pipetting scheme for cyt *c* assay

Reagents	for 100 wells	in one well
5mM cyt <i>c</i>	400 μl	4 μl
600 mM lactose	2 ml	20 μl
50mM KPB, pH 6.0	15.6 ml	156 μl
Enzyme (Supernatant)		10 μl

All reagents except for the enzyme were pre-mixed and 190 μl added to the well plate.

The raw output of the Tecan microplate reader is absorption units per minute [A min^{-1}] at room temperature. To standardize the data evaluation of 96-well plate screenings and for fast and easy measurements of catalytic activities a conversion factor to volumetric activity [U ml^{-1}] at 30°C was introduced. Results of samples measured in the well plate format [A min^{-1}] were plotted against results sharing the same assay composition of standard cuvette format with known enzyme factor to recalculate the results [U ml^{-1}]. The output is a linear relation (shown in the linear regression plots in Figure 9) with a slope representing the conversion factor and the coefficient of determination R^2 .

Conversion factor:

DCIP assay 3.2441 (Units*mL*A⁻¹*min⁻¹)

Cyt c assay 4.5757 (Units*mL*A⁻¹*min⁻¹)

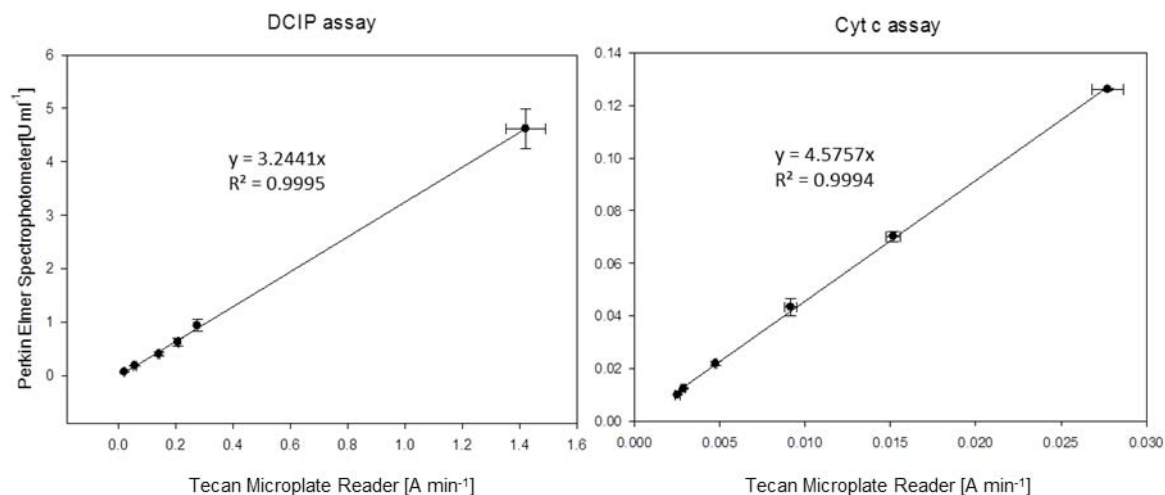


Figure 9: linear regression fit for Photometer – Platerreader relation for DCIP assay (U ml⁻¹ = 3.2441 ± 0.03 A min⁻¹) taken from Christian Schuster's diploma thesis (2014) and for cyt c assay (U ml⁻¹ = 4.5757 ± 0.06 A min⁻¹)

3.6.3 Amplex red assay

As reported previously in Kittl et al., (2012) a fast and robust enzyme assay allows the determination of LPMO activity in fermentation samples. The assay is based on a side reaction of LPMO; the production of hydrogen peroxide (H₂O₂), in the presence of CDH or other reductants. In case of successful electron transfer from CDH to LPMO, H₂O₂ is generated. In combination with horseradish peroxidase (HRP), Amplex red (AR) reacts with H₂O₂ to produce the red-fluorescent oxidation product, resorufin (excitation/emission: 570/585 nm). Thus the Amplex red activity assay is a highly sensitive assay to confirm LPMO activity and thus a good proxy for CDH-LPMO electron transfer.

Table 13: Pipetting scheme for Amplex red assay

Reagents	for 100 wells	in one well
0.5 mM Amplex red	2 ml	20 µl
143 U ml ⁻¹ Peroxidase	1 ml	10 µl
600 mM lactose	2 ml	20 µl
50 mM KPB, pH 6.0	11 ml	110 µL
3.5 µM LPMO (approx.)	2 ml	20 µL
Enzyme (Supernatant)		20 µL

All reagents except for the enzyme solution were premixed and 180 μl of the stock solution subsequently added to the microtiter plate.

In order to overcome the background activity caused by the formation of H_2O_2 by CDH itself and matrix effects, blank reactions without LPMO were conducted, which were then subtracted from the overall activities measured in the presence of LPMO.

Table 14: Pipetting scheme for AR-assay without LPMO

Reagents	for 100 wells	in one well
0.5 mM Amplex red	2 ml	20 μl
143 U ml^{-1} Peroxidase	1 ml	10 μl
600 mM Lactose	2 ml	20 μl
50 mM KPB, pH 6.0	13 ml	130 μL
Enzyme (Supernatant)		20 μL

3.6.4 Bradford assay

The protein concentration in each well was determined by Bradford assay using the Bio-Rad Protein Assay Kit (Bradford, 1976). For the sake of higher accuracy different concentrations of purified *Nc*CDH IIA, instead of bovine serum albumin were used for the preparation of a standard curve (Figure 10). Per well 180 μl of Bradford solution were added to 20 μl of enzyme and measured at the endpoint (after an incubation time of 10 min) the absorption at 595 nm with the Tecan microplate reader. The assay was used to standardize the results obtained from the other three assays, by means of protein concentration.

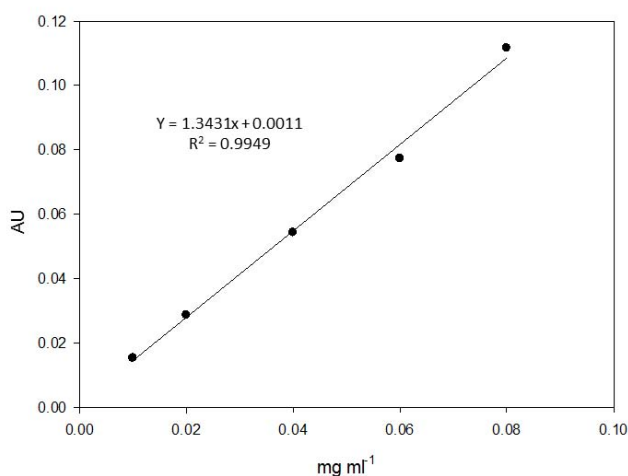


Figure 10: standard curve for Bradford assay made with *Nc*CDH IIA in the range from 0.01 mg/ml to 0.08 mg/ml.

3.7 Fermentation

The best producing clones were selected for methanol induced heterologous expression of CDH in *P. pastoris* adapted from the *Invitrogen Pichia Fermentation Process Guidelines* conducted in six Multifors fermenters (Infors HT, Bottmingen, Switzerland) with total volumes of 500 ml. Each of the bioreactors were filled with 300 ml of basal salts medium, sterilized and the pH adjusted to pH 5.0 with 28% ammonium hydroxide, which was maintained at this level throughout the whole fermentation process. The preculture was grown on 50 ml YPD medium in 250-ml baffled shaking flasks over night at 30°C and added to the bioreactor as well as 4.35 ml l⁻¹ PTM₁ (*Pichia* trace metal) to start the batch phase. The temperature was kept at 30°C the entire time while the stirrer speed varied between 600 and 1000 rpm. After the depletion of glycerol in the batch medium (after about 12 h), the fed-batch phase was started with a constant feed rate of 5 ml h⁻¹ of 50% w/v glycerol containing 12 ml l⁻¹ PTM₁ solution for approximately 8 h. Two hours prior the end of the glycerol fed-batch the methanol feed was initiated by adding 1.5 ml 100% methanol containing 12 ml l⁻¹ PTM₁ trace salts and the glycerol feed was reduced every 30 min for 50% in order to adapt the cells to methanol. Afterwards, the induction phase was started by changing the feed from glycerol to 100% methanol with 12 ml l⁻¹ PTM₁ following a pulse feeding strategy with intermediate pulse additions in response to an increased dissolved oxygen (DO) signal. Every time the DO exceeded 80% the methanol feed with a flow rate of 10 ml h⁻¹ was switched on and maintained for 10 min at the beginning of the induction phase. The methanol feed was increased to 20 min after 36 h. The fermentation was stopped after approximately 60 h on methanol.

Samples were taken regularly and clarified by centrifugation. The pellet was used to determine wet biomass. CDH activity and extracellular protein concentration were assayed in the supernatant. The activity of CDH was determined by monitoring the reduction of 0.3 mM DCIP as well as 20 µM cytochrome *c* in a 1 ml cuvette for 180 s at 30°C in a Perkin Elmer Spectrophotometer. All mixtures contained 30 mM lactose as substrate and 50 mM KPB buffer at pH 6.0. Protein concentrations were determined by the Bradford assay (Bradford, 1976) using bovine serum albumin (BSA) as the calibration standard and recorded at room temperature by a Hitachi U-3000 spectrophotometer.

3.8 Purification

Protein purification was started by centrifugation of the culture broth with 6000 g for 20 min at 4°C. A saturated ammonium sulfate ((NH₄)₂SO₄) solution was slowly added to the clear and chilled supernatant to a saturation of 30%. The precipitate was removed by centrifugation again and the

clear supernatant was used for a two-step purification method including a hydrophobic interaction as well as an anion exchange chromatography.

The chromatographic purifications were conducted by an ÄKTA Explorer chromatography system (GE Amersham Pharmacia, USA) and monitored by means of absorbance at 280 nm for total protein, 420 nm for the CYT domain, 450 nm for the FAD domain and conductivity. The enzymatic activity and the overall protein concentration of the most promising fractions was determined by DCIP-, cyt *c*- and the Bradford assay.

3.8.1 Hydrophobic interaction chromatography (HIC)

Hydrophobic interaction chromatography was done using a 70 ml Phenyl-Sepharose fast flow column (GE Health care Bioscience) equilibrated with HIC buffer A containing 30% ammonium sulfate to reach a conductivity similar to that of the supernatant. After loading the sample onto the column with a 20 ml min⁻¹ sample flow the column was washed with at least 3 column volumes (CV) of buffer A to remove unbound protein. The bound enzymes were eluted within a linear gradient from 0 to 100% buffer B within 3 CV and a flow rate of 10 ml min⁻¹ and collected in 5 ml aliquots. Fractions containing the enzyme were pooled and concentrated and desalted with a Vivaflow cross flow module (10 kDa MWCO) from Sartorius (Vienna, Austria) down to a conductivity of 3 mS cm⁻¹.

3.8.2 Ion exchange chromatography (IEC)

The received concentrate was applied onto a 20 ml Q-source column with a flow rate of 4 ml min⁻¹, after pre-equilibration with 25 mM sodium acetate buffer pH 5.5 (buffer A). Afterwards the column was rinsed with 3 CV of buffer A and a flow rate of 3 ml min⁻¹. The enzymes were eluted within a linear salt gradient from 0 to 1 M NaCl (buffer B) within 10 CVs. Aliquots of 2.5 ml were collected and the purest CDH fractions pooled, rebuffed and concentrated with the Vivaflow cross flow module (10 kDa MWCO) and stored in 50 mM KPB buffer, pH 6.0 at -80°C. These enzyme samples were used for subsequent analytical measurements.

3.9 Enzyme characterisation

3.9.1 Steady-state kinetic studies

Steady-state kinetics can be described by the Michaelis-Menten equation, which states the quantitative relationship between the velocity v_0 , the maximum velocity V_{\max} and the initial substrate concentration $[S]$, all related through the Michaelis-Menten constant K_M (Nelson et al., 2010).

The described kinetic constants were experimentally determined spectrophotometrically with DCIP as electron acceptor and two different substrates (cellobiose, lactose) as electron donors at varying concentrations. The assay was performed in 96-microtiter well plates using a Tecan microplate reader at room temperature as described above. In order to cover all significant sections of the Michaelis-Menten curve following substrate concentrations were added:

DCIP	3 mM
Lactose/cellobiose	0.025, 0.05, 0.1, 0.2, 0.4, 0.8 and 1.6 mM

The output [$A \text{ min}^{-1}$] was converted to [$U \text{ ml}^{-1}$] with the same conversion factor already described in an earlier section (3.6). The catalytic constants K_M and V_{\max} were calculated by fitting the observed data to the Michaelis-Menten equation (single rectangular hyperbola with two parameters) using a nonlinear regression (Sigma Plot 11, Systat Software, USA). Knowing these parameters the turnover number k_{cat} and the catalytic efficiency (k_{cat}/K_M) were calculated by using the molecular mass of CDH.

3.9.2 Presteady – state kinetic studies

By the use of stopped-flow technique it is possible to examine the presteady-state kinetics of fast, liquid-phase biochemical reactions by the rapid mixing of the reactants. In the present study a SX-20 stopped flow spectrophotometer (Applied Photophysics) was used to elucidate the electron transfer rates within CDH (k_2) and in between CDH and LPMO (k_3). In more detail a photodiode array detector (PDA; Applied Photophysics), which allows observation of absorbance at multiple wavelengths in the wavelength range 180 – 750 nm, was employed to monitor the rapid spectral changes at the isosbestic points of the heme cofactor (563 nm). An isosbestic point is defined as a specific wavelength at which curves of absorbance against wavelength all intersect at one point (Sanjeev et al., 2012). This means that the molar absorbance of two or more components remains constant during the whole chemical reaction. In Figure 11 the spectral changes from the oxidized to the reduced forms is outlined with focus on the isosbestic points. As shown in the Figure 11 the FAD has its isosbestic point at 449 nm, while the hemeprotein has two absorbing

bands in the 500 – 600 nm region at 533 nm (heme β -band) and 563 nm (heme α -band) with the α -band being chosen due to its higher absorption difference.

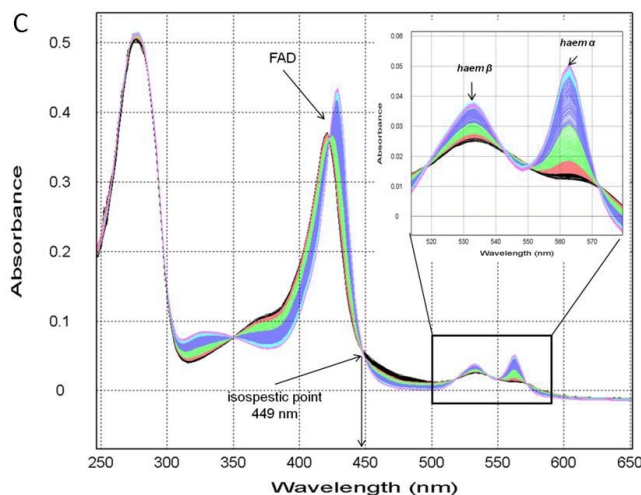


Figure 11: Presteady-state spectral changes of CDH upon mixing with cellobiose. Black arrows show the isosbestic point at 449 nm of the FAD and the α - and β -absorption bands of the heme at 563 nm and 533 nm, respectively (spectrum taken from Scheiblbrandner, 2012).

Single mixing experiment

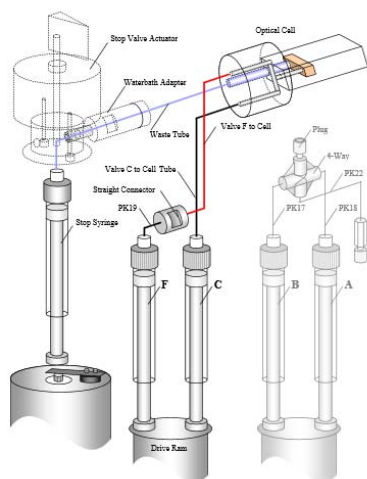


Figure 12: A simplified picture of a single mix flow circuit (Applied Photophysics, 2006)

In order to determine the intra-electron transfer (IET) rates inbetween the DH and the CYT domains the presteady-state reduction of the heme was monitored by the SX-20 spectrophotometer applying a single mixing mode. Therefore 5 μM CDH (final concentration) and an excess of cellobiose (50 μM final concentration) were pushed into an optical cell where the spectral data were collected by a photodiode array detection system, which was triggered after the flow has been stopped by a stop syringe (see Figure 12). Absorption changes at 563 nm were used to monitor heme reduction and the observed rate (k_{obs}) was estimated by fitting the experimental data to a single exponential curve.

Sequential mixing experiment

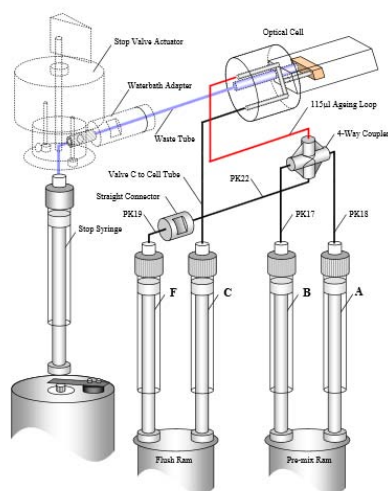


Figure 13: Simplified picture of a sequential mix flow circuit (Applied Photophysics, 2006)

cellobiose and CDH with LPMO) was determined for each CDH individually and ranges from 40 – 100 s.

The experiment was carried out with three increasing LPMO concentrations. The obtained rates (k_{obs} [s⁻¹]) estimated by fitting to a single exponential curve were plotted against each LPMO concentration yielding in the second order rate constant [sec⁻¹ μM⁻¹].

In order to eliminate background activity obtained with PDA, the absorbance at 700 nm was set as baseline wavelength and used to subtract versatile mixing effects.

All presteady-state measurements were carried out at least three times in 50 mM KPB buffer pH 6.0 at 30°C and the data was analyzed by the Applied Photophysics Pro-Data Viewer.

3.10 Kinetic studies of CDH-LPMO interaction on soluble and insoluble substrates

In order to elucidate the electron transfer rate from CDH to LPMO under in vivo conditions, enzymatic conversion on cellulose was performed and the multiple reaction products analysed and quantified by MS techniques. As the Institute of Food Biotechnology doesn't possess such analytical tools, I continued my studies in the group of Prof. Vincent Eijssink (PEP-group) at the University of

Natural Resources and Life Science (NMBU) in Ås, Norway. At NMBU I analysed, amongst others, the interaction of *Nc*CDH IIA and the mutant Q198F which have a fast and a slow IET, respectively, with LPMO-02916 on either a soluble substrate cellopentaose or an insoluble substrate Avicel (microcrystalline cellulose). Due to the lack of C₄-oxidized oligosaccharide standard solutions for HPLC, which are the main products of LPMO-02916, an approach was followed conducting analyses solely on mass spectrometry using an internal standard for the quantification.

The main research question addressed the kinetics of CDH-LPMO-substrate interaction if the substrate is soluble like cellopentaose (Glc₅) on the one hand or solid and crystalline like Avicel on the other hand. The rationale for the experiments was to create different reaction conditions to isolate individual reaction steps to become rate limiting and therefore measurable.

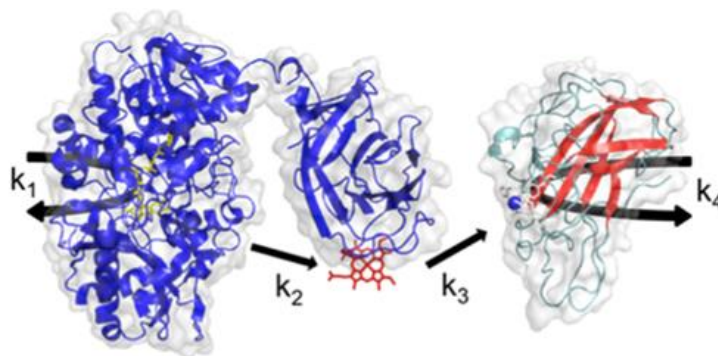


Figure 14: Electron transfer steps from CDH to LPMO and to its substrate (figure provided by Alfons Felice).

In order to avoid CDH side reactions and to start up the cellopentaose/cellulose degradation as fast as possible the CDH oxidation (k_1) was driven by a substrate with high affinity. CDH shows highest catalytic efficiency for lactose compared to possible reaction products of LPMO catalysis (cellotriose, cellotetraose, cellopentaose and their corresponding oxidized forms). Thus supplying a sufficient amount of lactose enables that the first electron transfer step (k_1) as well as the IET (k_2) were always at maximal rates.

The maximum electron transfer from CDH to LPMO (k_3) is governed by the LPMO substrate conversion rate (k_4). At low CDH-LPMO ratios k_3 is the rate limiting reaction step while at high CDH concentrations the LPMO monooxygenation (k_4) reaches a maximum and no further increase of the reaction rate is visible. Therefore reactions with increasing CDH-LPMO ratios at given substrate concentrations were conducted to reveal the rates of k_3 and k_4 on either soluble or insoluble substrate.

Experimental setup with cellopentaose as substrate

For the enzymatic conversion on cellopentaose reaction mixtures (50 μl of sample volume) contained 1 mM cellopentaose, 0.8 μM LPMO-02916, varying CDH concentrations from 0.32 – 8.0 μM as reductant for LPMO, 1 mM lactose, 0.05 mM of the internal standard chitobiose and 5 mM sodium acetate buffer, pH 5.5. The approximately 10-fold excess of lactose in the sample ensures the cleavage of cellopentaose only by LPMO while CDH exclusively binds to and oxidizes lactose. Thus the decrease in concentration of Glc_5 versus time could be used to assess the velocity of the reaction. For the quantification a standard curve was prepared with a set of calibration standards including increased concentrations of cellopentaose (0.01 – 1 mM) and a constant amount of chitobiose (0.05 mM). The standard solutions were detected by electrospray ionization mass spectrometry (ESI-MS) applying the same settings described below. The ratios of the peak intensities of cellopentaose to that of the internal standard were plotted against the corresponding Glc_5 concentrations. The output was a linear relation (shown in the linear regression plot above – Figure 15) including the response factor (slope) and a satisfying coefficient of determination R^2 . As the same amount of internal standard was added to both, samples and standards the concentration of the internal standard wasn't taken into account for the calculations of the calibration curve.

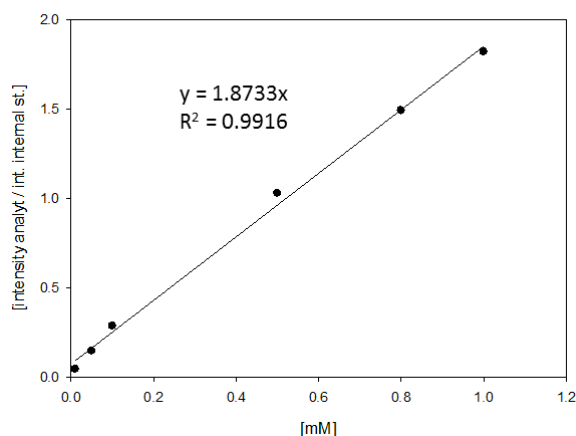


Figure 15: Linear regression fit for the ratio analyt-internal standard versus concentration of the analyt ($y_a/y_i=1.8733 * c_a$).

All reaction mixtures were incubated in a temperate autosampler of a UHPLC at 30°C during the entire reaction time which directly injected samples of 5 μl at given time points (after 0, 45, 90, 135, 180 min) into the mass spectrometer.

Experimental setup with Avicel as substrate

Avicel was incubated with LPMO and analyzed for soluble cello-oligosaccharides. The microcrystalline cellulose amount in 5 mM sodium acetat buffer (pH 5.5) was 25 mg ml⁻¹ and LPMO-02916 was added at a concentration of 0.8 μM. Chitobiose was employed as internal standard at 0.005 mM while CDH was used as reductant for LPMO at varying concentrations from 0.32 to 1.6 μM. CDH isn't able to oxidize microcrystalline cellulose. Therefore an additional electron donor is needed to start up the electron transfer between CDH and LPMO at the beginning of the reaction. Lactose was added to the reaction, but in contrast to the experiment with cellopentaose only in an equimolar amount (1 μM). A total volume of 100 μl was incubated at 30°C for 3, 6, 9 and 24 h in an Eppendorf Thermomixer with shaking at 800 rpm. After incubation the samples were centrifuged to remove remaining cellulose and the supernatant frozen at -70°C to stop the reaction. Immediately after the samples have been thawed again the released cello-oligosaccharides were detected by ESI-MS or fixed on a MALDI target plate for later analysis by MALDI-TOF MS (Matrix assisted laser desorption ionisation time-of-flight mass spectrometry)

For the quantification of ESI-MS data standard curves for each oligosaccharide (triose, tetraose, pentaose) were prepared (Figure 16) as described above balancing varying ionization effects of different sized species.

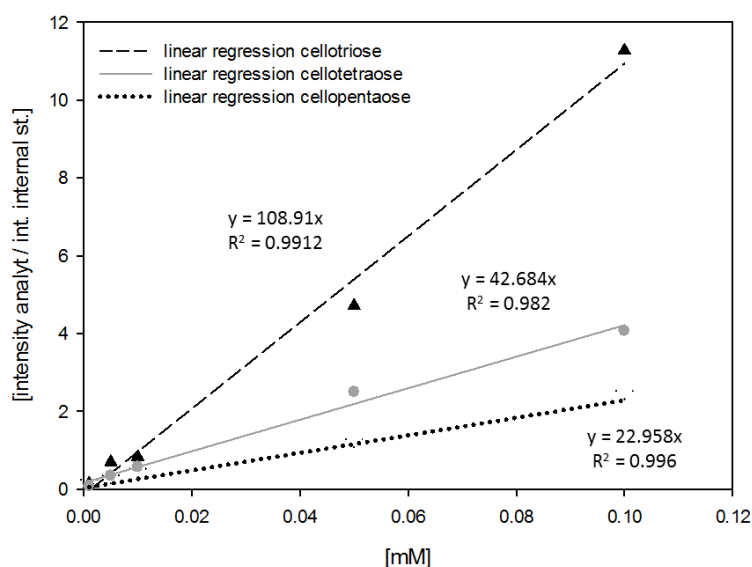


Figure 16: calibration curves for cellotriose, cellotetraose and cellopentaose.

For both experiments negative controls without CDH and LPMO were performed under the same conditions.

Product analysis by Electrospray Ionization Mass Spectrometry (ESI-MS)

The released products were detected by ESI-MS essentially identical to the method reported in Isaksen et al., (2014). The time resolved product analysis was performed with a Velos Pro ion trap mass spectrometer (Thermo Scientific, San Jose, USA) combined with an UltiMate 3000 RS UHPLC from Dionex (Sunnyvale, CA USA). The UHPLC delivered a constant flow of 0.2 ml min⁻¹ of 30/70 (v/v) 1 mM fluoroacetic acid and 100% acetonitrile and performed direct sample injections of 5 µl at given time points. The reaction mixtures were incubated without shaking in the autosampler of the UHPLC at 30°C and 4°C for reactions with either cellopentaose or Avicel, respectively. The electrospray was operated in positive mode at 4 kV spray current which leads to the formation of positively charged sodium adduct molecules. The MS run time was 0.4 min per injection and the scans were performed in the m/z 150 – 2000 mass range.

Product analysis by Matrix assisted laser desorption ionisation time-of-flight mass spectrometry (MALDI-TOF MS)

Additionally to analysis by ESI-MS reaction products released during Avicel degradation were detected by MALDI-TOF MS as described by Vaaje-Kolstad et al., (2010). For the sample preparation 2 µl of a DHB matrix solution (9 mg ml⁻¹ 2,5 -dihydroxybenzoic acid in 30% acetonitrile) were applied to a spot on a MALDI target plate ground steel TF (Bruker Daltonics) and mixed with 1 µl of the reaction mixture. After drying the DHB droplets the samples were analyzed with an Ultraflex MALDI-TOF/TOF instrument (Bruker Daltonics, Bremen, Germany). The mass spectrometer was operated in positive mode with an acceleration voltage of 25 kV, a reflector voltage of 26 kV and pulsed ion extraction of 40 ns. All spectra were acquired from averaging 300 arbitrary shots on each spot in a mass range from m/z 300 – 3000, with the lowest laser energy necessary to obtain sufficient signal to noise ratios (47-55 Hz). The instrument was controlled by FlexControl 3.3 software and the different spectra generated from the MS spectra using FlexAnalysis (Bruker Daltonics).

3.11 UV/visible spectra

UV/VIS spectroscopy was used to determine enzyme concentrations by measuring the absorbance of the overall protein concentration at 280 nm and of the CYT at 420 nm. The protein concentration was calculated according to Lambert-Beer's law ($A=c \times \epsilon \times d$) with a molar absorption coefficient for NcCDH IIA $\epsilon_{280}= 174 \text{ mM}^{-1} \text{ cm}^{-1}$ and $\epsilon_{420}= 103 \text{ mM}^{-1} \text{ cm}^{-1}$ (Sygmond et al., 2012). The spectra were recorded from 250 to 800 nm using a UV-Vis Diode Array Spectrophotometer (Agilent, USA)

3.12 SDS-PAGE

SDS_PAGE was done in order to assess purity of the fermentation samples with Mini-Protean TGX precast gels from Bio-Rad Laboratories (Vienna, Austria) containing a gradient of 4 to 15%. The protein samples were diluted to a concentration of 0.5 mg ml^{-1} and mixed 1:1 with Laemmli Buffer (Sigma-Aldrich) followed by a subsequent sample heating to 99°C for 3 min. Twenty μl of each sample as well as 10 μl of a standard ladder (Bio-Rad) were loaded onto the gel and run at 120 V for approximately 1 h. The protein bands were visualized by staining with Bio-Safe Coomassie blue according to the manufacturer's recommendations (Bio-Rad Laboratories).

4. Results & Discussion

4.1 Mutagenic studies of *Nc*CDH IIA

The genome of *N. crassa* encodes two different CDHs (*Nc*CDH IIA and *Nc*CDH IIB) with a sequence identity of only 53 % (Harreither et al., 2011; Sygmond et al., 2012). Several differences in their physical properties, size, redox potential and catalytic properties are described in Sygmond et al., (2012). Especially their differences in intra and inter electron transfer rates inbetween the CDH itself as well as to its reaction partner LPMO offer a promising basis for the elucidation of structural paradigms of the electron transfer mechanism from DH to CYT. Amino acids surrounding the redox cofactors FAD and heme *b* are found to have a substantial effect on the IET (Igarashi et al., 2005; Tan et al., 2015). Therefore several CDH variants with mutations around the DH - CYT interaction surface were engineered by structure-based site-directed mutagenesis. Accordingly, a homology model of *Nc*CDH IIB was constructed via SWISS-Model (Arnold et al., 2006; Biasini et al., 2014; Guex et al., 2009; Kiefer et al., 2009) based on the crystal structure of *Nc*CDH IIA recently published by Tan et al., (2015). Three-dimensional structures in closed confirmation of *Nc*CDH IIA and *Nc*CDH IIB were used to compare structural differences around the interaction surface of the two domains in both CDHs. A sequence alignment in combination with a structure alignment using PyMol were performed to identify these differences at the DH - CYT interface of *Nc*CDH IIA compared to *Nc*CDH IIB. Three clusters of close interaction were found and single point differences, as well as differences in the linker domain were selected for the mutagenesis study. These areas were assumed to have significant influences on the electron transfer between the redox centres.

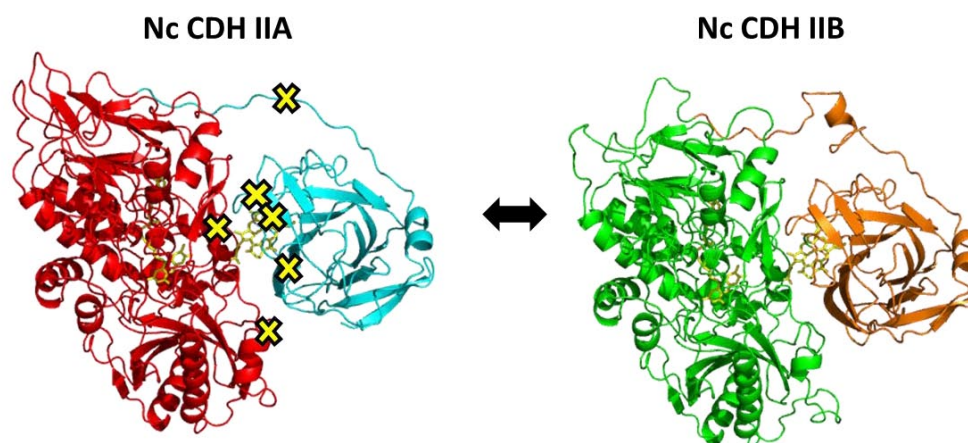


Figure 17: 3-D protein structure of the two CDHs from *N. crassa*. The structures were visualized with PyMol. Mutation sites at the interface as well as in the linker domain are marked with yellow crosses.

In Figure 18 the three clusters are depicted. The hot spots selected for mutagenesis are highlighted. The negatively charged side chains (green) were switched to more neutral (D200N, E629Q), thus altering the surface charge distribution. Hydrophobic side chains were introduced instead of neutral ones (Q198F) – colored in magenta – increasing hydrophobic and electrostatic forces. The structural differences coloured in grey found in the second cluster (A96Q, Y716P) include not only a change in hydrophobicity (hydrophobic to neutral - A96Q), but are also interesting sites addressing the contribution of steric effects (A96Q, Y716P). Another interesting point to assess all influences relevant for the electron transfer reaction is the long and flexible linker peptide. It connects the DH with the CYT domain and shows substantial differences in both CDHs in terms of length and structural composition. The linker peptide in *NcCDH IIB* is approximately 15 amino acids longer than that of *NcCDH IIA*, extended by an additional loop (illustrated in Figure 18). That loop was incorporated into the linker peptide of *NcCDH IIA* to reveal the contribution of the linker peptide in the electron transfer mechanism. These six CDH variants including the described mutation sites were produced and screened for altered intra- and inter-electron transfer properties employing the four assay HT-screening method (see 3.6 & 4.2).

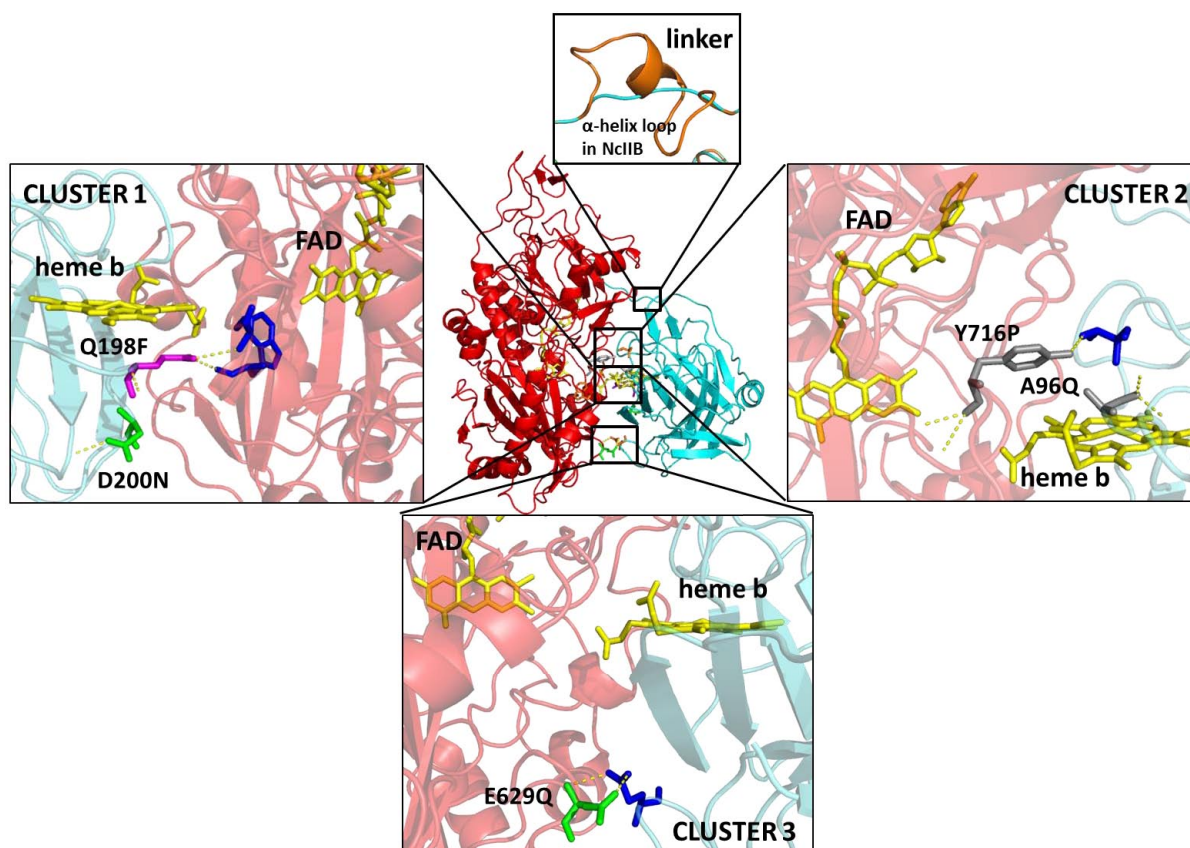


Figure 18: Close-up of the interface between the CYT and DH domains in *NcCDH IIA* showing the side chains targeted for mutagenesis. Amino acids for mutations highlighted in green (charge variants), magenta (hydrophobic changes), grey (steric differences) and orange (additional loop in linker peptide). Dashed yellow lines represent polar contacts to neighbouring residues.

Table 15: List of mutants engineered with site-directed mutagenesis and used for high throughput activity screening.

Single mutations on the DH domain				
Position in <i>NcCDH IIA</i> (Exchanged amino acid)	Position in <i>NcCDH IIB</i>	Mutated amino acid	Variant name	type of mutation
E629	Q650	Glutamine	E629Q	acidic in neutral
Y716	P738	Proline	Y716P	steric changes
Single mutations on the CYT domain				
Position in <i>NcCDH IIA</i> (Exchanged amino acid)	Position in <i>NcCDH IIB</i>	Mutated amino acid	Variant name	type of mutation
A96	Q104	Glutamine	A96Q	steric changes
Q198	F204	Phenylalanin	Q198F	neutral in hydrophob
D200	D206	Asparagine	D200N	acidic in neutral
Mutations on linker domain				
Position in <i>NcCDH IIA</i> (Exchanged amino acid)	Position in <i>NcCDH IIB</i>		Variant name	type of mutation
236-239 GPVT	246-256 α -helix loop		linker	steric changes

4.2 High-throughput activity screening

To develop and validate a screening method, that is sensitive to screen for the properties of interest and easy to use in order to apply it to larger enzyme libraries is one of the most challenging parts in a protein engineering experiment. The approach chosen for this study was to combine several photometric assays, directly applied to the supernatant of cultures grown in a deep well plate format.

The three enzyme activity assays – DCIP-, cyt *c*- and Amplex red assay – are approved tools to determine the activity of CDH and LPMO (Baminger et al., 2001; Canevascini et al., 1991; Kittl et al., 2012; Ludwig et al., 2003). In combination with the Bradford assay, they were used to determine the CDH-LPMO interaction as described in the materials and methodology section. However, before applying the four-assay screening method to CDH variants, several initial experiments were

performed addressing the sensitivity of each assay and the creation of an appropriate measuring protocol.

Detection limits were determined applying standard reaction conditions (described in 3.6) using the respective electron acceptor (DCIP, cyt *c*, AR/LPMO), varying concentrations of purified *Nc*CDH IIA plus lactose as electron donor. For the blank reactions, buffer instead of CDH was added. Even very low enzyme concentrations gave absorbance changes over time that could be clearly distinguished from the reaction blanks. The limit of detection (LOD) according to IUPAC guidelines (Nič et al., 2009) is the smallest concentration of an analyte that can be distinguished from a suitable blank value. It is mathematically defined in Equation 1 as:

Equation 1: limit of detection

$$x_{\text{LOD}} = x_b + 3 \cdot \text{stdev}_b$$

where x_{LOD} is the absorption signal at the detection limit, x_b the mean of the blank measurements and stdev_b the standard deviation of the blanks. The calculated LOD values were 0.0019 A min⁻¹ for the DCIP-assay, 0.00028 A min⁻¹ for the cyt *c*-assay and 31.61 counts min⁻¹ for the Amplex red-assay (Table 16).

An alternative approach to determine the detection limit is to plot the increasing CDH concentrations versus their corresponding absorbance change resulting in a linear correlation within the detection range. As depicted in Figure 19 the absorbance signal response was linear over the entire measuring range down to a CDH concentration of 0.03 μM (0.0052 A min⁻¹), 0.015 μM (0.0017 A min⁻¹) and 0.06 μM (134.33 counts min⁻¹) for DCIP, cyt *c* and Amplex red, respectively. The experimentally determined detection limits are higher than the calculated LOD values. However, the sensitivity of all three assays is high enough to enable measurements of CDH variants with even very low enzyme activities.

The robustness of the assays towards matrix effects of fermentation samples was tested in previous studies (Brugger et al., 2014; Kittl et al., 2012) rendering the background activity of media components and other oxidases as negligible. Thus not only the high sensitivity of the three assays but also the applicability to crude enzyme samples make the assays suitable for a high throughput screening of CDH variants cultivated in 96- deep well plates.

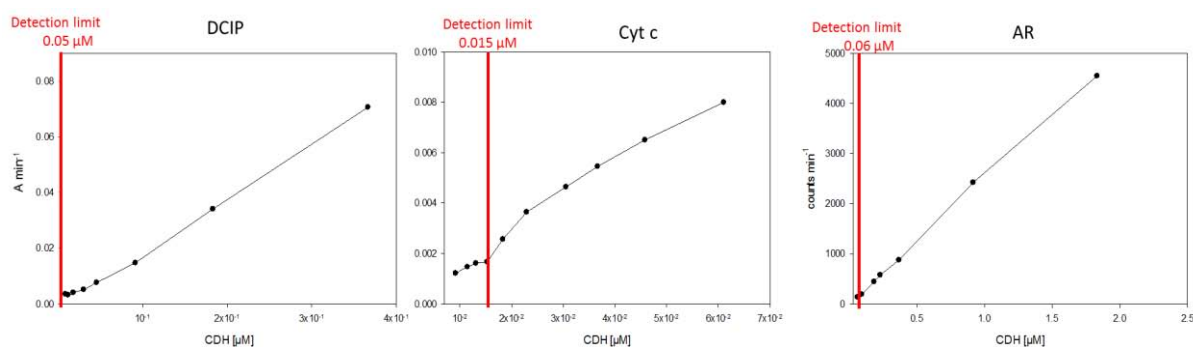


Figure 19: Determined detection limits for DCIP-, cyt *c*- and the Amplex red assay. A linear range for varying CDH concentrations was found from 0.05 – 0.5 μM (DCIP), 0.015 – 0.06 μM (cyt *c*) and 0.06 – 2 μM (AR).

Table 16: Detection limits determined after IUPAC guidelines (left column) and by plotting absorbance change vs. the corresponding CDH concentration (right column).

Assays	LOD (blank + 3*stdev _{blank})	LOD ($\Delta\text{abs vs [NcCDH IIA]}$)	
	A min ⁻¹ /counts min ⁻¹	A min ⁻¹ /counts min ⁻¹	NcCDH IIA [μM]
DCIP	0.0019	0.0052	0.03
Cyt <i>c</i>	0.0003	0.0017	0.02
Amplex red	31.61	134.33	0.06

A detailed measurement protocol can be found in the Appendix. It is the result of several iterations and reflects the optimal conditions used for all further experiments.

The developed high-throughput-screening including these four assays is easy to handle. With a smart combination of the assays, the help of the pipetting robot and the possibility to use a second microtiter plate reader a whole 96-deep well plate can be screened for improved and active variants in less than 45 min after 5 days of cultivation. As it is summarized in Figure 20 raw data were processed by removing outliers from the dataset applying the modified Thompson tau technique (Cimbala, 2011). Secondly, the obtained values were converted and standardized with the described conversion factors (3.6) and the determined protein concentration in each well, respectively. For the Amplex red assay activities of blank reactions without LPMO were subtracted from the overall activities measured in the presence of LPMO. Averages of five activity measurements of each mutant and their corresponding standard deviations as well as the ratio AR to cyt *c* were calculated and compared to the wild-type enzyme.

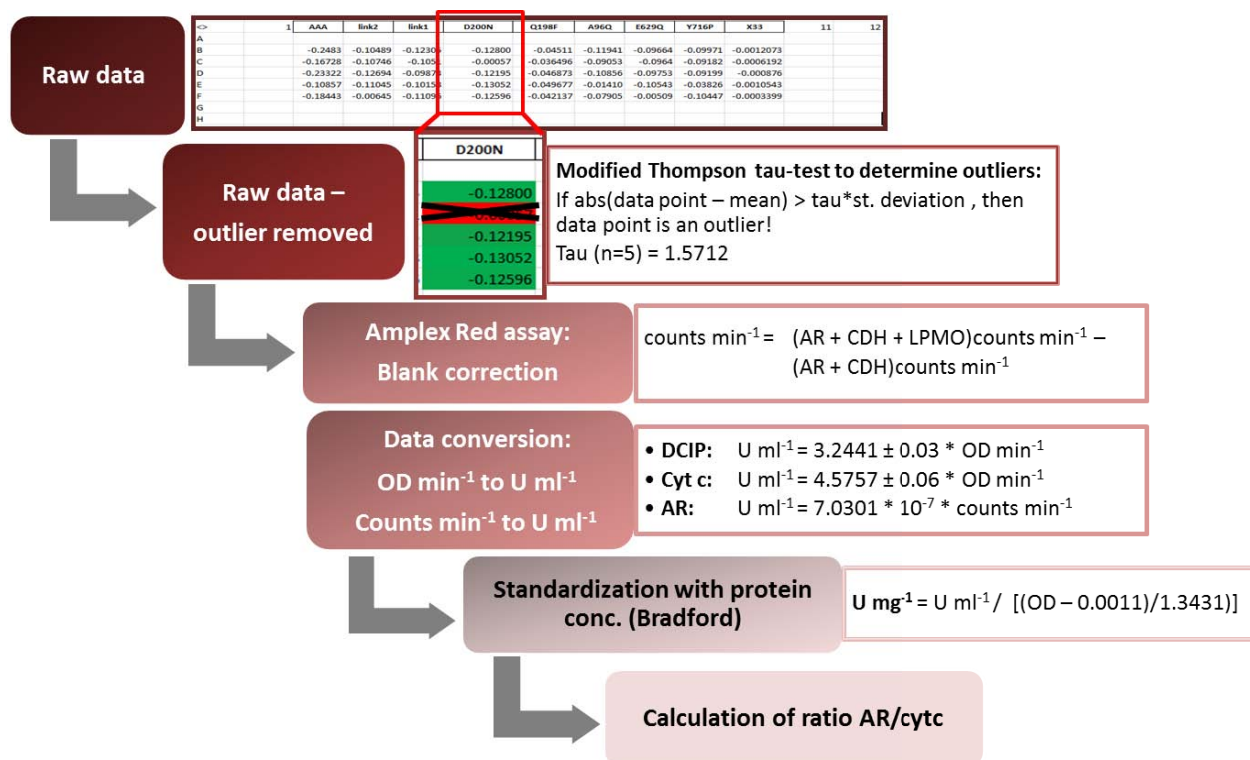


Figure 20: Data processing steps for the HTS from raw data to the enzyme factors and specific activities for all CDH variants.

Based on the initial tests for sensitivity, the correct handling procedure and the data processing, the HTS was applied to the CDH variants. As described in the methodology part, the CDH mutants were engineered by site-directed mutagenesis and confirmed by sequencing. For the deep-well plate cultivation five clones of each variant as well as of the *NcCDH IIA* wildtype were picked from a fresh YPD zeocin selection-plate and used for the methanol-induced expression in BMD medium. After 136 h the cultivation was stopped by a centrifugation step and the CDH remaining in the supernatant were analyzed for enzymatic activity. Five “empty” X33 cells, which did not express any CDH, served as negative controls.

Figure 21 displays the relative activities of all CDH-mutants compared to *NcCDH IIA*. As expected, all variants show less specific activity compared to the wild type with DCIP, cyt c and AR which implies a considerable influence of the mutation sites on the electron transfer rates. A percentage comparison of all measured activities in Table 17 illustrates the differences in more detail. It also contains the ratio of the catalytic activities between AR and cyt c. This ratio serves as good proxy for the electron transfer from CYT to LPMO. The linker mutant and in particular Q198F have considerable high AR/cyt c ratios compared to specific activities obtained by the AR-assay (illustrated in the right plot in Figure 21). This indicates an efficient electron transfer to LPMO, despite substantially low IET rates. This conclusion could be justified by stopped-flow experiments described below.

In contrast, the variant D200N with a relatively high *cyt c* activity, thus fast IET (similar to the wild-type), shows also higher specific activities with AR compared to Q198F. However the AR/*cyt c* ratio is much lower. Using AR/*cyt c* ratio instead of the individual values is therefore be a better indicator for the evaluation of altered CYT-LPMO reaction rates.

Reliable results with acceptable standard deviations within five repetitions (<15% for DCIP and *cyt c*; <30% for AR), were found for all the measurements of the catalytic activities in 96-well plates. No activity was observable for the five X33 blank cells. Additionally, the reliability of the HTS is emphasised by the two independently engineered linker variants (linker 1 and linker 2) which yielded similar results in all three assays.

All screened CDH mutants appear active and show intact IET as well as inter electron transfer properties to LPMO, except for the mutant Q198F with significantly low IET rates. Best producing CDH clones of all variants judged by DCIP- and *cyt c* activity were selected for production at large scale to produce enough enzyme for further characterization. Results of HTS were compared to the purified variants and analysed in more detail.

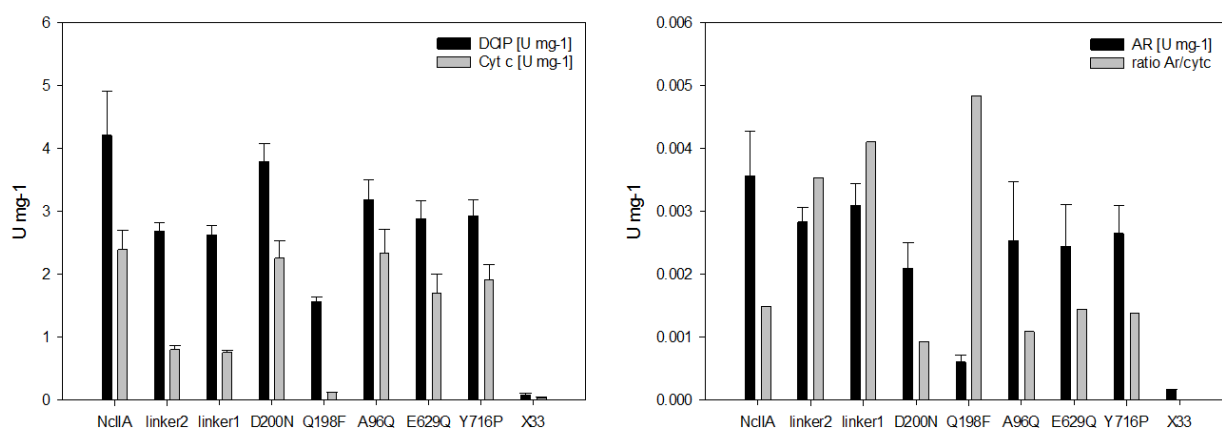


Figure 21: Shown on the left side the expressed activities of DH (DCIP) and of the holoenzyme (*cyt c*). The right plot displays LPMO activity (AR) which is an indicator for successful electron transfer from CDH to LPMO as well as the AR-activity in relation to *cyt c* activity. The specific activities are the mean of catalytic activities of five different clones including the same mutation.

Table 17: Screening results of each CDH variant in more detail.

Variant	Specific activity (U/mg)				Specific activity (U/mg)			AR/cyt c	
	DCIP		cyt c		Amplex red				
NcCDH IIA	4.21 ± 0.70	100%	2.39 ± 0.31	100%	0.0036 ± 0.0007	100%	0.0015	100%	
linker2	2.69 ± 0.13	64%	0.80 ± 0.06	34%	0.0028 ± 0.0002	79%	0.0035	237%	
linker1	2.63 ± 0.14	62%	0.75 ± 0.03	32%	0.0031 ± 0.0004	87%	0.0041	275%	
D200N	3.79 ± 0.29	90%	2.26 ± 0.28	94%	0.0021 ± 0.0004	59%	0.0009	62%	
Q198F	1.56 ± 0.08	37%	0.13 ± 0.00	5%	0.0006 ± 0.0001	17%	0.0048	324%	
A96Q	3.18 ± 0.31	76%	2.33 ± 0.38	98%	0.0025 ± 0.0009	71%	0.0011	73%	
E629Q	2.89 ± 0.28	69%	1.70 ± 0.30	71%	0.0024 ± 0.0007	69%	0.0014	97%	
Y716P	2.93 ± 0.25	70%	1.91 ± 0.23	80%	0.0026 ± 0.0005	74%	0.0014	93%	
X33 (neg.contr.)	0.07 ± 0.03	2%	-0.03 ± 0.02	-1%	0.0001 ± 0.0000	3%	/		

4.3 Production of CDH variants

Overproducing CDH transformants which have been selected during the screening were produced in 500 ml stirred and aerated six Multifors fermenters. The fermentations were performed simultaneously and as uniformly as possible. The time course of the wet biomass weight of the *P. pastoris* CDH expressing variants as well as the total protein concentration in the supernatant and the volumetric activity of CDH determined with the DCIP and cyt c assay, is depicted in Figure 22. By the end of the fed-batch phase (after about 30 h) all cultures showed similar cell densities (230 -260 mg ml⁻¹) except the culture of A96Q with a cell density of only 170 mg ml⁻¹. This was due to a lower feed caused by the defect feeding pump at the beginning of the fed-batch phase. However, the overall cellular yield was slightly higher than the expected 180 to 220 mg ml⁻¹ according to the Invitrogen Pichia Fermentation Process Guidelines (Invitrogen, 2002). At this time neither CDH activity nor extracellular protein was detectable. After inducing protein expression by a pulsed feed strategy with 100% methanol the specific growth rate μ was reduced to 10 – 15%. By the end of the fermentation process (after 93 h) the final cell densities varied between 200 and 310 mg ml⁻¹. The fermentation process of A96Q still had the lowest cell density while the linker fermentation showed the highest. The secretion of extracellular protein correlated with biomass production. It reached a total protein yield of about 0.4 – 0.5 mg ml⁻¹ for all CDH variants, which is even higher than the protein concentration (0.28 mg ml⁻¹) obtained for heterologous expression of NcCDH IIA in a previous report by Sigmund et al. (2012) . The maximum values for the volumetric activity determined with DCIP and cyt c were reached with the D200N variant with 4400 U L⁻¹ and 1200 U L⁻¹, respectively.

Significantly lower volumetric activities were obtained for Q198F with 1100 U L⁻¹ (DCIP) and 70 U L⁻¹ (cyt *c*), despite a high cell density of 290 mg ml⁻¹ and a total protein concentration of 0.4 mg ml⁻¹.

During the 5-day fermenter cultivations, mean volumetric activities of over 2700 U L⁻¹ and 640 U L⁻¹ with DCIP and cyt *c*, respectively, were achieved. These yields are higher compared with previous studies on the recombinant expression of CDH from *N. crassa* in *P. pastoris* (Sygmund et al., 2012) with a volumetric activity for NcCDH IIA of about 1700 U L⁻¹ and 360 U L⁻¹ obtained with DCIP and cyt *c*, respectively. Remarkably, some CDH variants were expressed with significantly different volumetric activities. As the extracellular protein concentration in each culture broth was similar (appr. 0.45 mg ml⁻¹) this was suggested to a higher specific activity of some variants. Nevertheless, all variants were successfully produced and yielded reasonable amounts of functional enzyme, which was purified by a two-step chromatographic purification procedure.

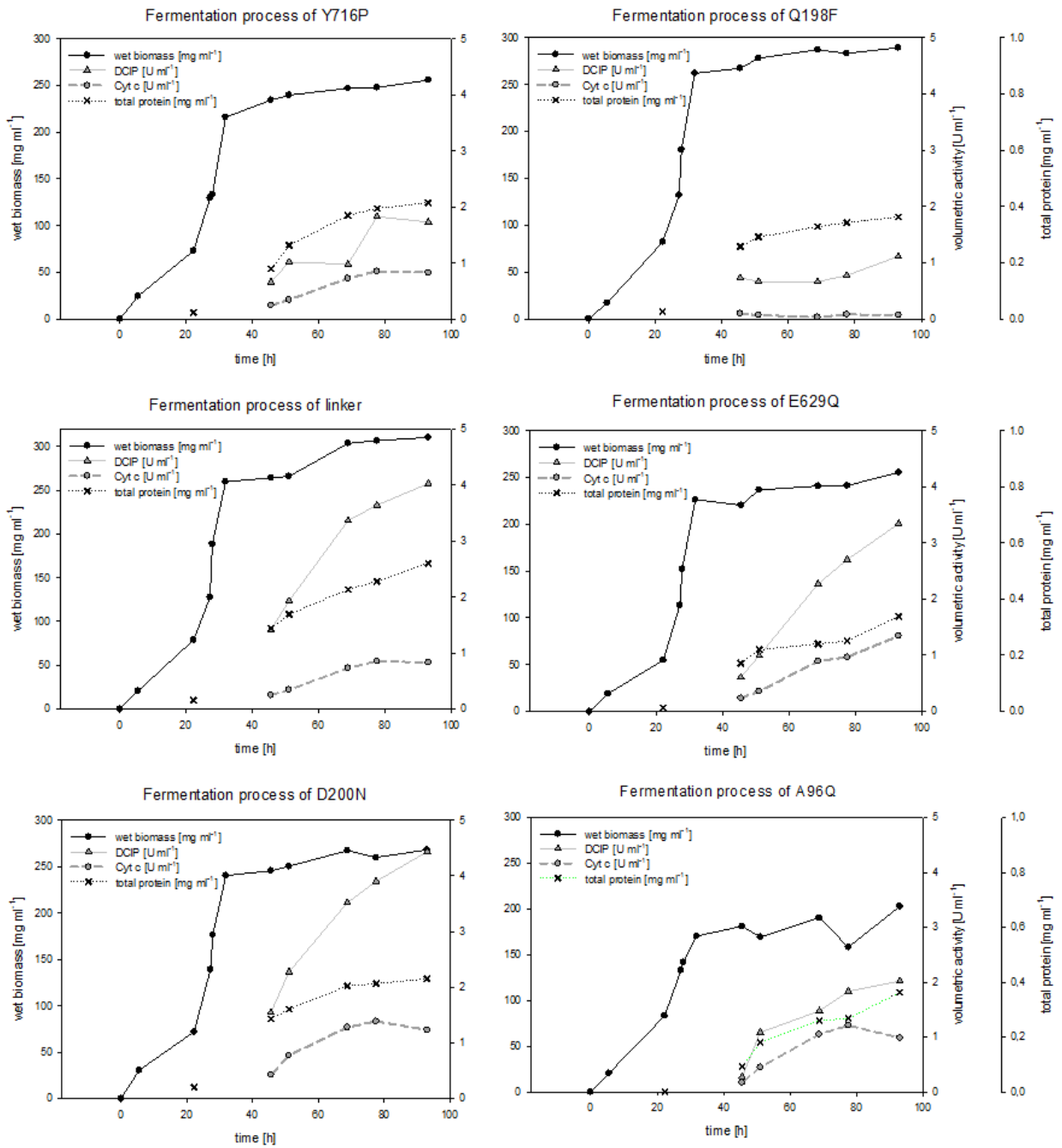


Figure 22: Production of *NcCDH IIA* variants in a *P. pastoris* X33. Time course of wet biomass, total protein concentration in the supernatant and enzymatic activity are shown.

4.4 Protein purification

N. crassa CDHs were purified to homogeneity in a standardized two-step purification procedure (Sygmond et al., 2012). All purifications were assayed in cuvettes using DCIP, cyt *c* and Bradford assays. Table 18 gives an overview of the whole process and the grade of purity reached by each step. The specific activity in the supernatant determined with cyt *c*, which only detects the intact

holoenzyme, reached values of up to 10 U mg⁻¹. The total protein amounts varied between 9 and 28 mg. Strict pooling of only the purest fractions resulted in low overall yields of about 18 - 45%, especially compared to enzyme activity yields obtained in other studies using a similar purification procedure with yields of up to 75% (Sygmond et al., 2013, 2012). However, sufficient amounts of all CDH variants were obtained for a detailed characterization. The purity of all variants was assessed with SDS-PAGE (Figure 23) and no considerable impurities were observed. The CDH variants as well as *NcCDH IIA* show sharp bands at around 110 kDa which are higher molecular masses as calculated from the amino acid sequence quite likely due to glycosylation (Sygmond et al., 2012). After the ion exchange chromatography, pooled fractions were concentrated, re-buffered and stored in 50 mM KPB, pH 6.0 at 4°C for further analysis.

Table 18: Purification scheme for *NcCDH IIA* variants. The purification factor was calculated from the specific activity obtained from the cyt *c* assay.

	Purification step	Volume [ml]	Total protein [mg]	Spec. act. [U mg ⁻¹]		Purification [fold]	Yield [%]
				DCIP	Cyt <i>c</i>		
A96Q	Crude extract	268.60	97.56	5.56	2.71	1	100
	HIC	67.00	20.47	8.97	7.77	3	60
	IEC	1.5	9.00	10.90	9.72	4	33
D200N	Crude extract	330.8	142.18	10.32	2.87	1	100
	HIC	190	37.83	11.50	6.47	2	60
	IEC	2	25.00	8.42	6.51	2	40
Q198F	Crude extract	341.3	123.58	3.07	0.18	1	100
	HIC	120	22.24	1.97	0.36	2	36
	IEC	0.7	10.33	2.56	0.40	2	18
Y716P	Crude extract	308.8	128.24	4.17	2.00	1	100
	HIC	158	38.95	4.61	4.16	2	63
	IEC	2.5	16.23	5.57	5.78	3	37
linker	Crude extract	328.90	171.16	7.74	1.83	1	100
	HIC	126.00	60.80	5.35	4.12	2	80
	IEC	4.60	27.94	12.55	5.02	3	45
E629Q	Crude extract	346.20	117.08	9.89	3.97	1	100
	HIC	150.00	37.29	12.16	7.26	2	58
	IEC	2.7	18.55	12.15	9.69	2	39

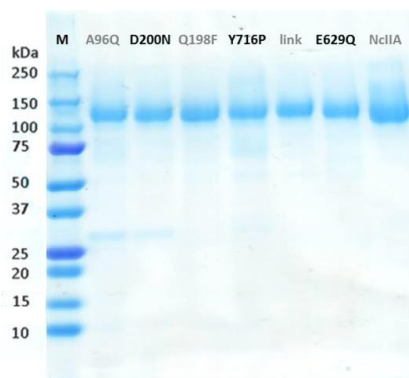


Figure 23: SDS-PAGE of *NcCDH IIA* variants and *NcCDH IIA* wild-type. All CHDs showed sharp bands at 110 kDa after the two-step purification.

4.5 Characterization

4.5.1 Steady-state kinetic constants

Catalytic constants of substrate turnover were recorded over a substrate range from 0.025 to 1.6 mM cellobiose and lactose for all variants using 3 mM DCIP as electron acceptor. The reaction mixtures were buffered with 50 mM KPB, pH 6.0. The enzyme concentrations used to calculate the results were determined by measuring the absorbance of the CYT domain at 420 nm. Due to the high amount of analysed samples the experiments were performed in 96-well microtiter plates and measured in a photometric plate reader. Although the determination of catalytic constants in microtiter plates saved time and resources, it also leads to difficulties in comparison of data obtained from activity measurements conducted in cuvettes. This may be a reason for the differences found when comparing the steady-state kinetic constants obtained for *NcCDH IIA* with recently reported data by Harreither et al., (2011). Whereas Harreither et al. measured K_M and k_{cat} values for cellobiose of up to 160 μM and 53.1 s^{-1} , respectively, in this study much lower K_M and k_{cat} values of only 57.5 μM and 11.7 s^{-1} were detected. However, the obtained catalytic efficiencies for cellobiose as well as lactose with $2.04 \cdot 10^5 \text{ M}^{-1} \text{ s}^{-1}$ and $1.00 \cdot 10^5 \text{ M}^{-1} \text{ s}^{-1}$, respectively, were comparable to data determined by Harreither and co-workers ($3.32 \cdot 10^5 \text{ M}^{-1} \text{ s}^{-1}$ for cellobiose and $1.6 \cdot 10^5 \text{ M}^{-1} \text{ s}^{-1}$ for lactose).

All kinetic data are listed in Table 19. The investigated CDH variants show very low Michaelis-Menten constants, all of them in the micromolar range and slight variations from 0.02 mM for the linker mutant up to 0.06 mM for *NcCDH IIA* and D200N. As expected all CDHs oxidize the natural substrate cellobiose more efficiently compared to lactose (Sygmund et al., 2012). The catalytic efficiencies (k_{cat}/K_M) vary from $7.77 \cdot 10^4$ to $2.83 \cdot 10^5 \text{ M}^{-1} \text{ s}^{-1}$ with the lowest efficiency found for the mutant Y716P and the highest for the linker variant. This implies that the additional loop in the linker domain and

therefore the increased flexibility of the DH domain results in accelerated substrate diffusion to the active site. On the contrary it seems that the variant Y716P, located on the DH domain near the FAD cofactor, has a negative effect on the substrate turnover.

Nevertheless, the catalytic constants of the other CDHs are similar. The steady-state kinetic constants using DCIP as electron acceptor are an indicator for substrate turnover by the DH. As the mutations mainly target the interface at the heme and FAD redox centers, no significant alterations in the substrate turnover rates were expected. Thus the results of each variant are in good agreement with its corresponding mutation. To fully elucidate the influence of the mutations on the reaction mechanism more elaborate presteady-state experiments were performed, as summarized in the next section.

Table 19: Steady-state catalytic constants of *NcCDH IIA* and six variants for cellobiose and lactose at pH 6.0 using DCIP as electron donor.

CDH	Cellobiose			Lactose		
	K_M [mM]	k_{cat} [s ⁻¹]	k_{cat}/K_M [M ⁻¹ s ⁻¹]	K_M [mM]	k_{cat} [s ⁻¹]	k_{cat}/K_M [M ⁻¹ s ⁻¹]
<i>NcCDH IIA</i>	0.06 ± 0.011	11,71 ± 0.016	2.04 × 10 ⁵	0.13 ± 0.010	12,48 ± 0.0147	9.72 × 10 ⁴
linker2	0.02 ± 0.002	6,61 ± 0.003	2.83 × 10 ⁵	0.09 ± 0.013	10,31 ± 0.0192	1.16 × 10 ⁵
D200N	0.06 ± 0.006	10,11 ± 0.008	1.76 × 10 ⁵	0.14 ± 0.009	10,91 ± 0.0127	7.97 × 10 ⁴
Q198F	0.03 ± 0.002	3,30 ± 0.002	1.29 × 10 ⁵	0.07 ± 0.004	4,43 ± 0.0060	6.53 × 10 ⁴
A96Q	0.05 ± 0.004	7,41 ± 0.006	1.61 × 10 ⁵	0.13 ± 0.009	8,46 ± 0.0136	6.76 × 10 ⁴
E629Q	0.03 ± 0.003	7,51 ± 0.004	2.52 × 10 ⁵	0.11 ± 0.014	11,75 ± 0.0203	1.04 × 10 ⁵
Y716P	0.05 ± 0.003	4,18 ± 0.005	7.77 × 10 ⁴	0.13 ± 0.008	6,11 ± 0.0112	4.79 × 10 ⁴

4.5.2 Presteady-state kinetic studies

Intramolecular electron transfer (IET)

Stopped-flow experiments in the single-mixing mode were carried out with 5 μM final enzyme concentration and an excess of cellobiose (50 μM) in

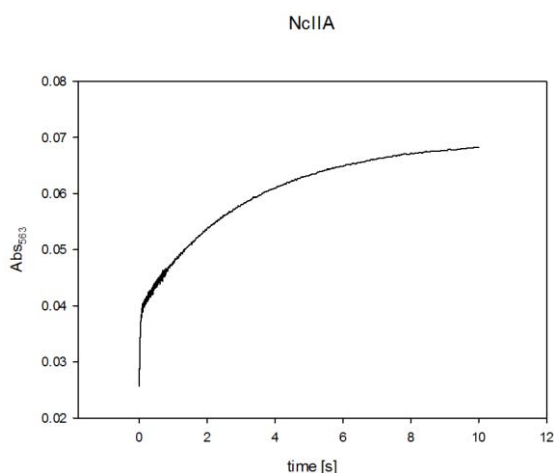


Figure 24: Time course of absorption at 563 nm for monitoring heme reduction of *NcCDH IIA*. The plot serves as an example of spectral changes obtained also for all other CDH variants.

50 mM potassium phosphate buffer at 30°C. On mixing CDH with cellobiose the spectrum of the enzyme rapidly changed from oxidized to reduced form. Initially, a decrease in absorption at 449 nm attributed to the FAD is observed, followed by an increase of α - and β -bands of the heme cofactor. For the determination of changed IET properties of the CDH variants solely the spectral changes at 563 nm were evaluated. Since the changes appear to be biphasic (example displayed in Figure 24), two rate constants -for the first fast and the second slow rate - were estimated by fitting each phase to a single

exponential function. The heme reduction was referred to the first $\sim 35\%$ (Δabs) of the absorption change, while the slow rate ($k_{\text{obs},2}$) remained ambiguous. In fact, no correlation could be found between the 2nd, slow rate and the CYT reoxidation using molecular oxygen, which is about 0.03 s^{-1} , thus even ten times slower than $k_{\text{obs},2}$ (detailed reoxidation rates can be found in the Appendix).

Similar IET rates were obtained for *NcCDH IIA* and A96Q with 45.13 ± 0.6 and $44.54 \pm 0.9 \text{ s}^{-1}$, respectively. Interestingly, the highest rate was observed for D200N with $66.22 \pm 0.4 \text{ s}^{-1}$, indicating a positive effect of neutral residues at the DH- CYT interface on IET. The significantly lowest rate was detected for Q198F with only $0.41 \pm 0.01 \text{ s}^{-1}$ which is in line with results observed during the high throughput screening process. A 5-fold decrease in IET rate compared to the wild-type was monitored for the linker mutant. The variants E629Q and Y716P show only a two-fold decrease in electron transfer rates from FAD to heme cofactor.

Table 20: Kinetic constants of IET rates and 2nd slow rates for all CDH variants. Delta absorbance describes the percentage absorbance change for each rate in relation to the complete absorbance change. Mean values and standard deviations were calculated from quadruplet measurements.

CDH	heme reduction			2 nd slow rate		
	k_{obs} [s ⁻¹]	Δ abs [%]		k_{obs} [s ⁻¹]	Δ abs [%]	
<i>NcCDH</i> IIA	45.13 ± 0.57	32		0.37 ± 0.00	66	
linker2	8.42 ± 0.35	38		0.86 ± 0.08	62	
D200N	66.22 ± 0.36	42		0.33 ± 0.02	55	
Q198F	0.41 ± 0.01	76		0.34 ± 0.01	24	
A96Q	44.54 ± 0.88	34		0.36 ± 0.01	63	
E629Q	24.05 ± 1.47	40		0.59 ± 0.02	60	
Y716P	34.65 ± 1.24	25		0.25 ± 0.01	72	

CDH-LPMO interaction

To monitor the electron transfer solely from CYT to LPMO excluding the electron transfer from FAD to heme, a sequential mixing mode was conducted. During the initial mixing electrons gained from cellobiose are transferred to CDH. By a slow side reactivity of CDH with molecular oxygen both cofactors begin to re-oxidize. After complete reoxidation of DH while still 70% of heme are in reduced state, three increasing LPMO concentrations (2, 6, 10 μ M) were added. The observed fast rates (k_{obs} [s⁻¹]) were estimated by fitting to a single exponential curve and plotted against each LPMO concentration (illustrated in Figure 25) revealing a consistent linear relation with a slope represent a second order rate constant k_{app} (s⁻¹ μ M⁻¹).

It shall be noted that the reactions for E629Q and Y716P appear biphasic at equimolar CDH-LPMO ratios. The k_{obs} values for the first data point may therefore be slightly inaccurate, as the rate was estimated over the first phase, where only 30-40% of heme-reoxidation was obtained. Here again, no correlation could be found between the biphasic heme-reduction and the oxygen reactivity of the heme-cofactor.

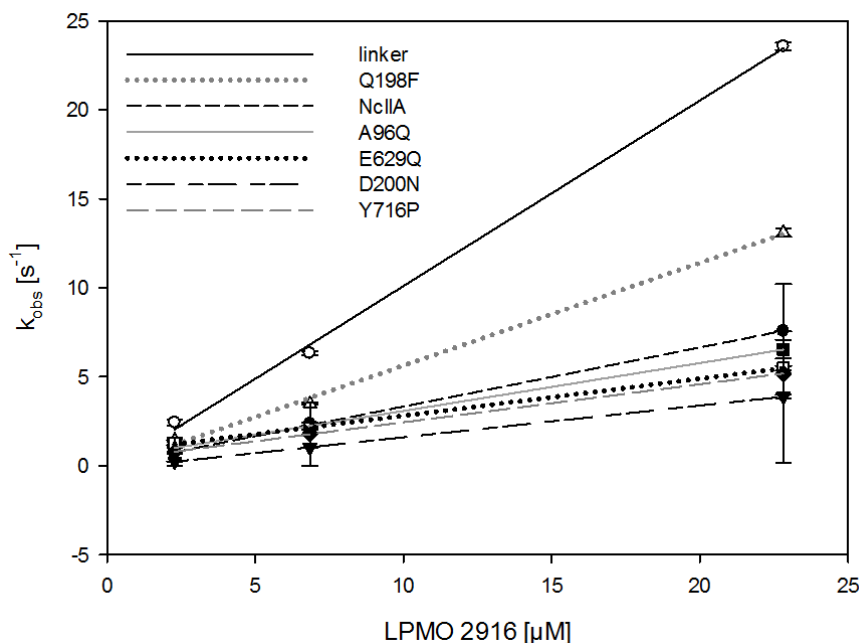


Figure 25: Observed rate constant k_{obs} for CDH-LPMO interaction plotted vs. the corresponding LPMO concentration. The slope equals k_{app} – a second order rate constant – that describes the CDH-LPMO reaction rate as a function of CDH-LPMO ratio.

Table 21: List of CDH-LPMO electron transfer rates. All CDH variants with each LPMO concentration were measured in triplicates.

CDH		$k_{obs} [s^{-1}]$			$k_{app} [s^{-1} M^{-1}]$
		LPMO-02916			
Variant	$[\mu M]$	2.28 μM	6.84 μM	22.82 μM	
		1:1	1:3	1:10	
		$k_{obs} [s^{-1}]$			
<i>NcCDH IIA</i>	1.99	0.71 \pm 0.03	2.35 \pm 0.07	7.57 \pm 0.02	3.68×10^5
linker2	2.01	2.42 \pm 0.17	6.33 \pm 0.11	23.57 \pm 0.21	1.16×10^6
D200N	1.99	0.24 \pm 0.01	1.02 \pm 0.01	3.89 \pm 0.10	1.78×10^5
Q198F	2.02	1.41 \pm 0.03	3.48 \pm 0.06	13.09 \pm 0.23	5.77×10^5
A96Q	1.95	1.07 \pm 0.06	2.15 \pm 0.04	6.55 \pm 0.53	2.69×10^5
E629Q	1.96	1.24 \pm 0.09	2.09 \pm 0.05	5.48 \pm 0.13	1.98×10^5
Y716P	2.01	0.78 \pm 0.03	1.79 \pm 0.06	5.18 \pm 0.09	1.95×10^5

As visible in Figure 25 and detailed in Table 21, the electron transfer rates differ significantly. The rates from *NcCDH IIA* to LPMO were $3.68 \times 10^5 s^{-1} M^{-1}$, which is approximately 3-fold higher than those of E629Q, Y716P and D200N and similar to k_{app} of A96Q. Apparently, an additional loop in the

linker domain and thus a higher flexibility of the CYT domain seems to have an accelerating effect on the electron transfer between CDH and LPMO as the linker mutant exhibits a 3-fold higher k_{app} rate compared to the wild-type. Interestingly, the mutant Q198F with an extremely low IET rate (0.41 s^{-1}) actually exhibits a two-fold higher electron transfer rate to LPMO compared to *NcCDH* IIA. A summary of all presteady-state kinetic constants is listed in Table 22.

Table 22: Reaction rates of heme reduction (IET) and 2nd order rate constants (CDH-LPMO interaction).

CDH	heme reduction		CDH-LPMO rate constant
	k_{obs}	[s^{-1}]	k_{app} [$s^{-1} M^{-1}$]
<i>NcCDH</i> IIA	45.13	± 0.57	3.68×10^5
linker2	8.42	± 0.35	1.16×10^6
D200N	66.22	± 0.36	1.78×10^5
Q198F	0.41	± 0.01	5.77×10^5
A96Q	44.54	± 0.88	2.69×10^5
E629Q	24.05	± 1.47	1.98×10^5
Y716P	34.65	± 1.24	1.95×10^5

The greatest changes in intra-electron as well as inter-electron-transfer properties compared to the wildtype *NcCDH* IIA can be found for the variants Q198F, D200N and the linker.

The side-chain of Q198 in *NcCDH* IIA is positioned adjacent to the heme *b* cofactor, close to its propionate-A group (shown in Figure 18). As recently reported the heme *b* propionate-A plays a key role in the IET mechanism as it actively participates in electron transfer events. It strongly interacts with four side-chains located on the DH at the CYT-DH interface referred to as propionate-docking site (Tan et al., 2015). The residue of Q198 shows polar contacts to two of the four amino acids in the propionate-docking site, namely W318 (equal to W295 in *MtCDH*) and S321 (S298 in *MtCDH*). A change from glutamine (Q) to phenylalanine (F) at this position most likely eliminates these interactions. It increases hydrophobic forces at the interface, which might slightly push the propionate docking site on DH away from the heme *b* propionate-A. This may explain the extreme breakdown of the IET observable in the variant Q198F. Interestingly, the electron transfer rate to LPMO is two-fold higher compared to *NcCDH* IIA. It is suggested that in solution the CYT domain docks favourable with its heme *b* to the copper site in LPMO (Tan et al., 2015). Thus, the mutation Q198F adjacent to the heme *b* may possibly alter the interaction interface to LPMO in a positive way. It can be also assumed that repulsion forces at the DH - CYT interface caused by the mutation Q198F, destabilize the closed state. The more loose attachment between the two domains may facilitate the

transition from the closed to the open conformation and thus accelerate the electron transfer to LPMO. However, more investigations have to be conducted to reveal the effect of this mutation on the ET to LPMO.

It is known that the electron transfer between the FAD and heme-*b* group in CDH is pH dependent (Igarashi et al., 2002; Kracher et al., 2015; Zamocky et al., 2006). Quite recently Kracher et al., (2015) explained the pH-dependency by the presence of negatively charged side chains at the interface of DH and CYT, preventing formation of a closed confirmation of both domains and thus IET. That indicates that a shift from negatively charged residues to neutral or positive ones decreases electrostatic repulsion of DH and CYT and allows more efficient and rapid electron transfer between the domains. That assumption was confirmed by results obtained for the variant D200N. A change from the acidic side-chain aspartate to the uncharged asparagine increases the IET in comparison to *NcCDH* IIA by about 50%. In contrast the ET to LPMO decreases by 50% which again correlates well with the assumed theory. This decrease of repellent interfacial surface forces may cause a stronger attachment between the two domains. That makes the CYT less accessible for reaction partners and negatively influences the electron transfer to other proteins, like LPMO or cyt *c*.

The opposite effect can be seen for the linker mutant. The incorporation of an additional loop exhibits a five-fold decrease in the heme-*b* reduction rate, but a three-fold increase of the electron transfer rate to LPMO. Therefore it seems that the increased flexibility of the extended linker peptide allows a more efficient association of the CYT to the copper site of LPMO. On the contrary the mutation in the linker domain might alter the position and distance between the CYT and DH domain in a manner that an efficient IET is not possible anymore.

The variant A96Q seems to be silent and neither affects the electron transfer rate inbetween the CDH itself, nor to LPMO. The mutants E629Q and Y716P, both located on the DH at the CYT- DH interface, also didn't show any significant differences to *NcCDH* IIA. That demonstrates that these three mutation sites aren't essential for IET as well as ET to LPMO.

However, the specific mutation of side chains at the interacting surface of CYT and DH corroborates the substantial influence of amino acids positioned at the interface of the domains on the reaction rates. The mutants D200N and Q198F indicate that the domain interaction is pH-dependent as well as affected by hydrophobic and electrostatic forces. Apparently, the linker peptide strongly contributes to the intra- and inter- electron transfer mechanism by affecting the overall domain interaction inbetween CDH as well as to LPMO. Interestingly, the electron transfer reaction rate from CYT to LPMO seems to be indirectly proportional to IET rates. Slow IET rates are accompanied by fast CYT-LPMO reaction rates and vice versa. This observation could be attributed to the accessibility of

the CYT domain, which either preferably associates with DH for efficient IET or interacts with LPMO for increased inter-electron transfer.

4.6 Comparison of HTS versus kinetic parameters

All CDH variants, screened with a combination four-assay method, were produced, purified and further characterized with steady- and presteady-state kinetic methods. These kinetic constants were then used to assess the reliability of the screening method by comparing them to the results gathered by stopped-flow technique applied on purified enzymes. All specific activities as well as reaction rates and rate constants were related to results obtained for *NcCDH IIA*. The cyt *c* assay is generally accepted as indicator for an intact IET. Its data should therefore be comparable to IET rates determined by fast kinetic measurements. The CDH-LPMO interaction was assessed by the AR/cyt *c* – ratio and the k_{app} rate constants, as both mainly focus on the electron transfer from CYT to LPMO. When comparing the relative values of the cyt *c* assay with k_{obs} rates (IET) and the AR/cyt *c* – ratio with the k_{app} rate constants (CDH-LPMO interaction), it can be seen that they match very closely and show the same trend. An exception represents the variant D200N, which shows an increased IET-rate determined by stopped-flow measurements, while the specific activity with cyt *c* was similar to that of *NcCDH IIA*.

However, the screening results obtained in culture supernatant correlate well with the fast-kinetic measurements conducted with the purified CDH-variants. Thus the screening method combining three enzyme-activity- as well as a Bradford-assay provides a rapid, simple and reliable method for the identification of changed intra- and inter-electron transfer rates. The microplate method applicable to culture supernatant and without time-consuming handling due to the use of a pipetting robot and fast and easy-to-use assays, has the potential for a high-throughput-screening of big enzyme libraries for altered electron transfer properties, rendering a directed evolution approach possible.

Table 23: Comparison of relative activities obtained from HTS with presteady-state kinetic data.

Variant	High-throughput-screening							Stopped-flow					
	Specific activity (U/mg)				Specific activity (U/mg)			AR/cyt c		IET k_{obs} [s ⁻¹]		CDH-LPMO k_{app} [s ⁻¹ M ⁻¹]	
	DCIP		cyt c		Amplex red								
NcCDH IIA	4.21	100%	2.39	100%	0.0036	100%	0.0015	100%	45.13	100%	3.68 x 10 ⁵	100%	
linker2	2.69	64%	0.80	34%	0.0028	79%	0.0035	237%	8.42	19%	1.16 x 10 ⁶	314%	
D200N	3.79	90%	2.26	94%	0.0021	59%	0.0009	62%	66.22	147%	1.78 x 10 ⁵	48%	
Q198F	1.56	37%	0.13	5%	0.0006	17%	0.0048	324%	0.41	1%	5.77 x 10 ⁵	157%	
A96Q	3.18	76%	2.33	98%	0.0025	71%	0.0011	73%	44.54	99%	2.69 x 10 ⁵	73%	
E629Q	2.89	69%	1.70	71%	0.0024	69%	0.0014	97%	24.05	53%	1.98 x 10 ⁵	54%	
Y716P	2.93	70%	1.91	80%	0.0026	74%	0.0014	93%	34.65	77%	1.95 x 10 ⁵	53%	

4.7 Kinetic studies of CDH-LPMO interaction on solid substrates

Two CDHs, *NcCDH IIA* and variant *Q198F* with a very high and a very low IET, respectively, were chosen to obtain a deeper understanding of the influence electron transfer rates on the LPMO conversion of crystalline cellulose (Avicel) and cellopentaose, when driven by CDH. This question was addressed, during a co-operation with the Norwegian University of Life Science applying a mass spectroscopy technique.

Several pre-tests were performed to find suitable internal standards and conditions; the purity of LPMO and CDH enzyme preparations and the identification of undefined peaks. After several experiments chitobiose was chosen as internal standard as it can be degraded neither by CDH nor by LPMO; even after three days of incubation at 30°C. The substrate to standard ratio was optimized for cellopentaose with 0.05 mM chitobiose and 0.005 mM for Avicel. LPMO and CDH preparations were checked for impurities and no unexpected products have been found in blank reactions where the LPMO reducing system CDH/lactose or LPMO itself were omitted. The identification of undefined peaks found during ESI-MS measurements was facilitated through comparison to ions detected in prior studies (Keller et al., 2008). Most unknown interferences could be identified (e.g. sodium acetate clusters by distinct repeating units) or were allocated to the electrospray ionization method itself (e.g. compounds in the eluents or instrument artefacts) as they didn't appear in the comprehensive analysis with MALDI-TOF.

4.7.1 Kinetic studies of CDH-LPMO interaction on the soluble substrate cellopentaose

For time resolved product analysis of products generated during degradation of cellopentaose ESI-MS was used. Cellopentaose (Glc₅) was treated with LPMO-02916 and varying *Nc*CDH concentrations in combination with an excess of lactose and analyzed after 0, 45, 90, 135 and 180 min. Main products of Glc₅ degradation were two species with *m/z* values 527 and 381, corresponding to the sodium adducts of cellotriose (Glc₃) and cellobiose (Glc₂) with a gemdiol (a hydrated keto group) at the nonreducing end (C₄), respectively (illustrated in Figure 26). The peaks at *m/z* 437 and 707 can't be assigned to masses of any reaction products and may be PEG (polyethylen glycol) contaminants (*m/z* 437) which are compounds in all plastic ware in laboratory (Keller et al., 2008) or background interferences from the ESI-MS itself. The *m/z* values 447 and 851 correspond to the sodium adducts of chitobiose and Glc₅, whereas the high intensity peak of lactose (*m/z* 365) can't be seen in this figure.

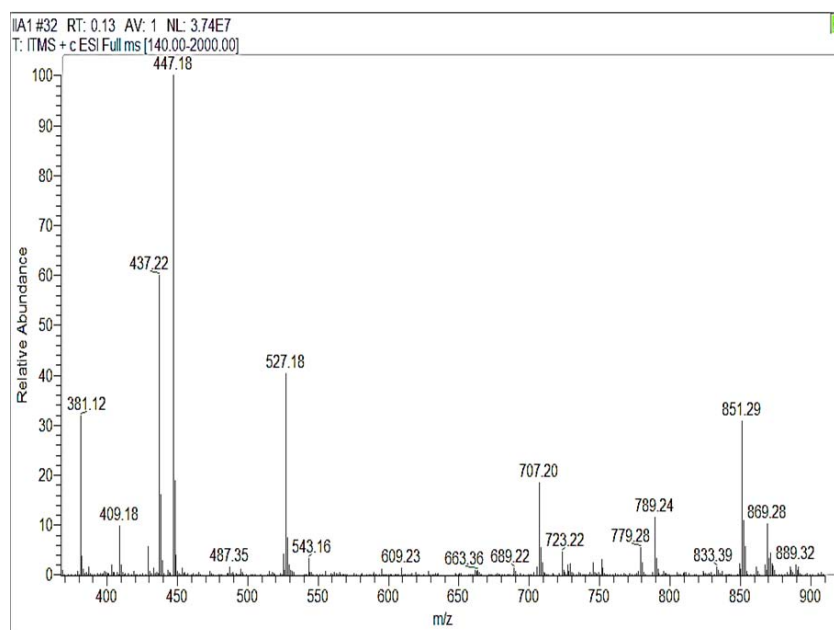


Figure 26: ESI-MS analysis of products generated over time during Glc₅ (*m/z* 851) degradation. The picture shows a spectrum from *m/z* 370 – 900 for the 180 min-sample of *Nc*CDH IIA (0.8 μM) to LPMO (0.8 μM) ratio of 1:1.

Figure 27 shows the results obtained for the ESI-MS product analysis. The cellopentaose concentration at each time point was calculated using the described standard curve and plotted vs. time. While the concentration of LPMO remained constant (0.8 μM) for all reactions, the CDH concentration varied from 0.32 μM to a 10-fold excess up to 8 μM (0.32, 0.8, 1.6, 4, 8 μM). For each ratio a substrate conversion rate k_{obs} [μM min⁻¹] was obtained as the slope of a linear regression fit

over the whole 180 min or only 135 min depending on the linearity (values are summarized in Table 24). In turn, k_{obs} [$\mu\text{mol L}^{-1}\text{min}^{-1}$] was converted to k [s^{-1}] by including the employed LPMO concentration and time. These values were then plotted versus their corresponding CDH concentrations (0.32, 0.8, 1.6, 4.0, 8.0 μM) and fitted to a single rectangular hyperbola with two parameters k_{lim} and K_D (depicted in Figure 28). At low CDH/LPMO ratios the reaction rate is increasing showing potentially a limitation of the electron transfer between CDH and LPMO (k_3) while at a five-fold excess of CDH the reaction rate didn't increase further, which is indicative for the LPMO monooxygenation step (k_4) becoming rate limiting. The corresponding kinetic constants were calculated by nonlinear least-square regression (Sigma Plot 12) and are listed in Table 25. Here, k_{lim} represents the maximum reaction velocity achieved by the CDH-LPMO system at maximum CDH/LPMO-ratio, whereas K_D denotes the affinity.

Although the IET rates of *Nc*CDH IIA and Q198F differ by a factor of 10, both variants show similar K_D as well as k_{lim} values in this experiments. This strongly suggests that the maximum rate (k_{lim}) represents the catalytic activity of LPMO-02916 on soluble substrate. In presence of a five-fold excess of CDH, the LPMO reaction becomes the rate limiting step, while the electron transfer within CDH appears negligible. As the observed turnover rates are below all observed electron transfer rates, it can be concluded that the overall reaction is governed by the LPMO substrate conversion rate (k_4 , see Figure 3 and Figure 14).

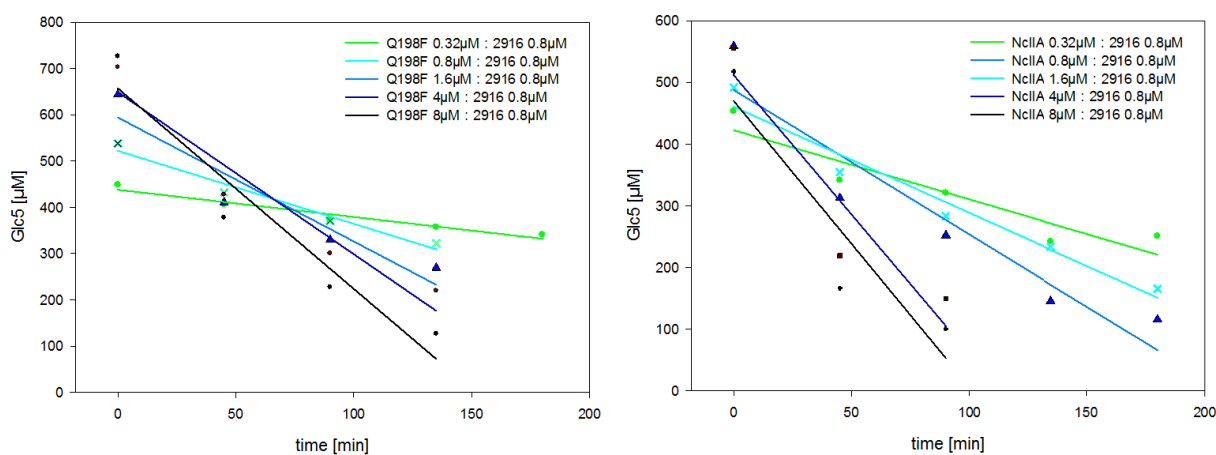


Figure 27: Linear relationship between cellopentaose conversion and time. The estimation of the substrate consumption rate was performed by a linear regression fit where k_{obs} [$\mu\text{M min}^{-1}$] equals the slope. The left plot shows the results of the experiments conducted with Q198F, the right plot with *Nc*CDH IIA.

Table 24: Reaction rates for different *NcCDH* IIA/Q198F – LPMO ratios reflecting cellopentaose degradation over time. Data were obtained from measurements of two separately prepared and analysed reaction mixtures.

CDH	k [s^{-1}]				
	CDH-LPMO ratio				
	0.4	1	2	5	10
<i>NcCDH</i> IIA	0.026 ± 0.004	0.045 ± 0.01	0.062 ± 0.02	0.092 ± 0.003	0.11 ± 0.02
Q198F	0.012	0.042 ± 0.01	0.058 ± 0.003	0.073 ± 0.0001	0.094 ± 0.005

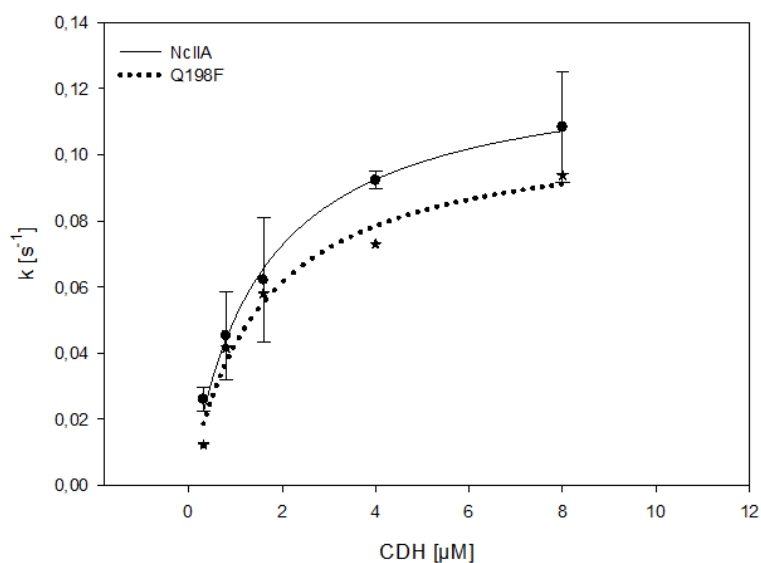


Figure 28: Determined reaction rates as a function of CDH concentration during cellopentaose conversion.

Table 25: Reaction rates for *NcCDH* IIA and Q198F determined by following the cellopentaose consumption over time and plotting the observed rates against their corresponding CDH concentration.

CDH	Cellopentaose		
	K_D [μM]	k_{lim} [s^{-1}]	k_{lim}/K_D [$s^{-1} M^{-1}$]
<i>NcCDH</i> IIA	1.51 ± 0.17	0.13 ± 0.01	8.61×10^4
Q198F	1.54 ± 0.39	0.11 ± 0.01	7.14×10^4

4.7.2 Kinetic studies of CDH-LPMO interaction on the insoluble substrate Avicel

For the investigation of CDH-LPMO interaction under *in vivo* conditions enzymatic conversion was performed on microcrystalline cellulose with varying CDH-LPMO ratios and analysed by ESI-MS, as well as MALDI-TOF MS. Figure 29 illustrates the complex product spectrum of oligosaccharides released upon degradation of 25 mg ml⁻¹ Avicel with an equimolar LPMO and CDH concentration (0.8 µM) after 9 h of incubation. It includes different species of cellotriose, cellotetraose and cellopentaose in the mass range m/z 520 – 590, m/z 680 – 743 and m/z 850 – 910, respectively (a detailed mass table can be found in Isaksen et al., 2014). The degradation of cellulose with LPMO driven by ascorbic acid as reductant yielded exclusively in native and single-oxidized cello-oligosaccharides. As already shown in Isaksen et al., (2014), the use of CDH/lactose as electron donor led to a change in the product profile. Native oligosaccharides (m/z 527 for cellotriose, m/z 689 for cellotetraose) were no longer observable because of their oxidation to aldonic acids by CDH (e.g. m/z 525 for cellotrionic acid and m/z 687 for cellotetraonic acid). Aldonic acids usually were transformed into a gemdiol by incorporation of a water molecule (m/z 543 & 705). Furthermore double-oxidized species appeared with a keto-group or a gemdiol at the non-reducing ends. The mass spectrum on the right side of Figure 29 displays the product pattern of cellotriose species in more detail.

In Figure 29 products taken into account for the product formation rate quantification are marked in red. The raw data of cellotriose, -tetraose and -pentaose plus their oxidized forms (trioses, tetraoses, pentaoses) were recalculated using the corresponding standard curve. The main reaction products were found in similar magnitude with oxidized cellotetraose being the most prevalent reaction product.

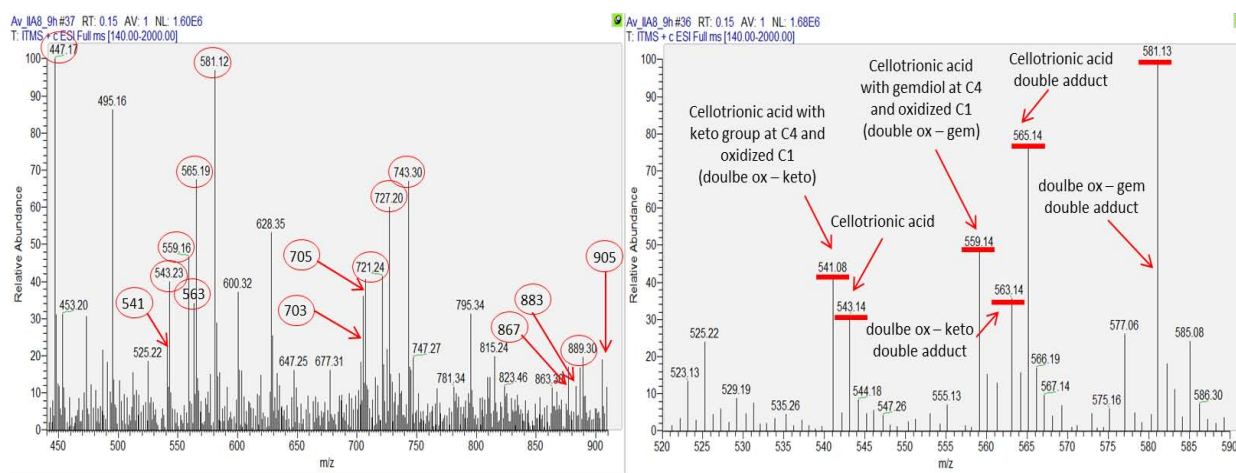


Figure 29: ESI-MS spectrum of multiple reaction products obtained after incubation of 25 mg ml⁻¹ Avicel with 0.8 µM LPMO-02916 and 0.8 µM *NcCDH* IIA with 1µM Lactose for 9 h, showing the sodium adducts or even double-adducts of their corresponding single- and double-oxidized cellotriose, cellotetraose, cellopentaose. The left picture displays a full spectrum from m/z 440 – 910, while the right one illustrates only the trimers found in a mass range from 520 to 590. The peak at m/z 447 corresponds to the mass of the internal standard chitobiose.

The further data processing was similar as described for cellopentaose degradation, but instead of following the cellopentaose consumption, a linear increase of LPMO reaction products over time was recorded. A linear regression analysis results in product formation rates for each CDH/LPMO ratio displayed in $\mu\text{M h}^{-1}$ (Figure 30). The analyses were conducted in triplicates with two independently prepared and analysed reaction mixtures.

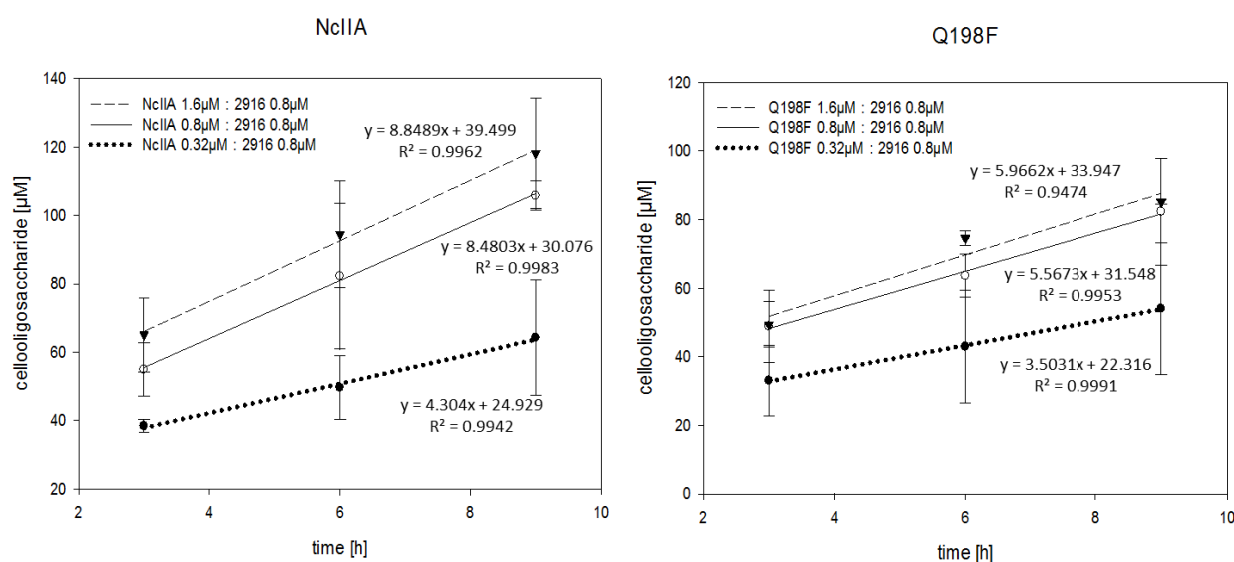


Figure 30: Linear increase of released products upon degradation of 25 mg ml⁻¹ Avicel with increasing CDH-LPMO ratios up to a two-fold CDH excess (0.32, 0.8, 1.6 μM CDH compared to 0.8 μM LPMO). The slope in the linear equation equals the product formation rate [$\mu\text{M h}^{-1}$] as a function of CDH:LPMO ratio.

For the sake of consistency the reaction rates were converted from $\mu\text{M h}^{-1}$ to $\text{k [s}^{-1}\text{]}$ and plotted against their corresponding CDH concentration (Figure 31). In comparison to cellopentaose, the reaction velocity only increased up to an equimolar CDH to LPMO ratio and couldn't be accelerated by addition of higher CDH concentrations. Quite the contrary, the product concentration at higher LPMO:CDH ratios from 1:5 even decreased after six hours of incubation (the corresponding plot Glc_x -concentration vs. time can be found in the Appendix).

This might be explained as CDH, like LPMO, has cellulose binding features and co-localizes on the cellulose surface. It seems, that a five-fold excess of CDH in the reaction may affect the LPMO/CDH synergy by occupying LPMO-binding sites on Avicel. This competitive binding might be a possible reason for the decreased product formation rate at high CDH concentrations. Another reason for that effect could be an augmented formation of reactive oxygen species (e.g. peroxide) by CDH, which may cause elevated enzyme denaturation and thus a decreased catalytic activity of LPMO.

The obtained k_{lim} – values as well as the catalytic efficiency for Avicel (listed in Table 26) appear marginally higher for NcCDH IIA than for Q198F. However, in consideration of the significant different

IET properties, both CDH/LPMO combinations show pretty similar catalytic constants which is again indicative for the LPMO reaction to be rate limiting. It should be noted that the overall fit to a hyperbolic dependency is not of high quality. Future work should therefore include experiments with lower CDH/LPMO ratios to cover the whole reaction range.

Nevertheless, the results provide compelling evidence that the LPMO reaction is approximately ten times slower on solid microcrystalline substrate than on soluble cellopentaose. Especially enzymatic conversion on soluble substrate revealed the LPMO reaction (k_4) to be the overall rate limiting step. As long as CDH is available in excess no influence of different electron transfer rates within CDH or to LPMO on cellopentaose degradation was observable. The slight differences in reaction velocity observable for Avicel might indicate an influence of the CDH-LPMO reaction on the LPMO degradation reaction on solid substrate. However, a potentially important effect of CDH electron transfer rates at lower ratios has to be confirmed by further analysis. A thorough validation and improvement of the parabolic fitting model would enhance the reliability of the results to allow for solid conclusions on this issue.

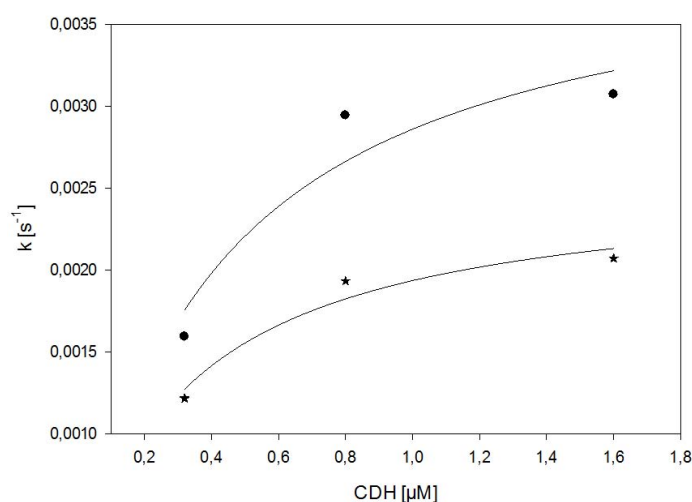


Figure 31: Product formation rates k [s^{-1}] at different CDH concentrations during Avicel conversion.

Table 26: Catalytic constants for *NcCDH* IIA and Q198F calculated by using nonlinear least-square regression by fitting the observed data to a single rectangular hyperbola.

CDH	Avicel		
	K_D [μM]	k_{lim} [s^{-1}]	k_{lim}/K_D [$s^{-1} M^{-1}$]
<i>NcCDH</i> IIA	0.42 ± 0.26	0.0041 ± 0.001	9.76×10^3
Q198F	0.32 ± 0.12	0.0026 ± 0.0003	8.13×10^3

4.7.3 Comparison ESI-MS vs MALDI-TOF MS

In order to confirm the reliability of results assessed with ESI-MS analysis, product analysis of already measured reaction mixtures including *NcCDH IIA* was conducted applying MALDI-TOF MS. MALDI-TOF MS and ESI-MS are highly sensitive analytical techniques. Both provide qualitative and quantitative information on analyte molecules after their conversion to ions (Ho et al., 2003). Nevertheless, there are also several differences in terms of molecule ionization, detection system or sample preparation. In MALDI-TOF MS the oligosaccharides are ionized with a short pulse of laser light and desorbed from the matrix into the vacuum system. Instead, ESI-MS uses a charged needle for dispersal of charged droplets and solvent evaporation to assist the transfer of ions from solution into the gaseous phase before they are subjected to the mass spectrometric analysis (Berg et al., 2009; Ho et al., 2003). Another variation is the totally different sample preparation for MALDI-TOF, where 1 μl of the sample was mixed with a matrix solution and fixed to a spot of a target plate, compared to ESI-MS, where 5 μl of the liquid sample preparation were directly injected into the MS.

Both analysis methods yield similar reaction rates for the analysed samples between 4.3 (ESI) and 4.5 (MALDI) $\mu\text{M h}^{-1}$ for the lowest CDH:LPMO ratio and 8.0 (MALDI) and 8.8 (ESI) $\mu\text{M h}^{-1}$ for the highest CDH:LPMO ratio (Figure 32 & Table 27) stressing the robustness of the experiment. A MALDI-TOF spectrum of the reaction products obtained from cellulose degradation by *NcCDH IIA* and LPMO-02916 can be found in the Appendix.

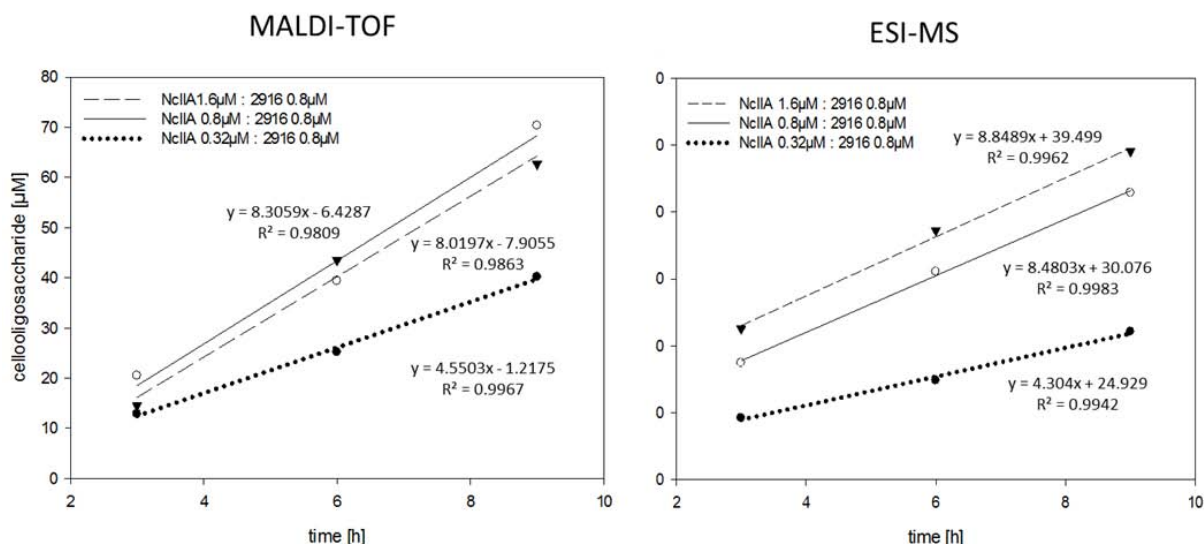


Figure 32: Linear regression plots of oligosaccharides increase versus time analysed by MALDI-TOF MS (left plot) and ESI-MS (left plot). The sample mixtures were identical for both analysis including 25 mg ml^{-1} Avicel, 0.8 μM LPMO-02916 and *NcCDH IIA* (0.32 – 1.6 μM) with 1 μM lactose.

Table 27: Comparison of reaction rates obtained for product analyses of the same reaction mixture with either ESI-MS or MALDI-TOF MS.

<i>N</i> cCDH IIA : LPMO ratio	k_{app} [$\mu\text{M min}^{-1}$]	
	ESI-MS	MALDI-TOF MS
0.4 : 1	0.072	0.077
1 : 1	0.141	0.139
2 : 1	0.147	0.134

5. Conclusions & Outlook

In the present work a screening method was developed for the rapid and simple screening for altered electron transfer properties of CDHs cultivated in deep-well plates by using a combination of four photometric enzyme activity assays. A screening-draft was step-by-step tested and improved in terms of assay sensitivity, data processing and an appropriate measuring protocol yielding in an elaborated screening protocol. The high sensitivity and robustness against interfering media components makes it applicable to culture supernatant. The screening results were reproducible and precise as confirmed by further characterization of purified enzyme samples with presteady-state kinetics. The microplate technique with a time efficient handling combining a pipetting robot and four easy-to-use assays, embodies real HTS potential for the search of interesting CDH variants with altered IET and ET properties to LPMO.

A rational enzyme design approach based on the comparison of the recently published crystal structure of *NcCDH* IIA with *NcCDH* IIB was used to engineer several CDH variants. The two CDHs of *N. crassa* show significant differences in intra and inter electron transfer rates within CDH as well as to LPMO. That offered a promising basis for the elucidation of the structural mechanism that governs the electron transfer between the FAD-, heme-*b*- and copper-cofactor of CDH and LPMO. To investigate this interaction mechanism and the influence of IET, the focus of the mutagenesis study has been on amino acid differences between *NcCDH* IIA and *NcCDH* IIB at the interaction surface of the DH and CYT domains.

Six interesting CDH variants were found with altered IET properties and produced at large scale in a six-force fermenter system. The recombinant production of the *NcCDH* IIA variants yielded reasonable amounts of functional holoenzyme. A subsequent two-step purification strategy applying a HIC and an IEC step resulted in sufficient amounts of 10 – 30 mg homogenous enzyme. These six CDH variants together with *NcCDH* IIA were used in steady-state and presteady-state experiments to elucidate substrate turnover by DH as well as IET and ET rates from CDH to LPMO in solution.

While similar turnover rates for cellobiose and lactose oxidation were obtained, significant differences were found for CDH-LPMO electron transfer rates, mainly for the variants Q198F, D200N and linker. Compelling evidence was provided that the electron transfer mechanism between DH and CYT depends on hydrophobic and electrostatic repulsion or attraction of polar or charged residues around the interface of the heme and FAD redox centres. Furthermore, the length and composition of the linker peptide strongly contributes to the intra- and inter electron transfer. An increased flexibility allows a more efficient electron transfer from CYT to the copper site in LPMO, while a change in environment between the FAD and heme-*b* cofactors results in dramatically lowered IET

rates. Apparently, CYT is the crucial domain for ET to LPMO or other reaction partners. A high compatibility of the redox center in CYT for the active site of LPMO favours efficient inter-electron transfer, while a strong association and attraction of DH and CYT results in fast IET rates but hampers electron transfer to LPMO.

For the investigation of the CDH-LPMO electron transfer mechanism *in vivo* during conversion of natural substrate, experiments on cellopentaose and Avicel with different CDH/LPMO combinations were conducted. A novel and robust method applying MS-techniques was developed during a visit at the Norwegian University of Life Science in Ås. Reaction products released during enzymatic degradation of soluble (cellopentaose) and insoluble microcrystalline (Avicel) substrate were quantified and reaction rates were calculated. The LPMO reaction on soluble substrate was shown to be ten-times faster compared to insoluble substrate. Conversion experiments on cellopentaose using two different CDH/LPMO combinations with CDHs showing either fast or slow IET rates, resulted in similar reaction rates. That reveals the LPMO substrate conversion rate to be the rate limiting step when CDH serves as reducing agent. The slight differences in reaction rates observable for Avicel might indicate an influence of CDH-LPMO reaction rates on the LPMO degradation reaction on solid substrate. However, the obtained results have to be confirmed by further experiments applying an improved experimental setup and testing more CDH/LPMO combinations.

The finding that cellulose conversion is mainly dependent on LPMO substrate conversion rate and that the reaction velocity can only be increase up to an equimolar CDH to LPMO concentration, can help to formulate more efficient, cost-effective enzyme solutions for biofuel production from lignocellulosic biomass. However, further research to find more efficient CDH/LPMO combinations for biomass saccharification is definitely required. Two powerful tools were provided in this work to investigate and thus improve not only CDH-LPMO, but also CDH-LPMO-cellulose interaction. Especially, the establishment of a quantification method of released oligosaccharides by means of mass spectrometry offers a great possibility to clarify the nature of CDH-LPMO-cellulose interaction in respect to efficient degradation of complex biomass for renewable chemicals and fuels.

The successful discovery of interesting CDH variants proves that the rational enzyme design method to generate CDH variants with varying IET properties to investigate CDH-LPMO interaction was an effective approach. Thus, ten additional variants were engineered by structure-based site-directed mutagenesis with respect to altered electron transfer rates. The CDH mutants have already been screened for changed IET and ET to LPMO by the newly developed HTS. The screening results are depicted in Table 28. Here, it becomes evident that mutations at the interaction surface of DH and CYT near the redox cofactors resulted in less active or even inactive CDH variants and have a

tremendous impact on CDH activity. Looking at the AR/cyt *c* ratio, interesting properties of CDH/LPMO interaction are expected. Promising variants can serve for further research to fully unravel the CDH-LPMO reaction mechanism towards a comprehensive understanding of this bi-enzymatic system.

Table 28: Specific activities of several CDH variants determined by the four-assay screening method combining DCIP-, cyt *c*- and Amplex red assay.

High-throughput-screening														
Variant	Specific activity (U/mg)							Specific activity (U/mg)				AR/cyt <i>c</i>		
	DCIP				cyt <i>c</i>			Amplex red						
NcCDH IIA	3,61	±	0,25	100%	2,48	±	0,09	100%	0,0031	±	0,0004	100%	0,0012	100%
N142A	2,03	±	0,28	56%	0,96	±	0,17	39%	0,0005	±	0,0003	15%	0,0005	40%
P183K	3,12	±	0,14	86%	0,90	±	0,13	36%	0,0008	±	0,0003	25%	0,0009	70%
P183D	3,04	±	0,64	84%	1,10	±	0,27	44%	0,0022	±	0,0003	73%	0,0021	166%
D320K	3,32	±	1,44	92%	2,23	±	0,94	90%	0,0018	±	0,0008	58%	0,0008	64%
D569K	0,22	±	0,01	6%	0,10	±	0,01	4%	-0,0001	±	0,0001	-4%	-0,0012	
D664K	3,21	±	0,36	89%	1,78	±	0,09	72%	0,0019	±	0,0004	61%	0,0010	85%
loop	2,22	±	0,18	61%	0,96	±	0,07	39%	0,0014	±	0,0004	46%	0,0015	118%
Y122L	2,06	±	0,20	57%	0,02	±	0,01	1%	-0,0003	±	0,0002	-11%	-0,0148	
W318L	2,06	±	0,04	57%	1,07	±	0,09	43%	0,0010	±	0,0002	33%	0,0010	77%
M332F	2,27	±	0,60	63%	0,91	±	0,20	37%	0,0002	±	0,0001	7%	0,0002	19%

6. References

- Adrio, J., Demain, A., 2014. Microbial Enzymes: Tools for Biotechnological Processes. *Biomolecules* 4, 117–139. doi:10.3390/biom4010117
- Applied Photophysics, 2006. SX20 Hardware User Guide. http://depts.washington.edu/cidb4bio/Applied_Photophysics_Manual.pdf (accessed 10 Aug. 2015).
- Arnold, K., Bordoli, L., Kopp, J., Schwede, T., 2006. The SWISS-MODEL workspace: a web-based environment for protein structure homology modelling. *Bioinforma. Oxf. Engl.* 22, 195–201. doi:10.1093/bioinformatics/bti770
- Baminger, U., Subramaniam, S.S., Renganathan, V., Haltrich, D., 2001. Purification and Characterization of Cellobiose Dehydrogenase from the Plant Pathogen *Sclerotium (Athelia) rolfsii*. *Appl. Environ. Microbiol.* 67, 1766–1774. doi:10.1128/AEM.67.4.1766-1774.2001
- Beeson, W.T., Vu, V.V., Span, E.A., Phillips, C.M., Marletta, M.A., 2015. Cellulose Degradation by Polysaccharide Monooxygenases. *Annu. Rev. Biochem.* 84, 923–946. doi:10.1146/annurev-biochem-060614-034439
- Berg, J.M., Tymoczko, J.L., Stryer, L., 2009. *Stryer Biochemie*, 6. Aufl. 2007, korr. Nachdruck 2010. ed. Spektrum Akademischer Verlag.
- Biasini, M., Bienert, S., Waterhouse, A., Arnold, K., Studer, G., Schmidt, T., Kiefer, F., Cassarino, T.G., Bertoni, M., Bordoli, L., Schwede, T., 2014. SWISS-MODEL: modelling protein tertiary and quaternary structure using evolutionary information. *Nucleic Acids Res.* 42, W252–W258. doi:10.1093/nar/gku340
- Bradford, M.M., 1976. A rapid and sensitive method for the quantitation of microgram quantities of protein utilizing the principle of protein-dye binding. *Anal. Biochem.* 72, 248–254. doi:10.1016/0003-2697(76)90527-3
- Brugger, D., Krondorfer, I., Zahma, K., Stoisser, T., Bolivar, J.M., Nidetzky, B., Peterbauer, C.K., Haltrich, D., 2014. Convenient microtiter plate-based, oxygen-independent activity assays for flavin-dependent oxidoreductases based on different redox dyes. *Biotechnol. J.* 9, 474–482. doi:10.1002/biot.201300336
- Cameron, M.D., Aust, S.D., 2001. Cellobiose dehydrogenase—an extracellular fungal flavocytochrome. *Enzyme Microb. Technol.* 28, 129–138. doi:10.1016/S0141-0229(00)00307-0
- Canevascini, G., Borer, P., Dreyer, J.-L., 1991. Cellobiose dehydrogenases of *Sporotrichum (Chrysosporium) thermophile*. *Eur. J. Biochem.* 198, 43–52. doi:10.1111/j.1432-1033.1991.tb15984.x
- Cimbala, J.M., 2011. Outliers. <http://www.mne.psu.edu/me345/Lectures/Outliers.pdf> (accessed 27 Oct 2015).
- Grigoriev, I.V., Nikitin, R., Haridas, S., Kuo, A., Ohm, R., Otilar, R., Riley, R., Salamov, A., Zhao, X., Korzeniewski, F., Smirnova, T., Nordberg, H., Dubchak, I., Shabalov, I., 2014. MycoCosm portal: gearing up for 1000 fungal genomes. *Nucleic Acids Res.* 42, D699. doi:10.1093/nar/gkt1183
- Guex, N., Peitsch, M.C., Schwede, T., 2009. Automated comparative protein structure modeling with SWISS-MODEL and Swiss-PdbViewer: A historical perspective. *ELECTROPHORESIS* 30, S162–S173. doi:10.1002/elps.200900140
- Hallberg, B.M., Bergfors, T., Bäckbro, K., Pettersson, G., Henriksson, G., Divne, C., 2000. A new scaffold for binding haem in the cytochrome domain of the extracellular flavocytochrome cellobiose dehydrogenase. *Structure* 8, 79–88. doi:10.1016/S0969-2126(00)00082-4

- Hallberg, B.M., Henriksson, G., Pettersson, G., Divne, C., 2002. Crystal structure of the flavoprotein domain of the extracellular flavocytochrome cellobiose dehydrogenase. *J. Mol. Biol.* 315, 421–434. doi:10.1006/jmbi.2001.5246
- Harreither, W., Sygmund, C., Augustin, M., Narciso, M., Rabinovich, M.L., Gorton, L., Haltrich, D., Ludwig, R., 2011. Catalytic Properties and Classification of Cellobiose Dehydrogenases from Ascomycetes. *Appl. Environ. Microbiol.* 77, 1804–1815. doi:10.1128/AEM.02052-10
- Himmel, M.E., Ding, S.-Y., Johnson, D.K., Adney, W.S., Nimlos, M.R., Brady, J.W., Foust, T.D., 2007. Biomass Recalcitrance: Engineering Plants and Enzymes for Biofuels Production. *Science* 315, 804–807. doi:10.1126/science.1137016
- Ho, C.S., Lam, C.W.K., Chan, M.H.M., Cheung, R.C.K., Law, L.K., Lit, L.C.W., Ng, K.F., Suen, M.W.M., Tai, H.L., 2003. Electrospray Ionisation Mass Spectrometry: Principles and Clinical Applications. *Clin. Biochem. Rev.* 24, 3.
- Horn, S.J., Vaaje-Kolstad, G., Westereng, B., Eijsink, V.G., 2012. Novel enzymes for the degradation of cellulose. *Biotechnol. Biofuels* 5, 45. doi:10.1186/1754-6834-5-45
- Igarashi, K., Momohara, I., Nishino, T., Samejima, M., 2002. Kinetics of inter-domain electron transfer in flavocytochrome cellobiose dehydrogenase from the white-rot fungus *Phanerochaete chrysosporium*. *Biochem. J.* 365, 521.
- Igarashi, K., Yoshida, M., Matsumura, H., Nakamura, N., Ohno, H., Samejima, M., Nishino, T., 2005. Electron transfer chain reaction of the extracellular flavocytochrome cellobiose dehydrogenase from the basidiomycete *Phanerochaete chrysosporium*. *FEBS J.* 272, 2869–2877. doi:10.1111/j.1742-4658.2005.04707.x
- Invitrogen, 2010. EasySelect™ Pichia Expression Kit manual. https://tools.thermofisher.com/content/sfs/manuals/easyselect_man.pdf (accessed 20 Sept 2015).
- Invitrogen, 2002. Pichia Fermentation Process Guidelines, Version B. Available from Invitrogen. https://tools.thermofisher.com/content/sfs/manuals/pichiaferm_prot.pdf (accessed 19 Oct 2015).
- Isaksen, T., Westereng, B., Aachmann, F.L., Agger, J.W., Kracher, D., Kittl, R., Ludwig, R., Haltrich, D., Eijsink, V.G.H., Horn, S.J., 2014. A C4-oxidizing Lytic Polysaccharide Monooxygenase Cleaving Both Cellulose and Cello-oligosaccharides. *J. Biol. Chem.* 289, 2632–2642. doi:10.1074/jbc.M113.530196
- Keller, B.O., Sui, J., Young, A.B., Whittall, R.M., 2008. Interferences and contaminants encountered in modern mass spectrometry. *Anal. Chim. Acta* 627, 71–81. doi:10.1016/j.aca.2008.04.043
- Kiefer, F., Arnold, K., Künzli, M., Bordoli, L., Schwede, T., 2009. The SWISS-MODEL Repository and associated resources. *Nucleic Acids Res.* 37, D387–D392. doi:10.1093/nar/gkn750
- Kittl, R., Kracher, D., Burgstaller, D., Haltrich, D., Ludwig, R., 2012. Production of four *Neurospora crassa* lytic polysaccharide monooxygenases in *Pichia pastoris* monitored by a fluorimetric assay. *Biotechnol. Biofuels* 5, 79. doi:10.1186/1754-6834-5-79
- Kracher, D., Zahma, K., Schulz, C., Sygmund, C., Gorton, L., Ludwig, R., 2015. Inter-domain electron transfer in cellobiose dehydrogenase: modulation by pH and divalent cations. *FEBS J.* 282, 3136–3148. doi:10.1111/febs.13310
- Langston, J.A., Shaghasi, T., Abbate, E., Xu, F., Vlasenko, E., Sweeney, M.D., 2011. Oxidoreductive Cellulose Depolymerization by the Enzymes Cellobiose Dehydrogenase and Glycoside Hydrolase 61. *Appl. Environ. Microbiol.* 77, 7007–7015. doi:10.1128/AEM.05815-11

- Ludwig, R., Ortiz, R., Schulz, C., Harreither, W., Sygmund, C., Gorton, L., 2013. Cellobiose dehydrogenase modified electrodes: advances by materials science and biochemical engineering. *Anal. Bioanal. Chem.* 405, 3637–3658. doi:10.1007/s00216-012-6627-x
- Ludwig, R., Salamon, A., Varga, J., Zámocky, M., Peterbauer, C.K., Kulbe, K.D., Haltrich, D., 2003. Characterisation of cellobiose dehydrogenases from the white-rot fungi *Trametes pubescens* and *Trametes villosa*. *Appl. Microbiol. Biotechnol.* 64, 213–222. doi:10.1007/s00253-003-1501-6
- Lutz, S., 2010. Beyond directed evolution—semi-rational protein engineering and design. *Curr. Opin. Biotechnol.* 21, 734–743. doi:10.1016/j.copbio.2010.08.011
- Lynd, L.R., Weimer, P.J., van Zyl, W.H., Pretorius, I.S., 2002. Microbial Cellulose Utilization: Fundamentals and Biotechnology. *Microbiol. Mol. Biol. Rev.* 66, 506–577. doi:10.1128/MMBR.66.3.506-577.2002
- Nelson, D., Cox, M., Heldmaier, G., 2010. *Lehninger Biochemie*, 4. Aufl. 2009, 3., korr. Nachdruck 2010. ed. Springer.
- Nič, M., Jirát, J., Košata, B., Jenkins, A., McNaught, A. (Eds.), 2009. *IUPAC Compendium of Chemical Terminology: Gold Book*, 2.1.0 ed. IUPAC, Research Triangle Park, NC.
- Perlack, R.D., Stokes, B.J., Jr, R.S.Z., Tatarko, J., 2011. U.S. Billion-Ton Update: Biomass Supply for a Bioenergy and Bioproducts Industry. ResearchGate.
- Perlack, R.D., Wright, L., Turhollow, A., Stokes, B., Erbach, D., 2005. Biomass As Feedstock for A Bioenergy and Bioproducts Industry: The Technical Feasibility of A Billion-ton Annual Supply. Report.
- Phillips, C.M., Beeson, W.T., Cate, J.H., Marletta, M.A., 2011. Cellobiose dehydrogenase and a copper-dependent polysaccharide monooxygenase potentiate cellulose degradation by *Neurospora crassa*. *ACS Chem. Biol.* 6, 1399–1406. doi:10.1021/cb200351y
- Quinlan, R.J., Sweeney, M.D., Leggio, L.L., Otten, H., Poulsen, J.-C.N., Johansen, K.S., Krogh, K.B.R.M., Jørgensen, C.I., Tovborg, M., Anthonsen, A., Tryfona, T., Walter, C.P., Dupree, P., Xu, F., Davies, G.J., Walton, P.H., 2011. Insights into the oxidative degradation of cellulose by a copper metalloenzyme that exploits biomass components. *Proc. Natl. Acad. Sci.* 108, 15079–15084. doi:10.1073/pnas.1105776108
- Ritter, S.K., 2008. Lignocellulose: A Complex Biomaterial. *Chem. Eng. News* 8649.
- Rubin, E.M., 2008. Genomics of cellulosic biofuels. *Nature* 454, 841–845. doi:10.1038/nature07190
- Sanjeev, R., Jagannadham, V., Vraha, R.V., 2012. Implications of a novel interpretation of the isosbestic point. *Chem. N. Z.* 76, 133–135.
- Scheiblbrandner, S., 2012. Biochemical and electrochemical characterization of cellobiose dehydrogenase for application in glucose biosensors. Univ. of Natural Resources and Applied Life Science, Vienna.
- Sygmund, C., Kracher, D., Scheiblbrandner, S., Zahma, K., Felice, A.K.G., Harreither, W., Kittl, R., Ludwig, R., 2012. Characterization of the Two *Neurospora crassa* Cellobiose Dehydrogenases and Their Connection to Oxidative Cellulose Degradation. *Appl. Environ. Microbiol.* 78, 6161–6171. doi:10.1128/AEM.01503-12
- Sygmund, C., Santner, P., Krondorfer, I., Peterbauer, C.K., Alcalde, M., Nyanhongo, G.S., Guebitz, G.M., Ludwig, R., 2013. Semi-rational engineering of cellobiose dehydrogenase for improved hydrogen peroxide production. *Microb. Cell Factories* 12, 38. doi:10.1186/1475-2859-12-38

- Tan, T.-C., Kracher, D., Gandini, R., Sygmund, C., Kittl, R., Haltrich, D., Hällberg, B.M., Ludwig, R., Divne, C., 2015. Structural basis for cellobiose dehydrogenase action during oxidative cellulose degradation. *Nat. Commun.* 6, 7542. doi:10.1038/ncomms8542
- Tian, C., Beeson, W.T., Iavarone, A.T., Sun, J., Marletta, M.A., Cate, J.H.D., Glass, N.L., 2009. Systems analysis of plant cell wall degradation by the model filamentous fungus *Neurospora crassa*. *Proc. Natl. Acad. Sci.* 106, 22157–22162. doi:10.1073/pnas.0906810106
- Vaaje-Kolstad, G., Westereng, B., Horn, S.J., Liu, Z., Zhai, H., Sørli, M., Eijsink, V.G.H., 2010. An Oxidative Enzyme Boosting the Enzymatic Conversion of Recalcitrant Polysaccharides. *Science* 330, 219–222. doi:10.1126/science.1192231
- Westermarck, U., Eriksson, K.-E., Daasvatn, K., Liaaen-Jensen, S., Enzell, C.R., Mannervik, B., 1974. Cellobiose:Quinone Oxidoreductase, a New Wood-degrading Enzyme from White-rot Fungi. *Acta Chem. Scand.* 28b, 209–214. doi:10.3891/acta.chem.scand.28b-0209
- Zámocký, M., Hallberg, M., Ludwig, R., Divne, C., Haltrich, D., 2004. Ancestral gene fusion in cellobiose dehydrogenases reflects a specific evolution of GMC oxidoreductases in fungi. *Gene* 338, 1–14. doi:10.1016/j.gene.2004.04.025
- Zamocky, M., Ludwig, R., Peterbauer, C., Hallberg, B., Divne, C., Nicholls, P., Haltrich, D., 2006. Cellobiose Dehydrogenase – A Flavocytochrome from Wood-Degrading, Phytopathogenic and Saprotropic Fungi. *Curr. Protein Pept. Sci.* 7, 255–280. doi:10.2174/138920306777452367

7. Appendix

7.1 List of figures

Figure 1: Structure of lignocellulosic biomass (Rubin, 2008)	8
Figure 2 : Scheme of fungal cellulolytic enzyme system. Exoglucanases (CBH1 and CBH2) act on chain ends. Endoglucanases (grey) and LPMO (here PMO – red, yellow and orange) cleave internal bonds in amorphous and crystalline cellulose, respectively, creating new chain ends for exoglucanases. CDH (violet) provides electrons for LPMO-dependent oxygen activation. Picture taken from Beeson et al., (2015).	9
Figure 3: Electron transfer steps of CDH and LPMO (provided by Alfons Felice)	11
Figure 4: Map of pPICzα vector. Adapted from (Invitrogen, 2010).....	20
Figure 5: schematic overview of the site-directed mutagenesis	21
Figure 6: Plate design for 96-deep well plate cultivation with <i>NcCDH IIA</i> wild-type, six CDH mutants and X33 cells.....	26
Figure 7: Layout of the pipetting robot for the transfer of supernatant: After a flushing and a washing step of the fixed tips (1), the robot picks up eight disposable tips (blue), takes up the supernatant from the deep well plate (violet) and transfers either 20 µl or 10 µl into the three microtiter plates (blue) until all wells are filled with culture supernatant. This procedure was repeated twice.	27
Figure 8: High-throughput-screening used for the detection of active CDH variants with intact electron transfer properties inbetween CDH as well as to LPMO	28
Figure 9: linear regression fit for Photometer – Platereader relation for DCIP assay ($U\ ml^{-1} = 3.2441 \pm 0.03\ A\ min^{-1}$) taken from Christian Schuster’s diploma thesis (2014) and for cyt <i>c</i> assay ($U\ ml^{-1} = 4.5757 \pm 0.06\ A\ min^{-1}$)	30
Figure 10: standard curve for Bradford assay made with <i>NcCDH IIA</i> in the range from 0.01 mg/ml to 0.08 mg/ml.	31
Figure 11: Presteady-state spectral changes of CDH upon mixing with cellobiose. Black arrows show the isosbestic point at 449 nm of the FAD and the α- and β-absorbtion bands of the heme at 563 nm and 533 nm, respectively (spectrum taken from Scheiblbrandner, 2012).	35
Figure 12: A simplified picture of a single mix flow circuit (Applied Photophysics, 2006).....	
Figure 13: Simplified picture of a sequential mix flow circuit (Applied Photophysics, 2006).....	

Figure 14: Electron transfer steps from CDH to LPMO and to its substrate (figure provided by Alfons Felice).	
Figure 15: Linear regression fit for the ratio analyt-internal standard versus concentration of the analyt ($y_a/y_i=1.8733 * c_a$).	38
Figure 16: calibration curves for celotriose, celotetraose and celopentaose.	39
Figure 17: 3-D protein structure of the two CDHs from <i>N. crassa</i> . The structures were visualized with PyMol. Mutation sites at the interface as well as in the linker domain are marked with yellow crosses.	42
Figure 18: Close-up of the interface between the CYT and DH domains in <i>NcCDH IIA</i> showing the side chains targeted for mutagenesis. Amino acids for mutations highlighted in green (charge variants), magenta (hydrophobic changes), grey (steric differences) and orange (additional loop in linker peptide). Dashed yellow lines represent polar contacts to neighbouring residues.	43
Figure 19: Determined detection limits for DCIP-, cyt <i>c</i> - and the Amplex red assay. A linear range for varying CDH concentrations was found from 0.05 – 0.5 μ M (DCIP), 0.015 – 0.06 μ M (cyt <i>c</i>) and 0.06 – 2 μ M (AR).....	46
Figure 20: Data processing steps for the HTS from raw data to the enzyme factors and specific activities for all CDH variants.	47
Figure 21: Shown on the left side the expressed activities of DH (DCIP) and of the holoenzyme (cyt <i>c</i>). The right plot displays LPMO activity (AR) which is an indicator for successful electron transfer from CDH to LPMO as well as the AR-activity in relation to cyt <i>c</i> activity. The specific activities are the mean of catalytic activities of five different clones including the same mutation.	48
Figure 22: Production of <i>NcCDH IIA</i> variants in a <i>P. pastoris</i> X33. Time course of wet biomass, total protein concentration in the supernatant and enzymatic activity are shown.....	51
Figure 23: SDS-PAGE of <i>NcCDH IIA</i> variants and <i>NcCDH IIA</i> wild-type. All CHDs showed sharp bands at 110 kDa after the two-step purification.....	
Figure 24: Time course of absorption at 563 nm for monitoring heme reduction of <i>NcCDH IIA</i> . The plot serves as an example of spectral changes obtained also for all other CDH variants.....	
Figure 25: Observed rate constant k_{obs} for CDH-LPMO interaction plottet vs. the corresponding LPMO concentration. The slope equals k_{app} – a second order rate constant – that describes the CDH-LPMO reaction rate as a function of CDH-LPMO ratio.....	

Figure 26: ESI-MS analysis of products generated over time during Glc₅ (m/z 851) degradation. The picture shows a spectrum from m/z 370 – 900 for the 180 min-sample of *NcCDH* IIA (0.8 μM) to LPMO (0.8 μM) ratio of 1:1. 62

Figure 27: Linear relationship between cellopentaose conversion and time. The estimation of the substrate consumption rate was performed by a linear regression fit where k_{obs} [μM min⁻¹] equals the slope. The left plot shows the results of the experiments conducted with Q198F, the right plot with *NcCDH* IIA. 63

Figure 28: Determined reaction rates as a function of CDH concentration during cellopentaose conversion.

Figure 29: ESI-MS spectrum of multiple reaction products obtained after incubation of 25 mg ml⁻¹ Avicel with 0.8 μM LPMO-02916 and 0.8 μM *NcCDH* IIA with 1μM Lactose for 9 h, showing the sodium adducts or even double-adducts of their corresponding single- and double-oxidized cellobiose, cellotetraose, cellopentaose. The left picture displays a full spectrum from m/z 440 – 910, while the right one illustrates only the trimers found in a mass range from 520 to 590. The peak at m/z 447 corresponds to the mass of the internal standard chitobiose. 65

Figure 30: Linear increase of released products upon degradation of 25 mg ml⁻¹ Avicel with increasing CDH-LPMO ratios up to a two-fold CDH excess (0.32, 0.8, 1.6 μM CDH compared to 0.8 μM LPMO). The slope in the linear equation equals the product formation rate [μM h⁻¹] as a function of CDH:LPMO ratio. 66

Figure 31: Product formation rates k [s⁻¹] at different CDH concentrations during Avicel conversion.

Figure 32: Linear regression plots of oligosaccharides increase versus time analysed by MALDI-TOF MS (left plot) and ESI-MS (left plot). The sample mixtures were identical for both analysis including 25 mg ml⁻¹ Avicel, 0.8 μM LPMO-02916 and *NcCDH* IIA (0.32 – 1.6 μM) with 1 μM lactose. 68

Figure 33: Product formation upon degradation of 25 mg ml⁻¹ Avicel with 0.8 μM LPMO-02916 and 4 μM *NcCDH* IIA. It can be seen, that the product concentration decreased and levelled off after 6 h of incubation possibly due to competitive binding of CDH and LPMO or the formation of harmful by-products (e.g. H₂O₂). 84

Figure 34: MalDI-TOF spectrum of multiple reaction products obtained after incubation of 25 mg ml⁻¹ Avicel with 0.8 μM LPMO-02916 and 0.8 μM *NcCDH* IIA for 3, 6, 9 and 24h. 84

7.2 List of tables

Table 1: List of primers used during the project	19
Table 2: List of enzymes used during the project.....	19
Table 3: List of kits used during the project	20
Table 4: Pipetting scheme for Phusion Master mix	22
Table 5: Pipetting scheme for Phusion PCR reaction	22
Table 6: Protocol for Phusion PCR reaction	22
Table 7: Pipetting scheme for Colony-PCR reaction.....	23
Table 8: Protocol for Colony-PCR reaction.....	23
Table 9: Pipetting scheme for DpnI digestion	24
Table 10: Pipetting scheme for MSSI digestion.....	25
Table 11: Pipetting scheme for DCIP assay.	28
Table 12: Pipetting scheme for cyt c assay.....	29
Table 13: Pipetting scheme for Amplex red assay	30
Table 14: Pipetting scheme for AR-assay without LPMO	31
Table 15: List of mutants engineered with site-directed mutagenesis and used for high throughput activity screening.....	44
Table 16: Detection limits determined after IUPAC guidelines (left column) and by plotting absorbance change vs. the corresponding CDH concentration (right column).....	46
Table 17: Screening results of each CDH variant in more detail.....	49
Table 18: Purification scheme for <i>NcCDH</i> IIA variants. The purification factor was calculated from the specific activity obtained from the cyt c assay.....	52
Table 19: Steady-state catalytic constants of <i>NcCDH</i> IIA and six variants for cellobiose and lactose at pH 6.0 using DCIP as electron donor.....	54
Table 20: Kinetic constants of IET rates and 2 nd slow rates for all CDH variants. Delta absorbance describes the percentage absorbance change for each rate in relation to the complete absorbance change. Mean values and standard deviations were calculated from quadruplet measurements.	56

Table 21: List of CDH-LPMO electron transfer rates. All CDH variants with each LPMO concentration were measured in triplicates.....	57
Table 22: Reaction rates of heme reduction (IET) and 2 nd order rate constants (CDH-LPMO interaction).....	58
Table 23: Comparison of relative activities obtained from HTS with presteady-state kinetic data.	61
Table 24: Reaction rates for different <i>Nc</i> CDH IIA/Q198F – LPMO ratios reflecting cellopentaose degradation over time. Data were obtained from measurements of two separately prepared and analysed reaction mixtures.	64
Table 25: Reaction rates for <i>Nc</i> CDH IIA and Q198F determined by following the cellopentaose consumption over time and plotting the observed rates against their corresponding CDH concentration.....	64
Table 26: Catalytic constants for <i>Nc</i> CDH IIA and Q198F calculated by using nonlinear least-square regression by fitting the observed data to a single rectangular hyperbola.	67
Table 27: Comparison of reaction rates obtained for product analyses of the same reaction mixture with either ESI-MS or MALDI-TOF MS.....	69
Table 28: Specific activities of several CDH variants determined by the four-assay screening method combining DCIP-, cyt <i>c</i> - and Amplex red assay.	72
Table 29: Heme reoxidation rates of all variants using molecular oxygen. The rates are determined by following the absorption at 563 nm and fitting the data to single exponential curves.....	83

7.3 List of abbreviations

AOX	Alcohol oxidase
AR	Amplex red
ARAA	Amplex red activity assay
BMD	Buffered minimal dextrose medium
BMM10	Buffered minimal methanol 10 medium
BMM2	Buffered minimal methanol 2 medium
CBM	Carbohydrate-binding module
CDH	Cellobiose dehydrogenase
CYT	Cytochrome domain CDH
Cyt <i>c</i>	Cytochrome <i>c</i>
DCIP	2,6 – dichloroindolphenol
DH	Dehydrogenase domain CDH
<i>E. coli</i>	<i>Escherichia coli</i>
ET	Electron transfer
FAD	Flavin adenine dinucleotide
HIC	Hydrophobic interaction chromatography
HTS	High throughput screening
IEC	Ion exchange chromatography
IET	Intra-domain electron transfer
k_{app}	Apparent second order rate constant
k_{cat}	Turnover number (Michaelis-Menten kinetics)
K_M	Michaelis constant (Michaelis-Menten kinetics)
k_{obs}	Observed reaction rate
LPMO	Lytic Polysaccharide Monooxygenase
<i>N. crassa</i>	<i>Neurospora crassa</i>
<i>NcCDH IIA</i>	<i>Neurospora crassa</i> CDH IIA
<i>NcCDH IIB</i>	<i>Neurospora crassa</i> CDH IIB
<i>P. pastoris</i>	<i>Pichia pastoris</i>
PDA	Photodiode array detector
SDS-PAGE	Sodium dodecyl sulfate - polyacrylamite gel electrophoresis
U	Unit of enzymatic activity [$\mu\text{mol min}^{-1}$]
V_{max}	Maximal reaction velocity (Michaelis-Menten kinetics)
YNB	Yeast Nitrogen Base

7.4 Supplemental information

7.4.1 High-throughput-screening protocol for CDH-LPMO interaction:

1. Premix all reagents necessary for each assay (DCIP, cyt *c*, Amplex red & Bradford) during the centrifugation of the *P. pastoris* cultures (3500 rpm for 15 min at 4°C) cultivated for 136 h in a deep-well plate.
2. Use a pipetting robot applying the program „Alf transfer deepwell to 3 96 well“ to transfer the culture supernatant including the CDHs automatically from the cultivation plate into three replica plates.
3. Repeat the procedure twice.
4. Immediately after the pipetting robot has finished its work, start the screening with the DCIP-assay by adding 180 µL of the premixed stock solution into the microtiter plate with a multi-channel pipette and put it into a photometric plate reader (Tecan).
5. While the absorbance change of DCIP is detected, the second assay (AR) is started and the enzymatic reaction followed in a fluorometric plate reader (Perkin Elmer).
6. After finishing the measurement of the DCIP reduction, replace the microplate by the third replica plate including cyt *c*.
7. Then start the second AR-assay without any LPMO to determine the expected oxygen background activity of CDH.
8. Finally conduct the Bradford assay by an endpoint measurement with the Tecan microplate reader after an incubation time of 15 min.

7.4.2 Oxygen heme reoxidation

CDH	Heme
	kobs [s ⁻¹]
NcCDH IIA	0.029 ± 0.001
linker2	0.033 ± 0.001
D200N	0.021 ± 0.001
Q198F	0.021 ± 0.001
A96Q	0.024 ± 0.001
E629Q	0.031 ± 0.001
Y716P	0.025 ± 0.001

Table 29: Heme reoxidation rates of all variants using molecular oxygen. The rates are determined by following the absorption at 563 nm and fitting the data to single exponential curves.

7.4.3 Avicel conversion by CDH/LPMO with a fivefold CDH excess

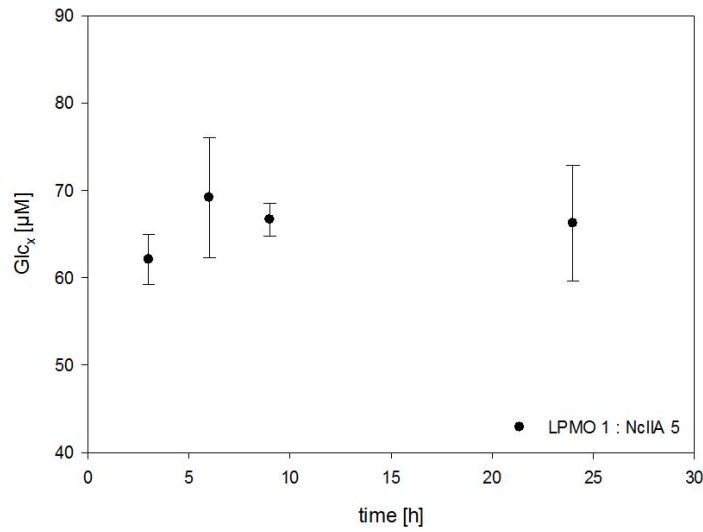


Figure 33: Product formation upon degradation of 25 mg ml⁻¹ Avicel with 0.8 µM LPMO-02916 and 4 µM NcCDH IIA. It can be seen, that the product concentration decreased and levelled off after 6 h of incubation possibly due to competitive binding of CDH and LPMO or the formation of harmful by-products (e.g. H₂O₂).

7.4.4 MALDI-TOF spectrum

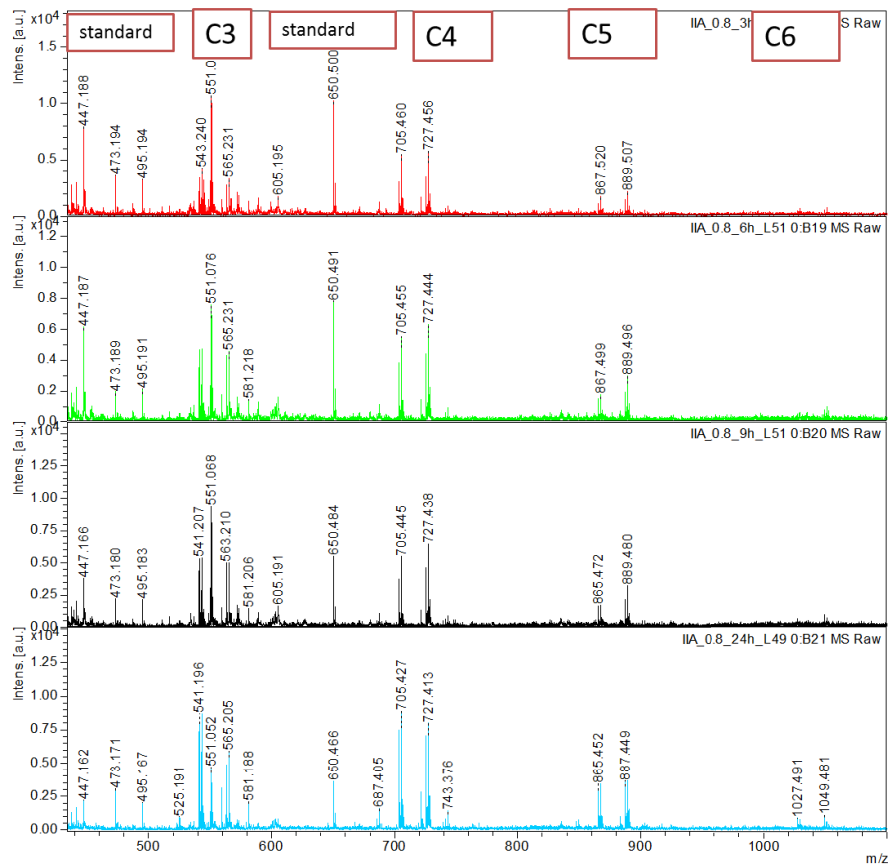


Figure 34: MalDI-TOF spectrum of multiple reaction products obtained after incubation of 25 mg ml⁻¹ Avicel with 0.8 µM LPMO-02916 and 0.8 µM NcCDH IIA for 3, 6, 9 and 24h.